LUND UNIVERSITY

Associative Polymer-Polymer and Polymer-Surfactant Systems: Phase Behaviour and the Influence of Chemical Reactions

Santos, Salome

2010

*Para os **meus pais**: as minhas mãos são o meu coração e com elas vos dou o melhor de tudo.*

*To **my parents**: my hands are my heart and with them I offer you the best of everything.*

…….....

"I'm digging my way to something better
I'm pushing to stay with something better
This thorn in my side is from the tree I've planted"
Metallica

Acknowledgments

My parents: you accepted my decision to stay in Sweden to do my PhD studies, even if it was extremely hard to endure. You devoted your lives to me and to only me, with a lot of hard work and huge sacrifices. There is nothing bigger than to spend one's entire life making it possible for others to live. This is love and I hope I never forget this lesson.

My Luís: you are the one I want to hear breathing by my side every night. I have no doubt. You are also the person I want to change the world with. Thank you for making me feel so special and encouraging me to go forward in my decisions. I always want to walk with you and we will always walk together.

My friend Zaida: my twin soul, thank you for so much and also for writing e-mails to me every day when I came to Sweden during 3 months. Without those e-mails I wouldn't have had the strength to stay. Sometimes I feel that without you I wouldn't exist.

My friends that I made in Lund: the associative behaviour in Lund was not only in the lab, but also in friendship. This association is not reversible and there are no changes that can make it weaker or be lost (to fully understand this part, you need to read the thesis ☺, and since you are my friends I am sure you will do it with pleasure ☺).

My friends in Portugal and outside Portugal (or Lund): thank you for never giving up on me because I was far. You always have hugs and smiles for me and I have my heart for you.

César and Paulina: thank you so much for all the love and care and for making things much easier in many situations. I am very fortunate because you became part of my life. Everything is much more "quentinho e porreiro" with you.

Maria: you took care of me, scientifically but not only, during the most difficult time in my life. Then you took me to Sweden and when I needed a Portuguese word to feel confident and move forward you were there. I will never forget it. Thank you for so many other things.

Björn: you are the responsible for many good things in my life. I thank you for your kindness, generosity and for teaching me so much.

Lennart: thank you very much for ALL the help you gave me from the beginning until the end of this journey. I learned a lot from you as a scientist, and you are a good friend too.

Ola: thank you for being so easy to talk to you. Thank you for the help, for all the care and fast replies that you gave me.

My co-authors: this Thesis would not have been possible without you. Thank you!

Physical Chemistry: this great place to work and make friends! I just want to say that I was very lucky to be here. Thanks to everyone who made this good feeling possible.

FCTand POPH/FSE: for funding my PhD studies (SFRH/BD/30929/2006).

Doctoral Thesis

Physical Chemistry
Center for Chemistry and Chemical Engineering
Lund University
P.O. Box 124
SE-221 00 Lund
Sweden

ISBN 978-91-7422-257-9
Printed by Media-Tryck, Lund University, Lund

Associative Polymer-Polymer and Polymer-Surfactant Systems: Phase Behaviour and the Influence of Chemical Reactions

Salomé dos Santos

LUND UNIVERSITY

Doctoral Thesis

The thesis will be publicly defended on Friday, 17th of December 2010, at 13.15 pm in lecture hall B, Center for Chemistry and Chemical Engineering, Lund, Sweden

The faculty opponent is the Senior Lecturer Per Hansson, from the Department of Pharmacy, Uppsala University, Uppsala, Sweden

Organization	Document name
LUND UNIVERSITY Physical Chemistry Center for Chemistry and Chemical Engineering POB 124, SE-221 00 Lund, Sweden	DOCTORAL DISSERTATION
	Date of issue December 17, 2010
Author(s) Salomé dos Santos	Sponsoring organization FCT(&POPH/FSE) (Portuguese Science and Technology Foundation) and VR (Vetenskapsrådet, Sweden)

Title and subtitle

Associative Polymer-Polymer and Polymer-Surfactant Systems:
Phase Behaviour and the Influence of Chemical Reactions

Abstract

Aqueous mixtures of two non-ionic polymers, poly(acrylic acid) (PAA) and the amphiphilic triblock copolymer, $(EO)_{27}(PO)_{67}(EO)_{27}$, known by its trade name Pluronic® P104, showed an associative phase separation (miscibility gap), which decreased with the decrease of PAA length. It was found that PAA is a much less selective "solvent" to P104 molecules than water. P104 aggregates are disintegrated and thus the liquid crystalline structures are destroyed upon replacement of water by PAA.

Oppositely charged polyelectrolytes, DNA (double- or single-stranded) and two cationic derivatives of the hydroxyethyl cellulose (cat-HMHEC and cat-HEC) were mixed in water. An asymmetric associative phase separation was observed: small amounts of cat-(HM)HEC could precipitate DNA but large amounts of DNA were needed to precipitate the polycations. The rheological properties of the off-stoichiometric one-phase mixtures were investigated. The viscosity increased as the polymer content was increased and showed an interesting non-monotonic behaviour for the cat-HEC/dsDNA/H_2O system.

Redissolution of insoluble polyion-surfactant ion complex salts by adding excess surfactant was investigated using the simple approach of preparing the complex salts and mixing them with excess surfactant. The complex salts contained poly(acrylate) homopolymer or copolymers containing acrylate and NIPAM or DAM. The phase diagram for the long homopolyions systems presented a large miscibility gap, while efficient redissolution was obtained for shorter polyions. Incorporation of neutral units (more hydrophobic) originated efficient redissolution.

Polymerizations in surfactant systems were performed. The acrylate counterion to the surfactant ion was polymerized under conditions where the growing poly(acrylate) chain was the sole counterion to the surfactant ion aggregates. Therefore the equilibrium phase diagrams constructed using the complex salts and excess surfactant predict the result of different pathways from polymerization reactions: phase diagrams come alive.

The structure of the polyion-surfactant ion concentrated phase was changed in situ through the degradation of the surfactant into alcohol. The used cationic surfactant (decyl betainate) had a hydrolyzing ester group sensitive to high pH. The degradation of the surfactant into decanol changes the curvature of the ordered structure of the concentrated phase. Multi-lamellar nano-particles were obtained.

Key words

Phase Behaviour, Polymer, Surfactant, Complex Salts, Redissolution, Chemical Reactions, Polymerizations, Association, SAXS, Rheology, Flory-Huggins, Curvature, Liquid Crystals, Phase Diagram, Templating, Hydrolysis

Classification system and/or index terms (if any)

Supplementary bibliographical information	Language English
ISSN and key title	ISBN 978-91-7422-257-9
Recipient's notes	Number of pages 140 / Price
	Security classification

Distribution by (name and address)

List of papers

I

Associative phase behaviour and disintegration of copolymer aggregates on adding poly(acrylic acid) to aqueous solutions of a PEO-PPO-PEO triblock copolymer

Salomé dos Santos, Bod Luigjes and Lennart Piculell, *Soft Matter*, 2010, **6**, 4756-4767

Reproduced by permission of The Royal Society of Chemistry
http://pubs.rsc.org/en/Content/ArticlePDF/2010/SM/C0SM00052C/2010-08-10

II

Phase behaviour and rheological properties of DNA-cationic polysaccharide mixtures: formation of highly viscoelastic solutions

Salomé dos Santos, Lennart Piculell, Bruno Medronho, M. Graça Miguel and Björn Lindman, submitted to *Soft Matter*

III

When do water-insoluble polyion-surfactant ion complex salts "redissolve" by added excess surfactant?

Salomé dos Santos, Charlotte Gustavsson, Christian Gudmundsson, Per Linse and Lennart Piculell, submitted to *Langmuir*

IV

Phase diagrams come alive: understanding how to create, destroy or change ordered surfactant structures by polymerizing the counterions

Salomé dos Santos, Lennart Piculell, Ola J. Karlsson and M. Graça Miguel, accepted for publication in *Soft Matter*

V

Responsive and evolving mixtures of a hydrolyzing cationic surfactant and an oppositely charged polyelectrolyte

Salomé dos Santos, Dan Lundberg and Lennart Piculell, manuscript

Contribution to the papers

I

I performed half of the experimental work, supervised the other half and wrote the paper together with the co-authors.

II

I performed all the experimental work and wrote the paper together with the co-authors.

III

I performed half of the experimental work, supervised the other half, performed the Flory-Huggins calculations and wrote the paper together with the co-authors.

IV

I performed all the experimental work and wrote the paper together with the co-authors.

V

I performed most of the experimental work and wrote the paper together with the co-authors.

Contents

Introduction

The wide number of studies performed in polymer-polymer or polymer-surfactant aqueous mixtures is a consequence of their significance in many different fields from fundamental science to industrial applications. Polymers and surfactants are present everywhere: they can be found in the human body, in cleaning products, in construction materials, in paper, in food, in pharmaceutical products, etc[1-6].

When mixed in water, under some circumstances, some polymers or polymers and surfactants attract each other and form complexes. These complexes can be soluble (homogeneous solution) or insoluble (separating out from the solution), depending on the chemistry of the molecules, the composition of the mixture and the ionic strength. Insoluble complexes can be used to create water-insoluble surface coatings by surface deposition techniques[7-10.] The insoluble complexes can separate out from water, forming a concentrated phase, which is in equilibrium with a dilute phase. For polymer-surfactant systems, the concentrated phase may display a variety of long-range ordered structures (liquid crystals) with diverse and interesting properties, due to the self-assembling tendency of surfactant molecules. These concentrated phases display structures that may be related to those formed by surfactants alone, but the presence of the polymer can facilitate the formation of the structures as well as modify their features. The long-range ordered structure of the concentrated phase depends largely on the chemistry of the molecules, the composition of the mixture and the interactions between the molecules. The structure of the concentrated phase can also be altered through chemical reactions performed directly in the system. When the mixtures exhibit long-range ordered structure, they can be used as templates to produce "mesoporous" materials[11,12] or to form structured nano-particles[13,14].

Different states of a mixture (soluble or insoluble) may find use in different states of an application. For instance, a shampoo is a homogeneous solution containing polymers and surfactants (or polymer-surfactant complexes) and during rinsing with water the polymer-surfactant complexes become insoluble and deposit onto the hair, creating a smooth coating[15].

Performing *in situ* chemical reactions is another way to produce mixtures with some properties at a certain stage and other properties at another stage. This method has been used in applications in paints and surface coatings[16].

Polymers and surfactants are widely used as rheology modifiers or gelling agents and their mixtures can exhibit interesting (sometimes non-monotonic) rheological behaviour, different from the individual polymer or surfactant solutions[3,17-22].

In this Thesis, interactions between polymers or polymers and surfactants in aqueous media have been studied, approaching the various systems (charged and non-charged) from different

perspectives. The work performed involved the study of phase behaviour of an uncharged polymer-polymer system, charged polymer-polymer and polymer-surfactant systems and the influence of chemical reactions in the polymer-surfactant systems.

The summary of this Thesis provides first a general background on polymers and surfactants and moves on to particular relevant aspects of the mixtures. For each mixture studied, a short overview of the related previous works is presented followed by a short summary of the main findings in this Thesis.

Polymers

Polymers are long chain molecules built from many smaller structural units called monomers (repeating units) which are covalently connected through polymerization reactions. The essential requirement for a small molecule to qualify as a monomer is that it contains reactive chemical bonds which under some conditions provide two or more bonding sites through which other monomers can covalently link and form the polymer chain. The number of repeating units in a chain is called the degree of polymerization.

Polymers can be ionic, and they are called polyions, or non-ionic (hydrophobic or hydrophilic). When charged, there is always an oppositely charged counterion neutralizing each charge of the polyion and the polyion together with its counterions constitutes a polyelectrolyte. They can be linear or branched (contain side groups attached to the backbone chain). Polymers can be homopolymers (built up from one kind of monomer) or copolymers (built up from different monomers). Copolymers can be amphiphilic if they contain both hydrophilic and hydrophobic repeating units. Copolymers can be made of blocks or be statistical (with a random distribution of the monomers). Polymers can have titratable or permanent charges. They can be flexible or rigid. Figure 1 shows examples of uncharged polymers, A, with titratable carboxylic groups, B, with neutral repeating units, and D, a triblock copolymer with poly(ethylene oxide) and poly(propylene oxide) groups, also called poloxamer; and polyelectrolytes (polyions + counterions): C, E, F and G. A, B and C, poly(acrylic acid), PAA, poly(NIPAM) (NIPAM = *N*,*N*-isopropylacrylamide) and sodium poly(styrene sulfonate), NaPSS, respectively, are obviously simpler polymers when compared to D, E, F and G, poloxamer, derivative of hydroxyethyl cellulose hydrophobically modified with $C_{12}H_{25}$, cat-HMHEC, cat-HEC (no hydrophobic modification) and deoxyribonucleic acid, DNA, respectively.

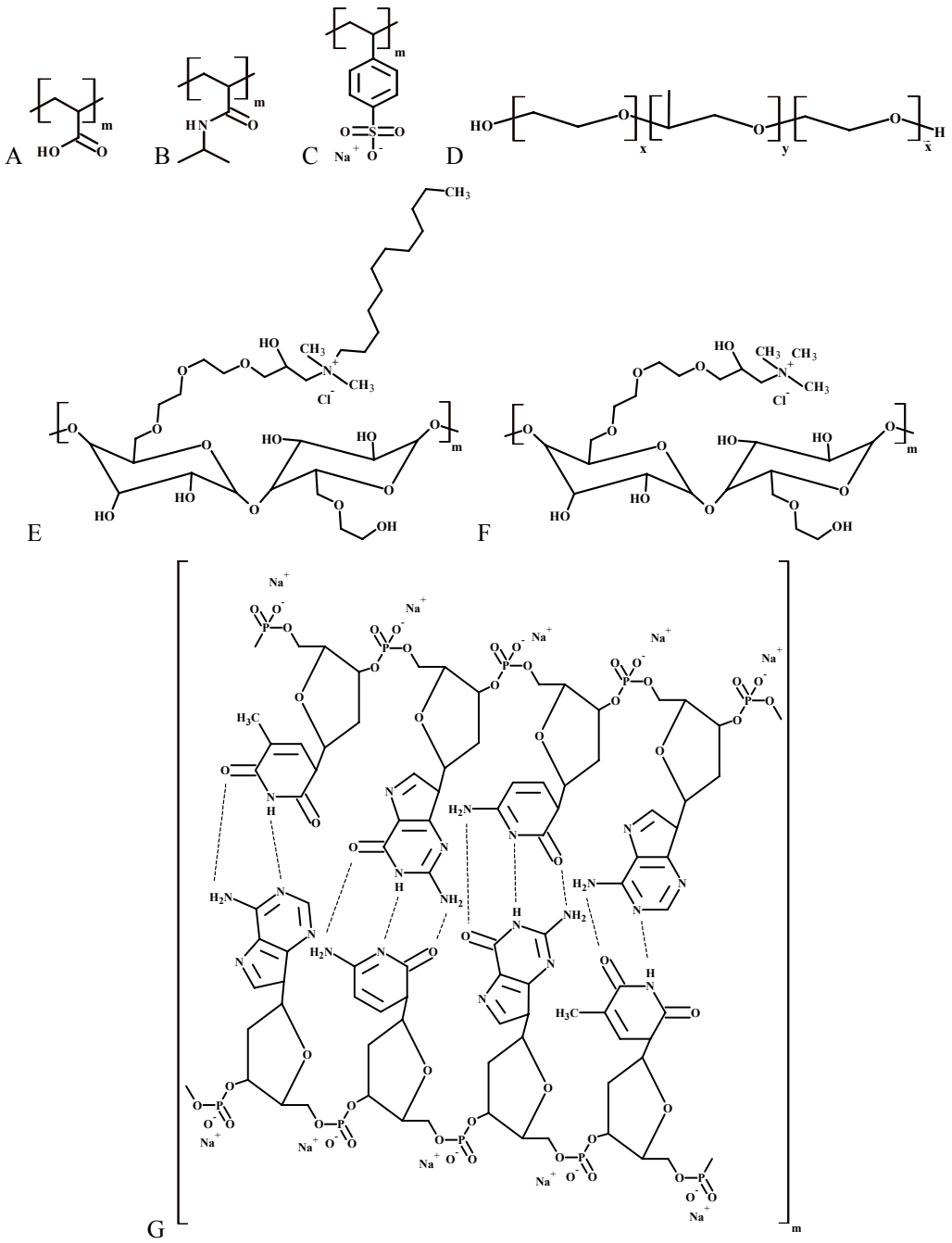

Figure 1 – Chemical structure of polymers relevant to this Thesis: A – poly(acrylic acid), PAA; B – poly(NIPAM) (NIPAM = *N*,*N*-isopropylacrylamide) copolymer; C – sodium poly(styrene sulfonate), NaPSS; D – poloxamer; E – derivative of hydroxyethyl cellulose hydrophobically modified with $C_{12}H_{25}$, cat-HMHEC, F – cat-HEC (no hydrophobic modification) and G – deoxyribonucleic acid, DNA.

Polymers can be synthesized by different methods (in bulk, suspension or emulsion). Bulk free radical polymerization is a simple polymerization reaction which initiates by the formation of radicals from an initiator by increasing temperature or using UV radiation. The radicals "attack" vinylic bonds creating a chain carrier and addition of monomers to a propagating chain occurs. Finally, the reaction is terminated by combination of radicals or disproportionation mechanisms[23].

Polymers in aqueous solution

Water-soluble uncharged polymers dissolve in water due to the gain in conformational entropy of the individual flexible polymer chains when these are diluted by the solvent. In general, charged polyions have a higher solubility in water than the corresponding uncharged polymer due to the dissociation of the counterions which increases the entropy of mixing[24]. The distribution of the counterions is enhanced close to the polyion and levels off with increasing the distance from the chain[25]. Some polyions, e. g. cat-HMHEC (Figure 1E), belong to the category of intrinsically insoluble polyions because the origin of its solubility is the presence of the charges (these polymers do not dissolve if their charges are screened by the addition of salt).

The amount of charged units per unit length in the polyion is referred to as the charge density. The charge density of polyions can vary considerably. Small distances between charges in the chain give a high charge density. Two examples of highly charged polyions are poly(acrylate) (PA^-) (Figure 1A in the acid form) and DNA (Figure 1G) with the distances between charges 0.25 nm and 0.34 nm (in each strand of DNA)[26], respectively. For cat-HMHEC and cat-HEC (Figure 1E and F) the distances between the charged groups projected onto the polyion backbone are roughly 10 nm and 2 nm, respectively,[27,28] corresponding to polyions of low charge density. The charges in the polyion can cause additional rigidity of the chain due to the electrostatic repulsion between charges of the same sign. Note that PA^- has a more flexible chain compared to cat-HEC or DNA.

For amphiphilic uncharged polymers (Figure 1D) and cat-HMHEC, the hydrophobic parts minimize the contact with water and self-assemble. This behaviour is similar to the surfactant behaviour that will be discussed below.

Flory-Huggins Theory

The entropy increases when mixing polymer and solvent. But, as said before, because the number of polymer chains is small, the most important contribution to the entropy of mixing comes from the increased number conformations available to individual flexible polymer chains when the latter are surrounded by small solvent molecules, rather than other polymer

chains. A lattice model to calculate the entropy of mixing for polymer solutions is given by the Flory-Huggins theory[29]. In the model one assumes a random distribution of the monomers despite the connectivity and that one monomer or one solvent molecule occupies one lattice unit (see Figure 2).

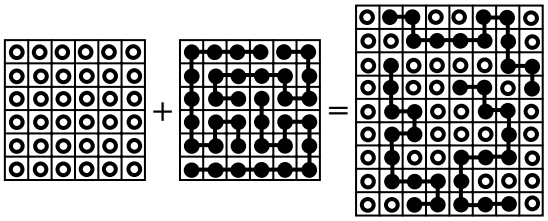

Figure 2 – Flory-Huggins lattice model for the mixture of a polymer and solvent.

The entropy of mixing can be calculated using Equation 1.

$$\Delta \boldsymbol{S}_{mix} = -k(N_1 + r_2N_2)[\phi_1 \ln \phi_1 + (\phi_2/r_2)\ln \phi_2] \qquad (1)$$

where $\phi_1 = N_1/(N_1 + r_2N_2)$ and $\phi_2 = r_2N_2/(N_1 + r_2N_2)$ are the volume fractions of solvent and polymer respectively. N_1 is the number of solvent molecules, N_2 is the number of monomer units, r_2 is the number of monomers per polymer (degree of polymerization).

$\Delta \boldsymbol{G}_{mix}$ is expressed as

$$\Delta \boldsymbol{G}_{mix} = kT(N_1 + r_2N_2)[\phi_1 \ln \phi_1 + (\phi_2/r_2)\ln \phi_2 + \chi_{12}\phi_1\phi_2] \qquad (2)$$

The entropy of mixing becomes more important the smaller the molecules are. The enthalpy is considered as being due to the balance of intermolecular interactions between the different molecules which is expressed by the χ parameter. This parameter can be negative or positive depending on whether the 12 interaction is more or less attractive than the average of the 11 and 22 interactions.[25,29]

Surfactants

Surfactants are amphiphilic molecules, containing both polar (hydrophilic) and non-polar (hydrophobic) parts. The polar part of the molecule can be charged or uncharged (non-ionic) and the non-polar part is typically a hydrocarbon chain. When charged, the head group of the surfactant ion is neutralized by a counterion. Due to their special properties, surfactants are surfaces active agents that can control surface and interfacial tensions, wettability, interfacial hydrodynamics, dispersion stability and rheology. Figure 3 shows examples of single-chain ionic surfactants (cationic surfactant ions + anionic counterions). In Figure 3 is seen that the alkyl chain length and the counterion type can vary. In Figure 3A, the common

cetyltrimethylammonium bromide surfactant is (C_{16}TABr) shown. The surfactant presented in Figure 3B has the dodecyltrimethylammonium ion neutralized by the organic counterion acrylate (C_{12}TAAcr). Acrylate (containing one vinylic bond) as seen in the Polymers section is the monomer which builds the poly(acrylate) polyion. Figure 3C shows a surfactant ion which contains an ester group which is very unstable under some pH conditions. Surfactants of the type shown in Figures 3B and C are used to manipulate surfactant action/properties through polymerization of the counterion or the hydrolysis of the ester bond, respectively[16,30].

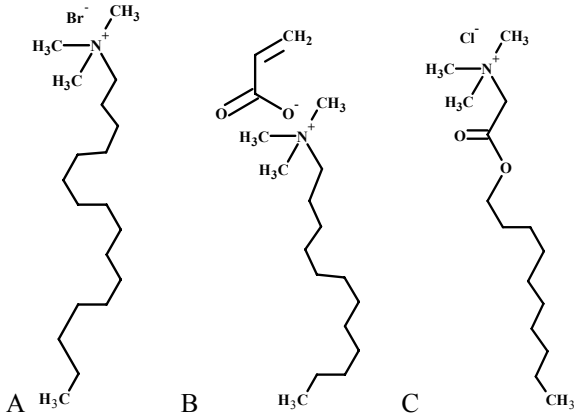

Figure 3 – Chemical structure of surfactant molecules relevant to this Thesis: A – cetyltrimethylammonium bromide (C_{16}TABr); B – dodecyltrimethylammonium acrylate (C_{12}TAAcr) and C – decyl betainate (DeB).

CMC

In water, the hydrophobic chains tend to associate spontaneously and the surfactant molecules form aggregates at some characteristic concentration. The simplest surfactant aggregate is the micelle. The micelles can have the shape of a sphere, an ellipsoid or a rod. The formation of micelles starts at the critical micellar concentration (*CMC*) and is a highly cooperative process. This concentration is approximately equal to the concentration of the free surfactant molecules, also called unimers (not aggregated) that remain in solution above *CMC*. Below the *CMC*, the surfactant behaves like a simple electrolyte. Above the CMC adding more surfactant to the solution only produces more micelles over a certain concentration range.

The balance between hydrophobic, electrostatic and steric effects determines the *CMC*[25]. Different surfactants have different *CMCs* depending on the chain length, type and valency of the counterion and type of head group[31,32]. The *CMC* of ionic surfactants can be lowered by: i) an increase in the alkyl chain length (not specific for ionic surfactants); ii) an increase in the valency of the counterion; iii) the presence of salt and iv) an increase in the counterion affinity to the surfactant ion.

The number of aggregated surfactant molecules in a micelle is called the aggregation number, N_{agg}.

Pseudo-phase separation model

When surfactant molecules are added to water, they are distributed between the bulk and the air-water interface (surface). The micelle has been considered as a separate phase in the pseudo-phase separation model, where the *CMC* is regarded as the saturation concentration for the single surfactant ions. The Gibbs adsorption equation, which connects the surface tension of a solution with the concentration of a solute, may be written in the form

$$-RT\Gamma_i = (\partial\gamma/\partial \ln a_i)_T = (\partial\gamma/\partial \ln x_i)_T \, (\partial \ln x_i/\partial \ln a_i)_T \qquad (3)$$

where Γ_i is the surface excess of the component i, γ is the surface tension, a_i the activity and x_i the mole fraction of the component i. The surface tension, γ, has a nearly constant value over a wide range of values of x_i in excess of the *CMC*. If Γ_i is finite and if $(\partial\gamma/\partial \ln x_i)_T$ is zero, it follows that $(\partial \ln x_i/\partial \ln a_i)_T$ is also zero. This is equivalent to the statement that a_i is independent of x_i above *CMC* and this is a signature of phase separation.[33]

Krafft point

The solubility of a surfactant varies with temperature. When the temperature decreases, the surfactant can precipitate out from solution as a solid crystal instead of forming micelles. The point at which the solubility equals the *CMC* is called the Krafft temperature. The solubility below this point is determined by the solubility of the surfactant monomers, whereas above it the high solubility of the micelles enables the formation of an homogeneous solution[25,31].

Surfactant number and mean curvature

The shape of the surfactant aggregates can be understood by two different approaches: the surfactant number or critical packing parameter, N_s, $N_s=v/la_0$, and the mean curvature of the surfactant-water interface, H, $H=1/2(1/R_1+1/R_2)$. v is the volume of the hydrophobic portion of the surfactant molecule, l is the length of the hydrophobic chain and a_0 is the effective area per surfactant head group. R_1 and R_2 are the radii of curvature of the surfactant-water interface in two perpendicular directions. Surfactant numbers relate the properties of the molecule to the preferred curvature properties of the aggregates. For a sphere: $N_s=1/3$ and $H=1/R$ ($R_1=R_2=R$); for a cylinder: $N_s=1/2$ and $H=1/2R$ ($R_1=R$ and $R_2=\infty$), for a planar bilayer: $N_s=1$ and $H=0$; and for bicontinuous structures: $N_s\geq1$ and $H\approx0$ ($R_1=-R_2$).[25]

Aggregates at high concentrations

In binary surfactant/water systems, a variety of structures can be found, ranging from disordered micellar solutions (referred to as **M** here and in the following sections) at lower concentrations to liquid crystalline structures (long-range order and short-range disorder) at higher surfactant concentrations. Liquid crystalline structures are composed of surfactant aggregates. The organization of surfactant aggregates can be in 3, 2 or 1 dimensions, corresponding to cubic (**C**), hexagonal (**H**) or lamellar (**L**) arrangements, respectively. The cubic structure can be bicontinuous or formed by discrete micelles packed in different arrangements (discontinuous). The micellar cubic structures can be divided into three main families: primitive, body centered and face centered. The unit cell, the smallest repeating unit in the 3D structure, in a cubic micellar structure contains different numbers of packed micelles in the different structures. The simplest is the primitive, which has only one micelle per unit cell. Body-centered (*BCC*) and face-centered (*FCC*) cubic structures have two and four micelles per unit cell, respectively, and the cubic structure with the *Pm*3*n* space group has eight slightly elongated micelles in the unit cell. The most common space group encountered for bicontinuous cubic structures is the *Ia*3*d* (**C_b**). Cubic structures are optically isotropic while hexagonal and lamellar are anisotropic. Figure 4 shows schemes for surfactant structures. Various factors that determine the relative stability of the different structures are discussed below.

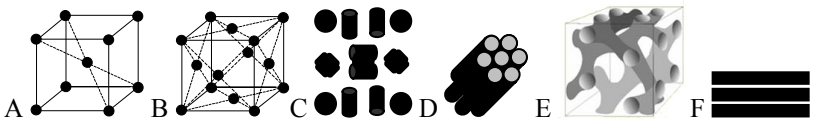

Figure 4 – Schemes of surfactant liquid crystalline structures relevant in this Thesis. From left to right: micellar cubic (**C**): A – ***BCC***, B – ***FCC***, C – ***Pm3n***; D – hexagonal (**H**); E – Cubic Bicontinuous *Ia*3*d* (**C_b**) and F lamellar (**L**).

Figure 5 summarizes sequences of surfactant aggregate structures appearing at high concentrations that will be discussed below.

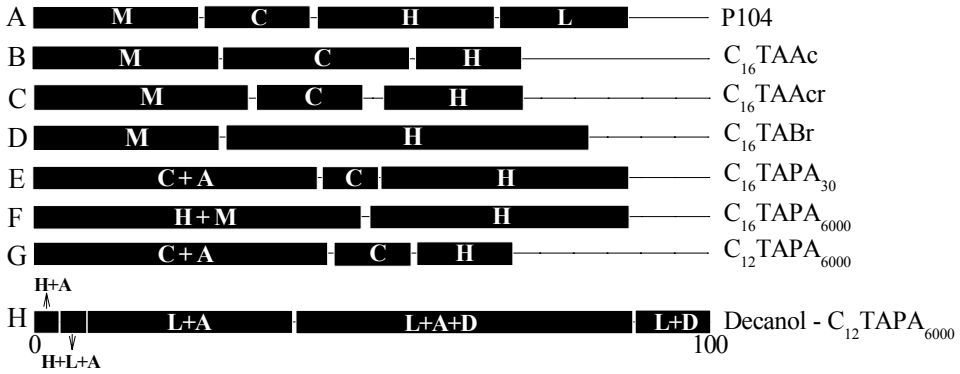

Figure 5 – The scale of the axis goes from 0 to 100 wt% for the respective compound in water. H shows the concentration of decanol. **A** – water phase, **M** – micellar, **C** – micellar cubic, **H** – hexagonal, **L** – lamellar and **D** – decanol.

Concentration

Concentration effects are apparent in the majority of the binary systems listed in Figure 5. In the top of the figure the phase sequence for P104/water binary mixtures is illustrated. The poloxamer P104 is composed of x=27 ethylene oxide (EO) units in each of the poly(ethylene oxide) blocks and y=61 propylene oxide (PO) units in the middle poly(propylene oxide) block (see scheme in Figure 1D). P104 in water presents a very rich phase behaviour: at low concentrations there is a micellar phase, then at intermediate concentrations a micellar cubic phase of *FCC* type emerges and at higher poloxamer concentrations the hexagonal and lamellar phases are found.

Examples of surfactant/water binary systems for the cetyltrymethylammonium cationic surfactant ion with the negative organic counterions acetate (Ac) and acrylate (Acr), C_{16}TAAc and C_{16}TAAcr, respectively, are shown in Figures 5B and C. These systems present a micellar phase for low concentrations, a cubic phase of the *Pm*3*n* symmetry, for intermediate concentrations and for the highest surfactant concentration shown they exhibit a hexagonal phase. These two counterions are chemically very similar and indeed the surfactant/water binary mixtures give the same phase sequence.

When the concentration is increased, the surfactant parameter does not change very much when moving from micellar to cubic structure, hence the micelles pack into a cubic arrangement. At a certain concentration surfactant molecules cannot be accommodated in the micelles unless they deform. When this happens the micelles grow in one dimension forming long-cylinder shaped aggregates, with a subsequent decrease of the aggregate curvature. The cylinders pack in a hexagonal arrangement. At higher concentrations, the surfactant aggregates must grow in one

other dimension to accommodate more surfactant molecules, hence they rearrange into lamellae (planar bilayers).

Counterion

The type of counterion to the surfactant ion might affect the phase behaviour. Strongly bound counterions decrease the repulsion between the charged head groups, resulting in a smaller head group size. Consequently, the micelles grow and become non-spherical at high concentrations. One example of this change of phase behaviour is given in Figure 5D for the cetyltrimethylammonium bromide, C_{16}TABr, in water. It shows a transition from micellar phase directly into a hexagonal phase, without an intervening cubic phase.

Theoretical and experimental studies have shown that the increase of the counterion valency gives rise to an additional attraction between the aggregates[34-38]. When a monovalent counterion is replaced by a polyion, the polyion gives rise to an attraction between the surfactant aggregates and even at very low surfactant concentrations, polyion-surfactant ion complexes separate out from water. The polyion-surfactant ion concentrated phase often has a long-range ordered structure. Figures 5E and F show two results for the systems with polymeric counterions, poly(acrylates), PA^-, with a degree of polymerization of 30 and 6000.

Chain length

The long chain surfactant has a higher propensity to form elongated aggregates when compared to a shorter chain surfactant, due to its lower surfactant parameter. This is shown in Figure 5G, for the PA^- with 6000 repeating units, which should be compared with Figure 5F.

Co-surfactant

Another way of changing the curvature of the surfactant aggregates is to add a so-called co-surfactant, normally an alcohol. Fontell et al showed that adding decanol to C_{16}TABr or $(C_{16}TA)_2SO_4$ aggregates in water caused the surfactant aggregates to change to a lamellar structure[39]. The small head group of the alcohol situates at the surface and decreases the average head group area of the surfactant + co-surfactant mixture, thereby increasing the surfactant number. The curvature is decreased and the sequence cubic→hexagonal→lamellar can be obtained increasing the alcohol content (see Figure 6). Figure 5H shows the phase sequence for the complex $C_{12}TAPA_{6000}$ with increasing concentration of decanol[40].

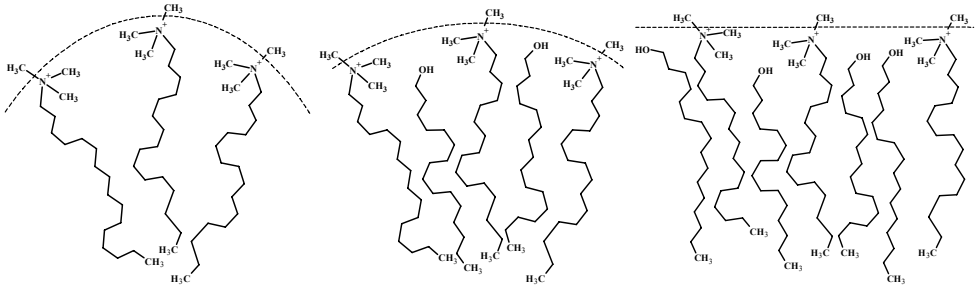

Figure 6 – Scheme showing the decrease in curvature and the transition from micelles to rods and planes, as the content of the alcohol is increased.

Ternary mixtures

Associative phase behaviour

When two polymers (P_2, P_3) or a polymer (P_2) and a surfactant (S_3) are mixed in water the compositions of the mixtures can be presented in a ternary phase diagram (Gibbs triangle) as the one shown in Figure 7. The sides of the triangle represent the three binary mixtures while the inside represents the ternary mixtures. Due the small contribution of the translational entropy of mixing for polymers and surfactant aggregates, their mixtures have a strong propensity to phase separate. Therefore when there is an attractive interaction between the polymers or the polymer and the surfactant, they associate and it is common to encounter a so-called associative phase separation (2ϕ region; in this context ϕ=phase) for the water-rich mixtures close to the water corner[16]. The mixture separates into two phases. (Water is represented by **W** here and in the next sections.) Typical features of an associative behaviour are depicted in Figure 7.

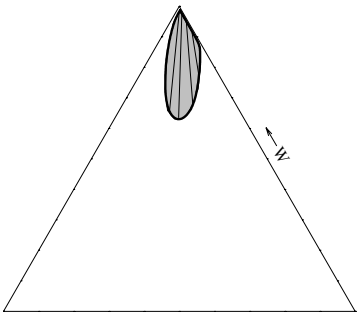

Figure 7 – Typical features of the phase diagram for an associative behaviour. Shadow – 2ϕ region.

In the associative phase separation, the 2ϕ region is anchored in the water corner of the ternary phase diagram and has the shape of a drop, which can be more or less symmetric in relation to the bisector of the water corner. The tie-lines, connecting the equilibrium compositions of the co-existing phases in the 2ϕ region, run from the water corner to the opposite side of the loop, showing that one phase is very dilute and the other is mostly constituted of the complexed molecules. Outside the 2ϕ drop one finds a 1ϕ region, meaning that the mixture of the two associating components can lead to the formation of soluble or insoluble complexes depending on the composition or ratio between the mixed components.

This association is quite general for oppositely charged mixtures, but can also be found for non-ionic mixtures. The size of the phase separation region increases with an increase of polymer molecular weight, alkyl chain length of the surfactant or charge density of the polyelectrolyte[42] and it decreases for instance with addition of salt, which screens the electrostatic interactions. For certain non-ionic systems, the extension of the phase separation region can also be strongly affected by temperature. An associative phase separation is favoured by a decreased hydrophilicity of one or both of the solutes[41].

Flory-Huggins Theory for three-component systems

The reason for the analogy in the phase behaviour between aqueous polymer-polymer and polymer-surfactant systems comes from the fact that the translational entropy of mixing is small for both the micellar and the polymer solution and that the phase behaviour is strongly influenced by the enthalpic effect.

The phase behaviour of ternary polymer-polymer-water or polymer-surfactant-water systems can be understood in the context of simple lattice Flory-Huggins theory for polymer mixtures. The Flory-Huggins theory can be extended to three components[43]:

$$\Delta \boldsymbol{G}_{mix} = kT(N_1 + r_2N_2 + r_3N_3)[\phi_1 \ln\phi_1 + (\phi_2/r_2)\ln\phi_2 + (\phi_3/r_3)\ln\phi_3 + \chi_{12}\phi_1\phi_2 + \chi_{13}\phi_1\phi_3 + \chi_{23}\phi_2\phi_3] \qquad (4)$$

where the subscript 3 refers to the second polymer or the surfactant.

Polymer-polymer systems

Non-ionic mixtures

Associative aqueous polymer-polymer or polymer-surfactant non-ionic mixtures have not received much attention with respect to detailed phase studies. Generally the mixtures were restricted to dilute regime. For instance poly(acrylic acid), PAA, poly(methyl methacrylic

acid), PMMA, and other polymers containing acrylic acid have been mixed with other non-ionic polymers such as polyethylene oxide (PEO), polypropylene oxide (PPO), poloxamers or non-ionic conventional surfactants[44-52]. In many of these studies, a macroscopic phase separation was seen. Saito concluded that complexation between PAA and PPO was weak compared to PMMA-PPO complexation[53] and Costa et al. inferred that PAA preferred to reside in the PEO corona of the poloxamer P123 micelles rather than in the PPO core[52]. At the other concentration extreme, there is recent work on PAA and poloxamers blends[54,55].

Associative mixtures of poloxamers and polymerized silica are used to prepare mesoporous silica materials because in dilute solutions of poloxamers, the poloxamer molecules remain aggregated and they separate out from solution, together with the polymerized silica in the form of a liquid crystalline structure[11,56,57]. This suggests a preference of the polymerized silica for the PEO blocks, compared to the PPO blocks. It is interesting to note that it was found for some systems that silica hydrophobic silica precursor (tetramethoxy orthosilane) initially penetrates into the PPO core of the poloxamer micelles, but the polymerized silica network partitions to the PEO corona[58].

In this Thesis, the aqueous phase behaviour for systems containing PAA of different lengths, *m* = 6000, 25 and 1 (*m* represents the number of repeating units or degree of polymerization, 1 corresponds to the repeating unit, propionic acid, PrA), and the poloxamer P104 was studied. As seen from the overview above, it is known that PAA interacts associatively with poloxamers in water, however the studies are restricted to the dilute regime. P104/water binary system presents a variety of structures, as can be seen in Figure 5A. This study bridges the studies in dilute regimes to the study in PAA-poloxamer blends of Watkins et al[54,55]. The obtained ternary phase diagrams are depicted in Figure 8.

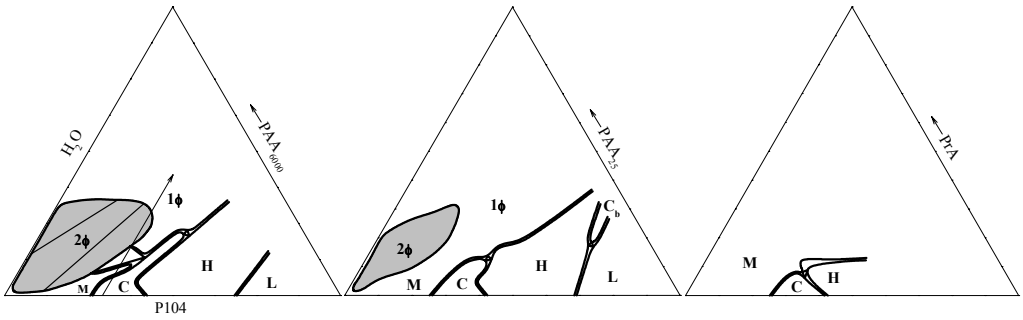

Figure 8 – Experimental P104/H_2O/PAA(PrA) phase diagrams.

The main observations/conclusions from this study are listed below.

→ Replacement of water by PAA (>10wt%) destroys the poloxamer self-assembly and thus the liquid crystalline phases giving place to disordered liquids or stiff gels. The decrease in PAA length, in the PAA_{6000} – PAA_{25} – PrA sequence, increased the efficiency to destroy the structured phases. PAA acts as a less "selective" solvent, for the PPO and PEO blocks, than water.

→ At low and intermediate concentrations of P104, an associative phase separation was found, appearing in a closed droplet-shaped miscibility gap with tie-lines confirming the association. This phase behaviour is similar to the one shown in Figure 7. The different 1ϕ regions are seen for all the compositions outside the miscibility gap.

→ Within the miscibility gap, none of the two phases in equilibrium showed long-range order. Here the self-assembly of the poloxamer, which occurs in water is largely irrelevant for the associative phase separation which involves individual poloxamer chains rather than aggregates of chains.

→ The phase separation was larger for the longer PAA and non-existing for PrA.

→ There was an asymmetry in relation to the water corner bisector in the sense that even very small additions of P104 to PAA solutions resulted in phase separation, whereas a significant amount of PAA could be added to P104 solutions before phase separation.

→ Similarities between this study and the study of Galatanu et al[59] on PAA mixed with a common non-ionic surfactant, Triton X-100, were found. An associative phase separation was observed at low concentration of PAA and Triton X-100 and, at higher overall concentrations, a variety of single-phase regions of different liquid crystalline or disordered structures was found.

Oppositely charged mixtures

Oppositely charged polyelectrolyte mixtures have been studied and some detailed phase studies have been performed to understand the role of molecular weight, charge density, chemical structure and ionic strength in phase behaviour and rheological properties[60,61].

When two neutral salts, for instance two polyions of opposite charges (P_2^- and P_3^+) with their respective counterions (A^+ and A^-), are mixed, the dissociation of the counterions and the different alternatives to combine the charged species into net neutral (mixed) salts turns the mixture into a 4-component system. Contrary to the non-ionic systems, presented above, for oppositely charged systems the classical triangular representation is generally not correct when 5 species are mixed. The Gibbs phase rule states that $f=c-p$, when pressure and temperature are fixed. f is the number of degrees of freedom, p is the number of phases in the system and c the

number of components. Due to the electroneutrality constraint all ionic species are independent but one. The latter constraint turns the system in a 4-component system, which has to be correctly described by a 3D figure and not a 2D triangle (since each one-phase region has three degrees of freedom in the compositional variables) (Figure 9).[62] Typically, the phase behaviours of two oppositely charged species have been represented by the so-called conventional mixing plane ($A^+P_2^-/P_3^+A^-/W$). In Figure 9 a hypothetical associative phase separation region (similar to Figure 7) is drawn in the conventional mixing plane. Again the associative interaction between the oppositely charged polyions leads to the formation of a concentrated phase enriched in the polyions and a dilute phase which in this case is enriched in the simple counterions. In Figure 9, there are two hypothetical tie-lines which pass through the two different phase-separating mixtures. In this hypothetical scenario, the tie-lines do not fall in the same plane; generally the separating phases are not restricted to the conventional mixing plane. The dilute phase has the composition corresponding to the location of the end of the tie-line closer to the water corner and the concentrated phase has a composition corresponding to the location of the opposite end (farthest from the water corner). Due to the difficulties in representing the mixtures in the 3D phase diagram, triangular representations are preferred in general. Often, for the sake of correctness, the mixtures of oppositely charged species are presented in the so-called phase maps rather than in phase diagrams. Each mixture is placed in the map accordingly to the number of phases that it presents. When experimental tie-lines are shown in the phase maps they are generally projections of the real tie-lines.

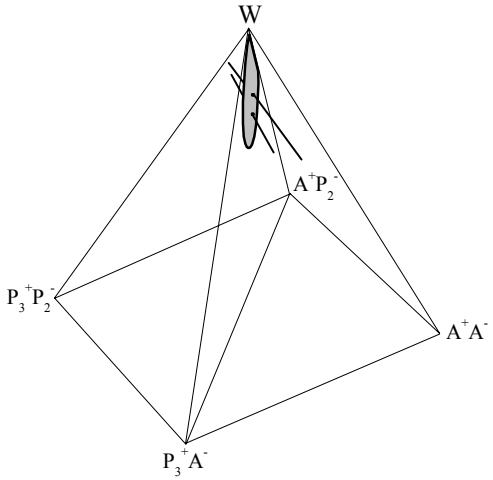

Figure 9 – 4-component system represented by a pyramidal phase diagram with an associative phase separation in the $A^+P_2^-/P_3^+A^-/W$ plane. The tie-lines are shown as straight lines passing through the mixing plane.

It is indeed possible to observe that oppositely polyion-polyion complexes do not separate out of the solution only at charge equivalence; mixtures of oppositely charged polyelectrolytes can show a pronounced asymmetry in relation to the charge equivalence. This asymmetry has its origin in some difference between the polyions other than the sign of the charge (a mixture of two polyions differing only in the sign of their charge must necessarily give rise to a symmetric phase diagram). For instance, a well established cause of asymmetry in phase behaviour in these systems is a pronounced difference in the number of charges per polyion[63].

The oppositely charged polyions interact mainly by Coulombic forces but if, for instance, the polyions contain hydrophobic moieties, hydrophobic interactions might play a major role and can modulate the thermodynamic phase behaviour, as reflected in the extent of the phase separation. When hydrophobic interactions are present, they are normally responsible for a decrease in extension of the phase separation. In some cases, due to the hydrophobic interactions, insoluble complexes only form in a narrow composition region (close to charge equivalence), largely reducing phase separation[60,61]. When both polyions are hydrophobically modified there is a tendency of the hydrophobic groups to associate and reside in one phase. When one of the polyions is in excess (charge-wise) in the mixture, the complexes acquire excess charge because the hydrophobes associate and the complexes redissolve (the mixtures go from two-phase to one-phase samples)[60,61,64,65]. The hydrophobic association can be the cause an asymmetry in the phase separation region in relation to the charge equivalence.

DNA is a widely studied polyion and it has been mixed with different oppositely charged polyions[66-70]. Some of the main ideas behind these studies are to understand the role of cationic molecules which interact with DNA using synthetic polycations as model molecules and to formulate DNA for gene therapy and drug delivery[66,69,70]. However, there are other more technological/methodological applications, such as immobilization of DNA onto solid supports, design of DNA-templated nano-materials, development of better strategies for DNA purification, etc[69]. From a fundamental point of view DNA is also a very interesting polyion; it is has a high charge density and a stiff chain (when it is in the double-stranded native form).

The previous studies of the oppositely charged polyelectrolyte mixtures containing DNA are often restricted to the dilute regime[67-69]. From all the studies involving DNA-polycation mixtures there are not many general similar conclusions that can be taken. In some systems, the associative phase separation occurs around charge equivalence, but below and above the charge equivalence soluble complexes exist[67,68]. Other mixtures show a more pronounced asymmetric phase behaviour[68].

In this thesis, single- and double-stranded DNA were mixed with dilute and semidilute solutions of cationic derivatives of cellulose, cat-HMHEC and cat-HEC (see Figure 1E and F).

(When these two polycations are referred to collectively, the notation cat-(HM)HEC is used). Phase behaviour and rheological properties of the off-stoichiometric homogenous mixtures were investigated. Figure 10 shows the phase behaviour of cat-HEC/DNA/H_2O system in two alternative ways, using either the equivalent charge concentration or the weight percent of the polyions as concentration units.

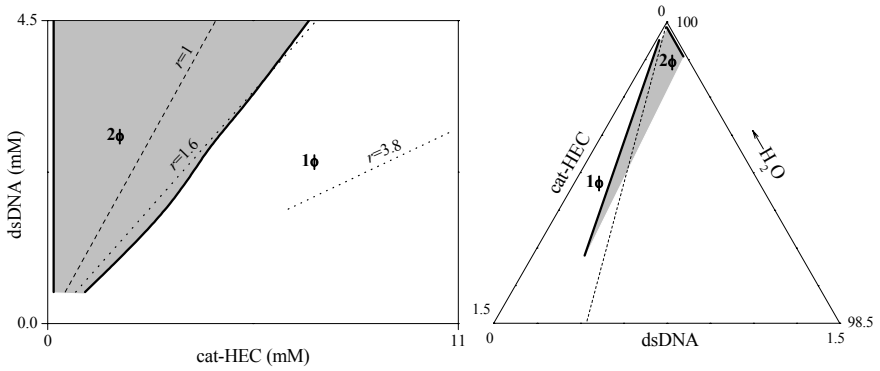

Figure 10 – Phase maps for cat-HEC/DNA/H_2O system. *r*=equivalent concentration of cat-(HM)HEC/equivalent concentration of DNA.

Some observations/conclusions from this study are listed below.

→ The associative phase separation was asymmetric: only minor additions of cat-(HM)HEC (both cat-HMHEC and cat-HEC) to DNA solutions lead to phase separation while mixtures dominated by the polycations did not phase separate on addition of DNA until some distinct global charge ratio of the mixture was reached.

→ Redissolution of the cat-(HM)HEC-DNA complexes (into a single homogeneous phase) occurred for a specific charge ratio (with modest excess of cationic polyelectrolyte) which was independent of the overall polyion concentration. The one-phase off-stoichiometric mixtures presented a viscoelastic character. The presence of DNA strengthened the viscoleastic behaviour of the cat-(HM)HEC solutions.

→ For the catHEC/dsDNA/H_2O system, the rheology showed a non-monotonic behaviour: the storage modulus, *G*', and the viscosity (both the complex viscosity, η^*, and the shear viscosity, η) showed pronounced maxima, roughly coinciding with a transition from bluish to clear samples, for all the series of samples where the cat-HEC concentration was increased at constant dsDNA concentration. (The rheological parameters are described in the Methods section at the end of this Thesis summary.)

→ Differences in the phase behaviour and rheology were observed, particularly between systems containing cat-HMHEC or cat-HEC, but also between dsDNA and ssDNA systems.

→ Similarities between these systems and the systems studied by Thuresson et al[60] for mixtures of cat-HMHEC with PA^- and $HMPA^-$ were found: a phase separation was observed over the most of the PA^- rich side of the mixing range and an efficient redissolution was obtained for a small charge excess. The replacement of PA^- by $HMPA^-$ led to an efficient redissolution on the $HMPA^-$ rich side. Owing to association of the hydrophobic groups cat-HMHEC and $HMPA^-$ molecules have the strong tendency to reside almost quantitatively in one and the same phase. In excess of cat-(HM)HEC or $HMPA^-$ the molecules partition strongly to the concentrated phase, associating into (mixed) hydrophobic aggregates. The overcharged concentrated phase swells, eventually it absorbs all the water and a 1ϕ mixture is formed.

Polymer-Surfactant systems

Early studies of polymer-surfactant systems were connected to the interest in the understanding of the interactions between surfactant and proteins or other biological polyelectrolytes, with the aim of investigating and understand the role and mechanisms of these macromolecules very abundant in the human body[71]. But the need to understand more about this topic drove the attention to synthetic systems which serve as models for the biological ones. The interest in these systems was further increased with the huge amount of applications that the systems find in the industrial world.

The fundamental feature of oppositely charged polymer-surfactant systems is the strong attraction between the charged polyions and the oppositely charged surfactant ion aggregates, both containing multiple charges leading to extensive association. Typically, a concentrated polyion-surfactant ion phase separates out when stoichiometric and neutral polyion-surfactant ion complexes are formed. However, certain off-stoichiometric mixtures produce 1ϕ solutions, whereas other remain phase separated at practically all mixing ratios.

Redissolution phenomenon by adding excess surfactant

Uncharged slightly hydrophobic polymers and charged polymers display important similarities in their interaction with ionic surfactants. In both cases, binding of the surfactant to the polymer chain can be observed, resulting in the formation of micelle-like clusters of surfactant molecules adsorbed to the polymer chain. The surfactant binding normally starts at a rather well-defined surfactant concentration, the so-called critical aggregation concentration (*CAC*), which is always lower than the *CMC* of the surfactant. The binding of the surfactant is

normally characterized by its marked cooperativity due to the hydrophobic interaction between the surfactant chains (the binding is actually a micelle formation at the surface of the polymer). Polyions associate strongly with oppositely charged surfactant ion aggregates due to the strong Coulombic attraction between the two multi-charged species. Phase separation often occurs, resulting in a concentrated phase enriched in polyions and surfactant ion aggregates in equilibrium with a dilute phase. When phase separation occurs, a dense "solid" or gel-like concentrated phase typically forms. In some systems, it is possible to bind a considerable amount of surfactant ions to the polyion before phase separation occurs[72]. There are other systems where phase separation occurs for a very low concentration of surfactant ions[73].

"Redissolution" of the concentrated phase, which occurs when non-stoichiometric complexes are redissolved into a single phase, is subject of very large interest. The redissolution can be accomplished by addition of excess surfactant or excess polyelectrolyte, but the mechanisms behind this phenomenon are not fully understood.

The focus in this Thesis in is on the redissolution phenomenon of polyion-surfactant ion complexes by adding excess surfactant.

The typical procedure to study this phenomenon is to fix the concentration of polyion (normally very low, <1 wt%) and then add surfactant stepwise. This corresponds to a line close to the surfactant/water binary axis in the phase map (conventional mixing plane) as shown in Figure 11. Another used procedure is to start with a macroscopic gel of crosslinked polyion which is immersed into a surfactant solution and observe what happens in terms of swelling behaviour. Note that in these studies the compositions of the concentrated phases that separate out are normally not determined.

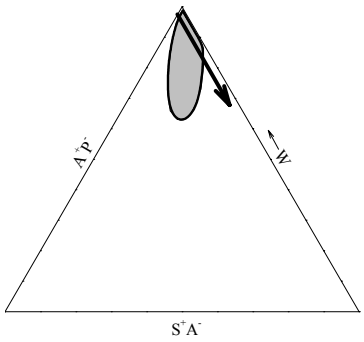

Figure 11 – Exemplification of composition line (thick arrow) used in redissolution studies in dilute systems.

As said above the surfactant starts to aggregate at the polymer backbone at the *CAC*. Macroscopic phase separation occurs at the *CAC* or slightly above depending on the polyion concentration and the characteristics of the system[74]. For the gel experiments the *CAC*

corresponds to a deswelling of the gel. When extra surfactant binds to the polyion above the charge equivalence, the complexes become overcharged. In some systems, a second cooperative binding of surfacatnt ions can occur at what is is called the *CAC*(2), which is sometimes referred to as the "hydrophobic" *CAC*, because cooperative binding happens due to a hydrophobic association of the excess surfactant ions to the neutral complex. This may lead to redissolution, and for the gel experiments the redissolution corresponds to the reswelling of the gel.

Goddard et al studied the complexation of cationic hydroxyethylcellulose (cat-HEC) and the oppositely charged NaDS[75,76]. Adding NaDS to cat-HEC resulted in precipitation at charge equivalence, followed by redissolution at excess surfactant. It was concluded that an overcharged polyion-surfactant complex had been created by hydrophobically bound excess surfactant. Note that it was observed that ionic surfactant binds to certain uncharged polymers, producing charged soluble complexes[77]. It was also found that it is more difficult to obtain redissolution if the charge density of the polyion was increased[78]. Precipitation and redissolution behaviour of cat-HEC/surfactant mixtures have also been studied by gel swelling experiments[79]. The collapsed gel (at charge equivalence) reswelled when excess surfactant was added to the solution. The reswelling was considered to be caused by the recharging of the complex due to hydrophobic binding of additional surfactant to the neutralized complex. The onset of the reswelling was sharp, and was identified as the *CAC*(2).

Gel swelling experiments were also performed for systems containing copolyions of acrylate with either isopropylacrylamide (NIPAM) or dimethylacrylamide (DAM) and it was shown that a sharp reswelling does not occur unless the co-polyion is hydrophobic enough[80,81]. Other studies with linear polymers clearly show that the hydrophobicity of the polyion is very important for the efficient redissolution of the polyion-surfactant ion complexes[9,10,82]. On the other hand, in some cases investigators of dilute mixtures have concluded that apparently redissolved complexes were, in reality, non-equilibrium dispersions of particles of the concentrated phase, stabilized by a surface covered with excess surfactant[83].

Different systems could in principle show different redissolution mechanisms. In conclusion, in some systems efficient redissolution occurs; however, there are other systems were efficient redissolution is not achieved by adding access of surfactant[73,84,85].

As exemplified above, a large amount of work in this field has been performed in very dilute polyion solutions (mixtures containing large amounts of water). More detailed phase studies have been performed in some multi-component polyelectrolyte-surfactant mixtures. For instance, in the studies performed by Thalberg et al, the NaPA/C_nTABr/H_2O (n=number of carbons in the alkyl chain) phase maps showed that a decrease of the alkyl chain length (from C_{14} to C_{10}) of the surfactant reduced the phase separation region in the phase diagram, keeping

the shape of the phase separation region and the slope of the tielines[86]. One of the explanations for this was the reduction of the aggregate size. Here the most significant reduction was when going to C_{10}. There was a difference from C_{14} to C_{12} but not huge. Note that with a shorten chain length, the aggregates formed are smaller and more numerous, and this originates higher entropy of mixing for the aggregates, which disfavors complexation. Also with shorter chain length there is a higher free surfactant (unimer) concentration (*CMC* is higher) and the electrolyte effect is stronger; this increases the solubility of the polyion-surfactant ion[86,87].

As it was explained before for multi-component systems, the tie-lines do not generally fall in the mixing plane and the full characterization of the separated phases involve a considerable amount of work. A few number of works have presented the fully characterization of the separated phases and the direction of the tie-lines in multi-component polyelectrolyte-surfactant systems[62,88,89]. Therefore, the study of the redissolution phenomenon by adding excess surfactant under multi-component conditions does not provide a clearest path for understanding, particularly because a varying level of simple salt is present in the separated phases screening more or less the interactions between polyion and surfactant ions.

From complex multi-component systems to simplified systems

To simplify the study of the phase behaviour, the number of components in the mixture can be reduced by synthesizing the pure "complex salt", that is, the pure salt resulting from the complexation of the polyion and surfactant ions (S^+P^-), and use this as one of the starting components. The complex salt can be then mixed with excess surfactant (S^+A^-). This mixture contains three components and thus represents a truly ternary mixture, corresponding to the $S^+P^-/S^+A^-/W$ face of the pyramid in Figure 9 (when P_2^+ is replaced by P and P_3^+ by S^+). This face of the pyramid is also called the surfactant ion mixing plane[87,90,91]. The schemes of the $NaPA/C_{16}TABr/H_2O$ phase map and the $C_{16}TAPA_{30}/C_{16}TABr/H_2O$ phase diagram are presented in Figure 12. The schemes are similar to the experimental phase diagrams in references 89 and 90. When comparing the phase map of $NaPA/C_{16}TABr/H_2O$ mixtures with the $C_{16}TAPA_{30}/C_{16}TABr/H_2O$ phase diagram, they both contain the same phases but the relation between the phases is not clearly illustrated. In the phase map in Figure 12A the hexagonal-micellar region has no connection with the hexagonal 1ϕ region. In the dilute part of the phase map, there is the appearance of the cubic phase. From the phase diagram we understand that this cubic phase is stable only when the mixture is composed of a concentrated phase containing essentially complex salt in equilibrium with almost pure water (compositions close to the complex salt/water binary axis in Figure 12B). In Figure 12B the connection between the hexagonal-micellar phase and the hexagonal 1ϕ region is observed.

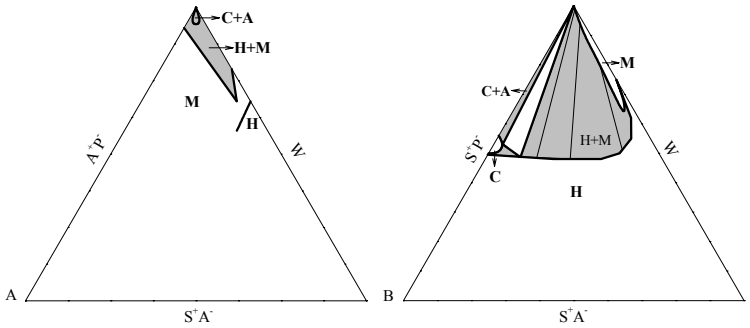

Figure 12 – $A^+P^-/S^+A^-/W$ phase map (A) and $S^+P^-/S^+A^-/W$ phase diagram (B). The figures are schematic reproductions from references 89 and 90.

With a simplified system, a true redissolution has been encountered in a study where the complex salt cat-HECDS (DS=dodecylsulfate) was prepared and mixed with excess NaDS[92]. The phase diagram is reproduced in Figure 13A. The redissolution of the polyion-surfactant ion complexes occurs for 5-10wt% of excess NaDS and the formation of a micellar one-phase occurs. The latter phase covers the major part of the phase diagram, stretching from the surfactant/water binary axis to the concentrated regions of the complex salt/water binary axis. For the most dilute region (>98wt% of water) the phase boundary between the two-phase and the one-phase regions was roughly linear, implying that both the complex composition and the free surfactant concentration at the redissolution were constant.

A number of ternary mixtures of complex salts C_{16}TAPA (S^+P^-) with added C_{16}TAX (S^+A^-) (X refers to the surfactant counterion) surfactant have been established (see Figures 12B and 13B and C). The phase diagrams referring to complex salts with short (30 repeating units) or long (6000 repeating units) poly(acrylate) polyions, and two different simple surfactant counterions are all very different. Moreover, all three phase diagrams are quite different from the phase diagram of cat-HECDS with NaDS. An efficient surfactant redissolution of C_{16}TAPA by added C_{16}TAAc is observed when the PA^- chain is very short. However, if instead a very long PA^- chain is used in C_{16}TAPA, or if C_{16}TABr is used instead of C_{16}TAAc (Figures 13C and 12B, respectively), a wide two-phase region results, which extends practically all the way across the phase triangle with an almost constant low water content of the concentrated phase - even when the latter phase is dominated by the added surfactant. The general conclusion is that added excess surfactant may redissolve oppositely charged polyion-surfactant ion complexes more or less efficiently or not at all, depending on the system. The ability to understand and control this variation is of considerable interest.

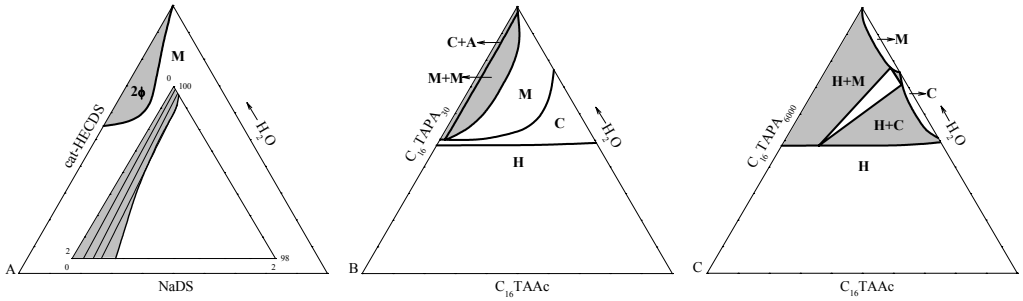

Figure 13 – Experimental cat-HECDS/NaDS/H_2O (A)[94],$C_{16}TAPA_{30}/C_{16}TAAc/H_2O$ (B) and $C_{16}TAPA_{6000}/C_{16}TAAc/H_2O$ (C) phase diagrams.[87,90]

The Flory-Huggins lattice model has been adopted to polyelectrolyte systems[93-95] and can be adopted here, to study the phase behaviour of these systems. The essence of this version of the Flory-Huggins theory, as applied to the present type of system, is to treat each of the solvent (W), the polyion (P^-), the surfactant ion aggregate (S^+), and the simple counterion of the surfactant (A^-) as a separate species, but with the additional constraint that each equilibrium phase in the mixture must be electroneutral. As in the real system, the latter constraint implies that the mixture of the four species considered is reduced to a three-component system. To incorporate the electroneutrality condition, each unit taken to occupy one lattice site (a polyion repeating unit, a surfactant ion, a simple ion or a water molecule) has a charge number. The Coulomb attraction between oppositely charged species is modelled by a strongly negative Flory-Huggins χ parameter. The essential features that the model captures are thus the strong attraction between oppositely charged species, the electroneutrality condition and the change in the translational entropy of mixing that accompanies a change of the degree of polymerization of an ionic species.

In this Thesis, the redissolution phenomenon was investigated systematically by experimental and theoretical phase equilibrium studies. Complex salts with linear polyions (C_nTAPA_m) and copolyions (C_nTA-co-NIPAM/DAM) were mixed with excess surfactants with different akyl chain lengths and different counterions. Flory-Huggins calculations were carried out to obtain further insight into the studied experimental systems.

The main observations/conclusions of this study were:

→ A large excess of small spherical micellar aggregates with simple counterions is not sufficient to redissolve complexes containing homopolyions. The ternary system with $C_{12}TAPA_{6000}/C_{12}TAAc/H_2O$ (Figure 14A) does not show a decrease of the phase separation region (miscibility gap) compared to the $C_{16}TAPA_{6000}/C_{16}TAAc/H_2O$ system (Figure 13C). The tie-lines for $C_{12}TAPA_{6000}/C_{12}TAAc/H_2O$ system show that the

distribution of the surfactant between the phases is almost equal; extra added micelles (as the surfactant concentration is increased) simply distribute equally between the phases. A large excess of surfactant in the concentrated phase is not sufficient to cause redissolution of the complex.

→ Redissolution of polyion-surfactant ion complexes containing poly(acrylate) is much more efficient when the homopolyion is short (Figure 14B). $C_{12}TAPA_{25}/C_{12}TAAc/H_2O$ system shows approximately the same features as the $C_{16}TAPA_{30}/C_{16}TAAc/H_2O$ system (Figure 13B).

→ Introducing a large fraction of uncharged slightly hydrophobic DAM or NIPAM comonomers into the poly(acrylate) chains makes the surfactant redissolution much more efficient even for long copolyion chains (Figure 14C – for the co-polyion containing 82 mol% of NIPAM). The efficient redissolution is explained by the formation of soluble polyion-surfactant ion complexes carrying an excess of surfactant ions through an additional hydrophobic attraction.

→ Acetate, rather than bromide, counterion makes the cationic surfactant more potent to redissolve the complex salt, in agreement with Figures 12B and 13B; bromide counterions are known to bind strongly to C_nTA^+.

→ A simple mean-field Flory-Huggins theory predicts the correct phase behaviour found for the complexes with long homopolyions (Figure 15A). The Flory-Huggins theory also predicts an increased tendency for surfactant redissolution when the complex salt contains very short polyions (Figure 15B) and it captures the effect of an additional attraction between the simple anion and the surfactant ion aggregate (Figure 15C), which corresponds to the experimental phase diagram presented in Figure 12B).

→ The agreement between the model and the experimental phase diagrams for the homopolyions suggests that the details of the polyions and surfactant aggregates do not need to be taken into account to explain the main entropy-enthalpy balance underlying the phase separation phenomenon and it shows that the entropy of the counterions is very important.

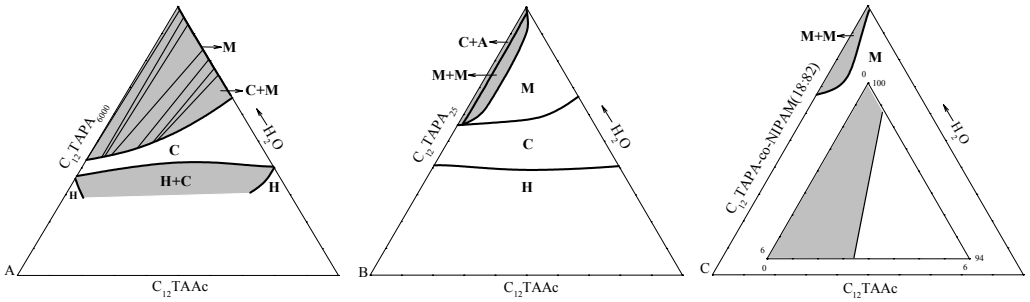

Figure 14 – Experimental $C_{12}TAPA_{6000}/C_{12}TAAc/H_2O$ (A), $C_{12}TAPA_{25}/C_{12}TAAc/H_2O$ (B) and $C_{12}TAPA$-co-NIPAM(18:82)/$C_{12}TAAc/H_2O$ (C) phase diagrams.

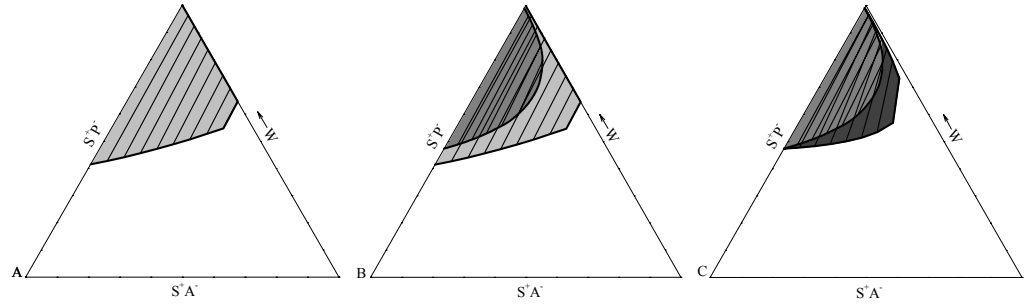

Figure 15 – Calculated phase diagrams using the Flory-Huggins model. A – long homopolyions, B – going from long (lighter) to short (darker) homopolyions and C – going from a less bound (lighter) to a strongly bound (darker) surfactant counterion.

Templating of ordered surfactant structures

In the studies shown above, the discussion did not focus on the structures presented in the systems but only on the redissolution of insoluble polyion-surfactant ion complexes regardless of their structure. Now the main focus will be the structure.

The concentrated ordered phases formed by surfactants or poloxamers are very interesting to be used as templates or "structure directing agents" for creation of the so-called mesoporous ordered materials. A common procedure for producing mesoporous materials is that the monomer or polymer precursor is mixed with the surfactant, either in a dilute the micellar phase[96] or in organized concentrated phases[97] and the polymerization reactions create a polymer around the surfactant aggregates which become embedded in a polymer matrix. After the reaction is finished the surfactant template can be removed from the mixture and mesoporous materials are created. In case of direct or "true" templating , the templated material is a copy of the template structure, and no changes in order or length scale of the template structure occur[98].

Several different approaches have been taken using many kinds of polymerizable surfactants or just polymerizing some kind of water- or oil-soluble monomer in the organized surfactant

systems. Both organic and inorganic polymers have been used. What comes out from the polymerizations is not always the desired product/result. Sometimes, the structures resulting from the reactions are different from the original template structure. One reason for such changes is that when a polymer is formed in an original concentrated surfactant phase it can be excluded from the space in between the aggregates due to so-called depletion forces, if no attractive interactions keep the polymer and the surfactant together.[98]

Silicate-surfactant/silicate-poloxamer aggregates are precursors for the synthesis of mesoporous materials. The most common procedure to produce inorganic mesoporous materials is to use mixtures containing large amounts of water. The synthesis of the materials involves the mixing of the silica precursor with a dilute micellar solution of surfactant/poloxamer aggregates and the polymerization at different temperatures in basic or acid media. An attractive interaction between the silica oligomer/polymer which is formed by silicate condensation and the surfactant/poloxamer aggregates drives the system towards an associative phase separation, resulting in the formation of concentrated phase with a long-range ordered structure. Removal of the surfactant by calcination results in an ordered mesoporous silica material. In the silica material the polymer is not linear but is extensively crosslinked. The curvature of the resulting structures depends on the ratio between surfactant and inorganic material, the strength of the interaction between the silica polymer and the aggregates, the ionic strength, the presence of simple ions and the chemistry of these, the temperature of the synthesis reaction and the presence of non-polar additives[96].

The interaction between the different components (surfactant/poloxamer aggregates and formed polymers) in the system should be attractive in order to create long-range ordered structures containing both polymer and surfactant[99]. After this description, it is obvious that there are similarities between the equilibrium polymer-surfactant phase diagrams, described in the earlier section and silicate-surfactant systems. Indeed, complex salts also separate out from water forming concentrated long-range ordered phases.

Difficulties in making mesoporous soft materials

Most of the nano-structured materials (nano-particles or meso- and microporous) produced via templating are inorganic. The the use of organic (soft) templates to produce organic (soft) mesoporous materials is much more restricted. One reason for this restriction is that organic polymer chains can generally adjust their shape to pack more efficiently and maximize the intermolecular interactions; porous and structural details are not normally thermodynamic favourable, and pores can close. Therefore the maintenance of the mesopores in an organic material normally requires a stiff and highly cross-linked polymer network.[98] Nevertheless it is very attractive to produce nano-structured soft materials. However, most approaches to

polymerization reactions in soft systems so far seem to have been based on trial and error and most of the resulting structures have often been different from the original surfactant template[100,101].

Phase diagrams come alive

There is another way to view the phase diagrams showed earlier for the $C_nTAPA_m/C_nTAAc/H_2O$ systems: These equilibrium phase diagrams illustrate what happens when simple monomeric counterions to the surfactant (Ac) are partially or completely replaced by polymeric counterions (PA^-_m). This is shown as an example by the arrows in the phase diagrams in Figure 16. This replacement process is a process that closely resembles a polymerization reaction and the phase diagrams can therefore serve as guidelines for polymerization reactions. In the phase diagrams showed in Figure 16 the arrows show different polymerization cases.

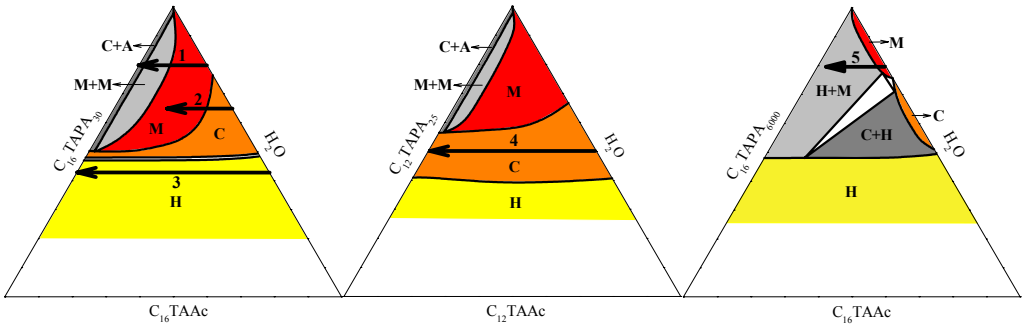

Figure 16 – $C_{16}TAPA_{30}/C_{16}TAAc/H_2O$, $C_{12}TAPA_{35}/C_{16}TAAc/H_2O$ and $C_{16}TAPA_{6000}/C_{16}TAAc/H_2O$ phase diagrams illustrating (arrows) predicted results of polymerization reactions (cases 1-5).

In this Thesis, polymerization reactions were performed in systems of minimum complexity by the use of akyltrimethylammonium surfactants with polymerizable acrylate counterions (one example is shown in Figure 2B). Therefore, the synthesis was done under conditions where the surfactant aggregates were the sole counterions to the growing polyion chains. C_nTAAcr was used instead of C_nTAAc and different polymerization reactions, under different conditions, such as different monomer-to-initiator ratio and different concentrations, were performed.

Some of the observations/conclusions from this study are listed below.

→ The outcome from polymerization reactions agreed with the predictions from the equilibrium phase diagrams. The polymerization of the counterions in a disordered micellar solution results in the formation of a concentrated, ordered cubic phase, containing polyions and the surfactant aggregates with essentially pure water (case 1). A partial polymerization of the counterions in an originally cubic phase results in a change of

the system to a viscous disordered micellar solution (case 2). It is possible to polymerize the counterions of an originally cubic or hexagonal phase without changing the structure (case 3 and 4, respectively). Increasing the molecular weight of the polyion in the $C_{16}TA^+$ system leads to a hexagonal phase instead of a cubic phase separating out from the originally micellar phase (case 5). Thus, the phase diagrams "come alive" as the systems evolve through the polymerization reactions.

→ The synthesized polymer is not excluded from the surfactant phase but rather aids in the formation of long-range order.

→ The conditions to create, destroy or change ordered structure through polymerization reactions were established for the studied systems.

→ The polymerization reactions in these organic systems agree, indeed, with trends seen for the silica-surfactant systems.

Structural changes through the degradation of the surfactant molecule

The addition of decanol to complex salts of the $C_{12}TAPA_m$ type (m=30 or 6000) was investigated previously by Bernardes et al[40]. The phase behaviour for the $C_{12}TAPA_{6000}$/Decanol/H_2O system in the decanol dilution line (adding decanol) was presented in Figure 5H.

Along the decanol dilution line, the effects caused by the incorporation of oil into the surfactant aggregates can be followed. The complex salt/water binary mixture presents a 2ϕ system of a concentrated phase with the micellar cubic structure in equilibrium with excess water. The addition of alcohol changes the shape and size of the surfactant aggregates; the general feature is that oil favors the development of structures with reduced curvature (hexagonal or lamellar). Note that a small amount (<2wt%) of decanol changes the structure of the concentrated phase into hexagonal.

Recently, nano-particles formed by poly(acrylate) and alkyltrimethylammonium surfactant ions at low concentrations were investigated[14]. These nano-particles, observed by means of cryo-transmission electron microscopy (cryo-TEM) presented a long-range ordered structure. The studied systems by Nizri et al involved the mixture of NaPA and C_nTABr (n=8,10,12,14 or 16).[14]

Long-chain betaine esters are surfactants as the one shown earlier in Figure 2C. The hydrolysis of the betaine esters shows a rather dramatic pH dependence and these esters are much more prone to alkaline hydrolysis than esters in general[102,103]. The alkaline hydrolysis of the ester group of a surfactant molecule, such as the one shown in Figure 17, starts by the nucleophilic attack by hydroxyl ions to the ester carbonyl carbon, producing an alcohol and a betaine. The reaction produces protons that lower the pH of the reaction medium.

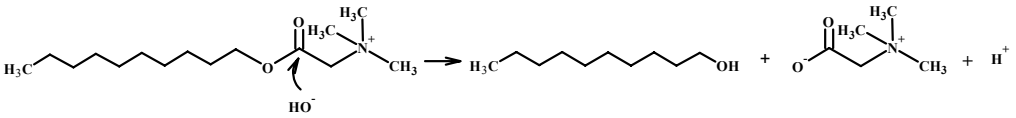

Figure 17 – Base-catalyzed hydrolysis of decyl betainate, DeB, into decanol and betaine.

In this thesis, the change in curvature of the structures of the concentrated polyion-surfactant ion phases (possibly containing small counterions) or of nano-particles were produced *in situ* by the hydrolysis of DeB. The studied mixtures are, thus, responsive and evolving systems. DeB was used either as the only surfactant or together with a stable surfactant, dodecyltrimethylammonium chloride C_{12}TACl (referred to as DoTAC), in mixtures with the anionic polyelectrolyte. Introduction of DoTAC was done in order to control the maximum amount of alcohol formed. Three different systems were studied: mixtures containing the titratable PA^- polyion (both NaPA or PAA), DeB and DoTAC, and mixtures of DeB, DoTAC and the non-titratable NaPSS (see Figure 1C).

The main observations/conclusions are listed below.

→ The mixtures containing NaPA, DeB and DoTAC are "self-degrading" mixtures due to the fact that the pH of the mixture immediately after mixing is ~8, and no addition of base is needed to start the reaction. The mixtures are also "self-quenching" because the decrease in pH as the reaction evolves makes the reaction stop by itself. A change in structure of the polyion-surfactant ion concentrated phases was observed, going from cubic to hexagonal and to lamellar when the amount of DeB was increased in the mixture.

→ For the most dilute samples of NaPA and DeB, where polyion-surfactant ion nano-particles were observed, these evolved into multi-lamellar "onion-like" particles with a size distribution of 30-80 nm were obtained when the samples were left untouched for 17 days (see cryo-TEM images in Figure 18).

→ For the mixture containing NaPSS, DeB and DoTAC, the concentrated polyion-surfactant ion phase containing no long-range order was exposed to NaOH solution and the degradation of DeB produced a polyion-surfactant ion concentrated phase with a hexagonal structure.

→ The hexagonal structure obtained for the mixtures containing NaPSS, DeB and DoTAC presented a dramatic swelling when washed with large amounts of water for the samples containing the highest amounts of DeB in the starting mixture.

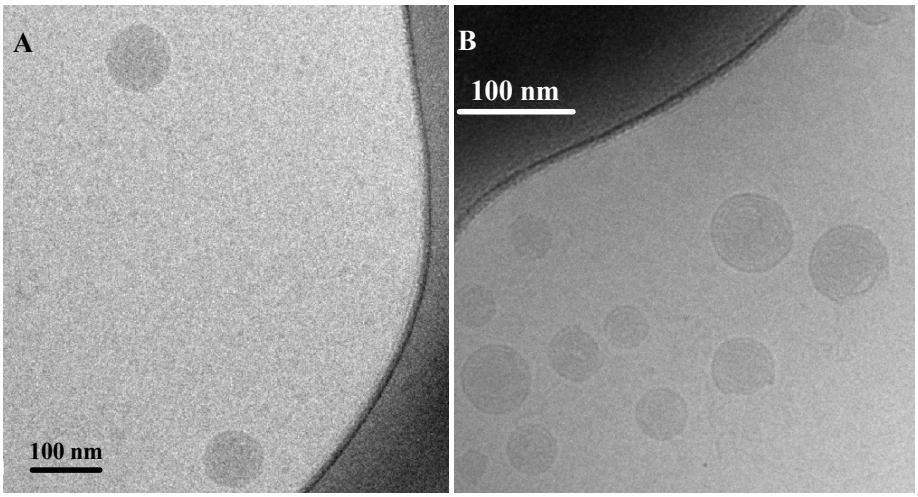

Figure 18 – Cryo-TEM images for two mixtures of 10 mM NaPA and 5 mM DeB, one freshly mixed (A) and one 17 days old (B).

Advanced methods

SAXS

The structures in the liquid crystalline phases were identified by small angle X-ray scattering (SAXS).

The phenomenon of diffraction is the interference caused by objects in the path of electromagnetic waves. In the case of SAXS, the incoming waves interact with the electrons in the sample. From both crystals and liquid crystals, which have long-range structural order, characteristic diffraction patterns, which reveal the crystal symmetry, can be obtained. The crystal can be modeled as stacks of reflecting lattice planes separated by a distance d. When the diffraction angle satisfies Bragg's law, $n\lambda=2d\sin\theta$, constructive interferences give rise to peaks in the SAXS profile; n is an integer, λ is the wavelength and θ the diffraction angle. SAXS peaks are normally referred to as reflections. The SAXS profile is normally presented as intensity (a.u) as a function of the scattering vector, q, $q=n(2\pi/d)$, which relates to θ by $q=(4\pi/\lambda)\sin(\theta/2)$. SAXS measurements give structural information in the size range from 10-1000 Å. SAXS profiles reflect the organization and the electron density of the sample. High organization and high electronic density result in higher intensity and higher number of observed reflections. From the scattering profiles it is possible to identify the structure and obtain values for distances, sizes, and aggregation numbers. The unit cell is the smallest repeating unit of a crystalline structure. There are an infinite number of ways to divide the crystal into planes. The Miller indices, h, k and l denote the number of parallel planes that intersect with each unit axis and are therefore used to define the lattice planes in the crystal. For a cubic structure, the unit cell size, α_{cub}, is calculated by

$$\alpha_{cub} = (2\pi/q)(h^2 + k^2 + l^2)^{1/2} \qquad (5)$$

For the hexagonal structure the order is in 2D and the distance between the centers of two rods, d_{hex}, is given by

$$d_{hex} = (2/(3)^{1/2})(2\pi/q_1) \qquad (6)$$

For lamellar structure the order is in 1D and the distance between equivalent planes in neighbouring lamellae, d_{lam}, is simply

$$d_{lam} = 2\pi/q_1 \qquad (7)$$

q_1 is the scattering vector of the first reflection in the profile.

SEC-MALLS

The molecular weight of the synthesized polymers was determined by size exclusion chromatography coupled with a multi-angle laser light scattering instrument (SEC-MALLS).

The SEC column set is used to separate the polymer molecules according to size. After leaving the column, the molecules flow past a light scattering detector (using one or more angles) and then to a concentration detector. The usual choice for the concentration detector is a differential refractive index instrument (RI). Using this method, absolute molecular weights can be obtained.

The relationship between the experimental data and the molecular parameters of the system is described by Equation 8[104].

$$R_\theta/Kc = M_w P(\theta) - 2A_2 c M_w^2 P^2(\theta) \qquad (8)$$

The excess Rayleigh ratio, R_θ, which describes the scattering after the contribution of the pure solvent is subtracted, is the light scattered by the pure solution at an angle θ in excess of that scattered by the pure solvent, divided by the incident light intensity. c is the molecular concentration, M_w the weight average molar mass, A_2 is the second virial coefficient (related to polymer-solvent interactions in the system), and K is an optical constant that contains the refractive index increment, dn/dc. $P(\theta)$ is the form factor which describes the scattered light's angular dependence ($P(\theta) \sim \sin^2(\theta/2)$). It is possible to solve Equation 8 in a variety of ways, leading to a number of different fit methods (Debye, Zimm, Bery and Random Coil methods). In the Debye fit method (used in this Thesis), first a Debye plot, R_θ/Kc versus $\sin^2(\theta/2)$, is constructed. Second, a polynomial in $\sin^2(\theta/2)$ is fitted to the data, thereby obtaining the intercept at zero angle, R_0/Kc. Note that as θ approaches zero, $P(\theta)$, approaches unity. Therefore Equation 8 becomes

$$R_{\theta \to 0}/Kc = R_0/Kc = M_w - 2A_2 c M_w^2 \qquad (9)$$

If A_2=0, then

$$M_w = R_0/Kc \qquad (10)$$

Otherwise

$$M_w = [2(1-(1-8A^2c(R_0/Kc))^{1/2})]/8A^2c \qquad (11)$$

The degree of polydispersity of the polymer chains is calculated from the relation between number and weight average molecular weights (M_w/M_n). $M_w=(\Sigma(c_i M_i))/\Sigma c_i$ and $M_n=(\Sigma c_i)/\Sigma(c_i/M_i)$, c_i and M_i are the weight concentration and the molar mass of the ith data slice.

Rheology

Rheology is a technique which gives information on deformability and/or flow properties of materials, elasticity, fluidity and viscosity. When an external pressure is exerted on a material (for instance a polymer-polymer mixture), the material responds to the action in different ways depending on its properties. The response varies according to the liquid or solid (elastic)

character of the material. Many polymeric materials are viscoelastic showing a combination of liquid-like and solid-like properties. Rheology is used in many industrial processes where control of viscosity, elasticity and/or fluidity is required and is an excellent technique for comparing between different materials.

The measurements performed can be linear (oscillatory) or non-linear (rotational). In linear measurements, a constant sinusoidal shear stress, σ, (at one or in an interval of frequencies, ω) is applied in alternating directions (oscillation) to the material, and the deformation (shear strain, γ) of the material is measured. Shear stress is defined as the force applied per unit area of the material. The deformation depends on both applied stress and frequency. In non-linear experiments a stress is applied to the material and viscosity of the material is measured. The first assumes no destruction of the sample and the second can destroy the physical arrangement of the sample.

In the oscillatory experiment, the solid-like response of the material is characterized by the storage modulus, G', which is in phase with the input shear stress.

$$G' = (\sigma_0/\gamma_0)\cos\delta \qquad (12)$$

σ_0 is the amplitude of the shear stress, γ_0 is the amplitude of the shear strain and δ is the phase angle between the shear stress and the shear strain. G' is a measure of the energy stored and recovered per cycle (stored elastic energy). It is dependent on the strength and number of entanglement connections in the material.

The liquid-like properties in the sample are obtained by the loss modulus, G'', which is 90º out of phase with the input shear stress.

$$G' = (\sigma_0/\gamma_0)\sin\delta \qquad (13)$$

G'' is a measure of the dissipated or lost energy, in the form of heat, per cycle of sinusoidal deformation.

When G' is higher than G'', the behaviour is predominantly elastic. For viscolelastic systems this happens at high frequencies whereas at low frequencies, G' is lower than G''. The intersection time (inverse of frequency) can be regarded as a relaxation time for the disengagement of the entanglements in the network of polymer chains, together with the G' reveal the relative strength of the entanglements.

The complex viscosity, η^*, is a combination of G' and G'':

$$\eta^* = (G' + G'')^{1/2}/\omega \qquad (14)$$

The shear viscosity, η, is obtained in non-linear experiments and is defined as the stress divided by the shear rate (defined as the change in shear strain with time) and measures the resistance of the material to flow.

Bibliography

1 *E. D. Goddard, R. B. Hannan and G. H. Matteson, J Colloids Interface Sci, 1977, 60, 214.*

2 *P. S. Leung and E. D. Goddard, Colloids Surf, 1985, 13, 47.*

3 *P. S. Leung and E. D. Goddard. Langmuir 1991, 7, 608.*

4 *B.-H. Lee, S. D. Christian, E. E. Tucker and J. F. Scamehorn, Langmuir, 1991, 7, 1332*

5 *B. Magny, I. Iliopoulos, R. Zana and R. Audebert, Langmuir 1994, 10, 3180.*

6 *I. Iliopoulos, Current Opinion Colloid Interf Sci 1998, 3, 493.*

7 *G. Decher, Science, 1997, 277, 1232.*

8 *Y. Hiwatari, K. Yoshida, T. Akutsu, M. Yabu and S. Iwai, Int J Cosmet Sci, 2004, 26, 316.*

9 *A. V. Svensson, L. Huang, E. Johnson, T. Nylander and Lennart Piculell, Appl Mater Interfaces, 2009, 11, 2431.*

10 *O. Santos, E. S. Johnson, T. Nylander, R. K. Panandiker, M. R. Sivik and L. Piculell, Langmuir, 2010, 26, 9357.*

11 *D. Y. Zhao, J. L. Feng, Q. S. Huo, N. Melosh, G. H. Fredrickson, B. F. Chmelka and G. D. Stucky, Science, 1998, 279, 548.*

12 *A. Thomas, F. Goettmann and M. Antonietti, Chem Matter, 2008, 20, 738.*

13 *G. Nizri, S. Magdassi, J. Schmidt, Y. Cohen and Y. Talmon, Langmuir, 2004, 20, 4380.*

14 *G. Nizri, A. Makarsky, S. Magdassi and Y. Talmon, Langmuir, 2009, 25, 1980.*

15 *P. Hössel, R. Dieing and R. Nörenberg, A. Pfau, R., Sander International Journal of Cosmetic Science, 2000, 22, 1-10.*

16 *Surfactants and Polymers in Aqueous Solution, K. Holmberg, B. Jönsson, B. Kronberg and B. Lindman, John Wiley & sons Ltd, 2003, pages 235-259.*

17 *A. Dualeh and C. A. Steiner, Macromolecules, 1990, 23, 251.*

18 *F. Guillemet and L. Piculell, J Phys Chem, 1995, 99, 9201.*

19 *K. Thuresson, S. Nilsson and B. Lindman, Langmuir, 1996, 12, 530.*

20 *K. Thuresson, B. Lindman and B. Nyström, J Phys Chem B 1997, 101, 6450.*

21 *L. Piculell, M. Egermayer and J. Sjöström, Langmuir, 2003, 19, 3643.*

22 *M. Karlberg, K. Thuresson, L. Piculell and B. Lindman, Colloids Surf A: Physicochem Eng Aspects, 2004, 236, 159.*

23 *Polymers: Chemistry & Physics of modern materials, J. M. G. Cowie, CRC Press, 1991, pages 52-58.*

24 *L. Piculell and B. Lindman, Adv Colloid Interface Sci, 1992, 41, 80.*

25 *The Colloidal Domain: Where Physics, chemistry, Biology and Technology meet, D. Fennell Evans and Håkan Wennerström, Ed.: Wiley-VCH, 1999.*

26 *Biochemistry, J. M. Berg, J. L. Tymoczko, L. Stryer, Ed.: W H Freeman and Company, 2002.*

27 *S. Dhoot, E. D. Goddard, D.S. Murphy and M. Tirrel, Colloids Surf, 1992, 66, 91.*

28 *K. Thuresson, S. Nilsson and B. Lindman, Langmuir, 1996, 12, 530.*

29*, Principles of Polymer Chemistry, P. J. Flory, Cornell University Press, Ithaca, 1953.*

30 *S. R. Kline, Langmuir, 1999, 15, 2726.*

31 *B. Lindman and H. Wennerström, Top. Curr. Chem., 1980, 87, 1.*

32 *G. Gunnarsson, B. Jönsson and H. Wennerström, J. Phys. Chem., 1980, 84, 3114.*

33 *K. Shinoda and E. Hutchinson, J Phys Chem, 1962, 66, 577-582.*

34 *L. Guldbrand, B. Jonsson, H Wennerström and P. Linse, J Chem Phys, 1984, 80, 2221.*

35 *P. Linse, V. Lobaskin, Phys Rev Lett, 1999, 83, 4208.*

36 *A. Svensson, L. Piculell, B. Cabane and P. Ilekti, J Phys Chem B, 2002, 106, 1013.*

37 *A. Svensson, J. Norrman and L. Piculell, J Phys Chem B, 2006, 110, 10332.*

38 *J. Norrman and L. Piculell, J Phys Chem B 2007, 111, 13364.*

39 *K. Fontell, A. Khan, B. Lindström, D. Maciejewska and S. Puangngern, Colloid Polym Sci, 1991, 269, 727.*

40 *J. S. Bernardes, J. Norrman, L. Piculell and W. Loh, J Phys Chem, 2006, 110, 23433.*

41 *K.Bergfeldt, L. Piculell and P. Linse, J Phys Chem, 1996, 100, 3680.*

42 *B. Lindman, A. Khan, E. Marques, M. G. Miguel, L. Piculell and K. Thalberg, Pure & Appli. Chem., 1993, 65,953.*

43 *R. Scott, J Chem Phys 1949, 17, 268.*

44 *R. J. Hefford, Polymer, 1984, 25, 979.*

45 *M. K. Chun, C. S. Cho and H. K. Choi, J Appl Polym Sci, 2001, 79, 1525.*

46 *Macromolecular Complexes in Chemistry and Biology, E. Tsuchida and S. Takeaka, Eds.: Dublin/Bock/Schulz/Thies, © Springer-Verlag Berlin Heidelberg 1994.*

47 *S. Shenkov and V. Y. Baranovski, J Polym Sci Part A: Polym Chem, 1994, 32, 1385.*

48 *M. L. Cole and T. L. Whateley, J Colloid Interface Sci, 1996, 180, 421.*

49 *Y. Wang, E. J. Goethals and F. E. Du Prez, Macromol Chem Phys, 2004, 205, 1774.*

50 *R. Berreiro-Iglesias, C. Alvarez-Lorenzo and A. Concheiro, Int J Pharm, 2003, 258, 165.*

51 *D. F. Anghel and Sjuji Saito, Recent Res Devel Surface Colloids, 2004, 1, 301.*

52 *T. Costa, K. Schillén, M. G. Miguel, B. Lindman and J. Seixas de Melo, J Phys Chem B, 2009, 113, 6194.*

53 *S. Saito, Colloids and Surfaces, 1986, 19, 351.*

54 *V. A. Tirumala, A. Ronang, S. Agarwal, E. K. Lin and J. J. Watkins, Adv Mater, 2008, 20, 1603..*

55 *V. A. Tirumala, V. Daga, A.W. Bosse, A. Romang, J. Ilavsky, E. K. Lin and J. J. Watkins, Macromolecules, 2008, 41, 7978.*

56 *K. Flodström and V. Alfredsson, Microporous Mesoporous Mater, 2003, 59, 167.*

57 *P. Linton and V. Alfredsson, Chem Mater, 2008, 20, 2878.*

58 *S. Ruthstein, V. Frydman and D. Goldfarb, J Phys Chem B, 2004, 108, 9016.*

59 *A. N. Galatanu, I. S. Chronakis, D. F. Anghel and A. Khan, Langmuir, 2000, 16, 4922.*

60 *K. Thuresson, S. Nilsson and B. Lindman, Langmuir, 1996, 12, 530.*

61 F. E. Antunes, B. Lindman, M. G. Miguel, Langmuir, 2005, 21, 10188.

62 *K. Thalberg, B. Lindman and G. Karlström, J Phys Chem, 1991, 95, 6004.*

63 *A. V. Kabanov and A. B. Zezin, Makromol. Chem. Suppl. 1984 6, 259.*

64 *M. Tsianou, A. L. Kjoniksen, K. Thuresson and B. Nyström, Macromolecules, 1999, 32, 2974.*

65 *I. A. Nyrkova, A. R. Khokhlov and M. Doi, Macromolecules, 1994, 27, 4220.*

66 *A. V. Kabanov and V. A. Kabanov Bioconjugate Chem., 1995, 6, 7.*

67 *V. A. Izumrudov, P.-O. Wahlund, P.-E. Gustavsson, P.-O Larsson and I. Yu. Galaev, Langmuir 2003, 19, 4733.*

68 *E. Raspaud, J. Pelta, M. De Frutos and F. Livolant, Physical Review Letters, 2006, PRL 97, 068103.*

69 *DNA interactions with polymers and surfactants, Wiley-Interscience, ed. R. S. Dias and B. Lindman, 2008.*

70 *L. Zonghua, Z. Ziyong, Z. Changren and J. Yanpeng, Progress in Polymer Science, 2010 (in press).*

71 *E. D. Goddard, B. A. Pethica, J Chem Soc, 1951, 2659. T. C. Laurent, J. E. Scott, Nature, 1964, 2002, 661.*

72 *P. Hansson and M. Almgren, Langmuir, 1994,10, 2115.*

73 *R. Dias, S. Mel'nikov, B. Lindman and M. G. Miguel, Langmuir, 2000, 16, 2164.*

74 *E. D. Goddard, Colloids Surf, 1986, 19, 301.*

75 *K. P. Ananthapadmanabhan, P. S. Leung and E. D. Goddard, Colloids and Surfaces, 1985, 13, 63.*

76 *P. S. Leung, E. D. Goddard, C. Han and C. J. Clinka, Colloids Surf, 1985, 13, 47.*

77 *M. N. Jones, J Colloid Interface Sci, 1967, 23, 36.*

78 *E. D. Goddard, R. B. Hannan J Am Oil Chem Soc, 1977, 54, 561.*

79 *J. Sjöström, L. Piculell, Colloid Surf A, 2001, 183-185, 429.*

80 *J. Sjöström and L. Piculell, Colloids and Surfaces A: Physiochem. Eng. Aspects, 2001, 183-185, 429.*

81 *Lynch, J. Sjöström and L. Piculell, J. Phys. Chem, 2005, 109, 4258.*

82 *F. Guillemet and L. Piculell, J. Phys. Chem., 1995, 99, 9201.*

83 *A. Mezei, K. Pojják and R. Mészáros, J. Phys. Chem112, 2008, 9693.*

84 *K. Thalberg and B. Lindman, J Phys Chem, 1989, 93, 1478.*

85 *K. Thalberg B. Lindman and K. Bergfeldt, Langmuir, 1991, 7, 2893.*

86 *Thalberg, B. Lindman and G. Karlström, J Phys Chem, 1990, 94, 4289.*

87 *A. Svensson, J. Norrman and L. Piculell, J Phys Chem B, 2006, 110, 10332.*

88 *P. Ilekti, L. Piculell, F. Tournilhac and B. Cabane, J Phys Chem B, 1998, 102, 344.*

89 *P. Ilekti, T. Martin, B. Cabane and L. Piculell, J Phys Chem B, 1999, 103, 9831.*

90 *A. Svensson, L. Piculell, B. Cabane, and P. Ilekti, J Phys Chem B, 2002, 106, 1013.*

91 *A. Svensson, L.Piculell, L. Karlsson, B. Cabane and B. Jönsson, J Phys Chem B, 2003, 107, 8119.*

92 *A. Svensson, J. Sjöström, T. Scheel, and L. Piculell Colloids and surfaces A: Physcochem. Eng Aspects 2003, 228, 91.*

93 *L. Piculell and B. Lindman, Adv. Colloid Interface Sci. 1992, 41, 149.*

94 *Michael Gottschalk, P. Linse and L. Piculell, Macromolecules, 1998, 31, 8407.*

95 *L. Piculell, B. Lindman and G. Karlström, In "Polymer-Surfactant Systems" (J. C. T. Kwak, ed.), Marcel Dekker, New York, 1998.*

96 *K. J. Edler, Aust J Chem, 2005, 58, 627.*

97 *G. S. Attard, J. C. Glyde and C. G. Göltner, Nature, 1995, 378, 366.*

98 *A. Thomas, F. Goettmann and M. Antonietti, Chem Mater, 2008, 20, 738.*

99 *L. Piculell, A. S. Svensson, J. Norrman, J. S. Bernardes, L. Karlsson and W. Loh, Pure Appl Chem, 2007, 79, 1419.*

100 *M. Antonietti, C. Göltner, and H.-P. Hentze Langmuir 14 (1998) 2670.*

101 *H.-P. Hentze and E. W. Kaler, Curr. Opin. Colloid. Interf. Sci. 8 (2003)164.*

102 *D. Lundberg and K. Holmberg, J Surfactants and Detergents, 2004, 7, 239.*

103 *M. Lindstedt, S. Allenmark, R. A. Thompson and L. Edebo, Antimicrob Agents Chemother, 1990, 34, 1949.*

104 *Zimm J Chem Phys 16, 1093.*

Popular science summary in English

Polymers are long chain molecules, built from smaller repeating units (monomers) which are connected through polymerization reactions. Polymers can be charged or uncharged. When they are charged the building blocks (monomers) contain charges. For each charge there must be a small charge of opposite sign (called counterion) in order to keep the electroneutrality requirement. In this case, the long charged polymer chain is sometimes referred to as a polyion, because it contains many ions in the chain.

Surfactants (also called detergents or soaps) are molecules that contain one part which likes water (hydrophilic) and another that dislikes water (hydrophobic). These molecules with a dual nature are called amphiphilic. Due to this special characteristic, when they are put in water the hydrophobic parts of the surfactant molecules hide from water forming aggregates (called micelles) of different shapes depending on a number of parameters, such as the molecule structure and the solution properties. The hydrophilic part of the surfactant can be charged or uncharged. Again when the hydrophilic part is charged there is a counterion which neutralizes this charge.

Two polymers can attract each other, either if they are uncharged or if they are oppositely charged (the latter is immediately understood because opposite charges attract each other). Polymers and surfactants of oppositely charge also attract each other. Sometimes for the mixtures where these big molecules attract each other, water-insoluble polymer-polymer or polymer-surfactant complexes are obtained and they separate out from water. The complexes can also be soluble in water under certain conditions, for instance when an excess of one of the species (polymer or surfactant) is added to the mixture. It is very interesting to understand under which conditions soluble or insoluble complexes are obtained. One very important application of these insoluble/soluble complexes is found in a conditioning shampoo. Getting a smooth hair texture is a good example when colloid chemistry comes into play. The shampoo that we apply on our hair contains both charged polymers and charged surfactants in a soluble mixture. When we rinse the hair with lots of water the polyion and the surfactant ions complex together and form an insoluble layer that deposits onto our hair giving rise to the smooth texture. Other processes are used to deposit layers of insoluble polymer-polymer or polymer-surfactant complexes onto different kinds of surfaces, changing their roughness.

Surfactants can form very highly ordered structures at high concentrations, because surfactant aggregates (micelles) pack into different arrangements, such as cubic (packed micelles in a cube), hexagonal (long rods of surfactants aggregates packed in a hexagonal way) or lamellar (planes packed on top of each other). These structures can be transformed through *in situ* chemical reactions. One example is when the small counterions to the ionic surfactant ion

aggregates are monomers. These monomers can be connected through polymerization reactions and form a long polymer chain. This means that the surfactant structures can be created, destroyed or changed through polymerization reactions, when the structures formed in the presence of polymer are the same or different from those of surfactant alone.

When a long-chain alcohol (a molecule that looks like a surfactant but has a very small uncharged hydrophilic part is mixed with a surfactant it can change the ordered surfactant structures, in the cubic→hexagonal→lamellar sequence as the concentration of alcohol is increased in the structure. Some surfactants can be transformed into alcohols through chemical reactions. These surfactants are called degradable or cleavable surfactants, because part of the surfactant molecule breaks into two and gives rise to an alcohol, when the pH of the mixture is increased. In a mixture of degradable, non-degradable surfactants and an oppositely charged polymer, the cleavable surfactant can be transformed into alcohol *in situ* and the structure of the polymer-surfactant mixtures can be changed. *In situ* reactions can find use when a certain structure is desired in a stage but another structure is desired in another stage.

All the above presented examples are manifestations of complex phase behaviour in polymer-polymer or polymer-surfactant systems.

Populärvetenskaplig sammanfattning på Svenska

Polymerer är molekyler bestående av långa kedjor, vilka byggs upp av repeterande enheter, monomerer, som binds samman vid polymerisationsreaktioner. Polymerer kan antingen vara laddade (polyelektrolyter) eller oladdade. Till varje eventuell polymerladdning finns en motladdning (motjon) för att elektroneutralitetsvillkoret ska vara uppfyllt. Då en polyelektrolyt sätts till en vattenlösning dissocierar den i mer eller mindre hög grad, och den laddade kedjan kallas då för en polyjon.

Tensider (detergenter) är molekyler som har en hydrofil (”vattenälskande”) och en hydrofob (”vattenhatande”) del. De kallas således för amfifila molekyler. En konsekvens av tensiders lösningsegenskaper är att de aggregerar då de löses i vatten, och dessa aggregat kan anta olika former beroende bland annat på tensidens kemiska struktur och lösningens egenskaper. Tensidens hydrofila del kan antingen vara laddad eller oladdad. Om den är laddad är den försedd med en neutraliserande motjon.

Polymerer i en vattenlösning kan attrahera varandra, både om de är neutrala eller motsatt laddade (det senare fallet är mer uppenbart, då det alltid finns en attraktionskraft mellan två motsatta laddningar). Polymerer och tensider (av motsatta laddningar eller oladdade) kan också attrahera varandra. Då dessa förekommer tillsammans i lösning leder ofta attraktionskraften till att vattenolösliga komplex bildas, vilket i sin tur resulterar i en fasseparation. Om polymererna är laddade frisläpps de små motjonerna i lösningen varpå de laddade polyjonerna blir varandras neutraliserande motjoner. Detta resulterar återigen i en fasseparation. Under vissa betingelser kan komplexen återupplösas, till exempel då en av komponenterna (polymer eller tensid) tillsätts i överskott. Det är av stort intresse att förstå under vilka förhållande dessa komplex är lösliga eller olösliga. Ett viktigt användningsområde för dessa olösliga/lösliga komplex är vid formulering av hårschampo. Då ett lent hår eftersträvas blir förståelsen för kolloidkemi av hög vikt! Schampot som vi löddrar in vårt hår med är i själva verket en blandning av bland annat lösliga komplex av laddade polymerer och motsatt laddade tensider. Då schampot sköljs bort med (överskott av) vatten bildar polyjonerna och de motsatt laddade tensidjonerna olösliga komplex som i sin tur skapar en beläggning på hårstråna, vilket resulterar i ett mjukt och lent hår. Andra viktiga sammanhang där olösliga komplex av antingen motsatt laddade polymer-polymer- eller polymer-tensid system förekommer är vid beläggning av olika sorters ytor. Dessa kan således ges nya egenskaper, såsom förändrad skrovlighet.

Vid höga koncentrationer kan tensider bilda flertalet väldigt ordnade strukturer, såsom kubiska, hexagonala och lamellära. Detta beror på att olika strukturer blir olika gynnsamma då tensidkoncentrationen förändras. Vidare kan dessa strukturer omformas genom kemiska reaktioner *in situ*. Ett exempel på detta är då en laddad tensids motjon är en monomer. Då en

polymerisationsreaktion initieras förbinds motjonerna till en långkedjig motjon (polyjon), varpå den befintliga strukturen kan förstöras och nya strukturer kan skapas och förändras, ifall strukturen för tensid ensam skiljer sig från polymer-tensidsystemets struktur.

Då en långkedjig alkohol (en molekyl lik en oladdad tensid, men med en hydrofil del som är betydligt mindre) blandas med en tensid i en vattenlösning förändras systemets struktur enligt sekvensen kubisk→hexagonal→lamellär vid en ökande alkoholkoncentration. Vissa tensider kan förändras till alkoholer genom kemiska reaktioner. De kallas då för nedbrytbara eller klyvbara tensider, eftersom en del av tensiden bryts av som en alkohol. I en blandning av klyvbara, icke-klyvbara joniska tensider och en motsatt laddad polyjon kan den klyvbara tensiden omvandlas till en alkohol *in situ*, vilket kan resultera i en strukturförändring av systemet. Dessa system brukar kallas för responsiva eller evolverande system. *In situ* – reaktioner kan vara användbara då en viss struktur önskas i ett visst skede, men en annan struktur eftersträvas i ett annat skede.

Alla ovan beskrivna exempel är manifestationer av komplexa fasbeteenden hos polymer-polymer eller polymer-tensid system.

Paper I

Associative phase behaviour and disintegration of copolymer aggregates on adding poly(acrylic acid) to aqueous solutions of a PEO-PPO-PEO triblock copolymer

Salomé dos Santos, Bob Luigjes† and Lennart Piculell*

Received 3rd March 2010, Accepted 20th May 2010
DOI: 10.1039/c0sm00052c

The influence of adding poly(acrylic acids) of two different chain lengths (PAA_{25} and PAA_{6000}) on the phase behaviour of the amphiphilic triblock copolymer Pluronic® P104 (P104 = $(EO)_{27}(PO)_{61}(EO)_{27}$, where EO = ethylene oxide, PO = propylene oxide) in H_2O was investigated. The resulting phase equilibria and structures were investigated by visual inspection, using crossed polarizers, and small angle X-ray scattering (SAXS). At low and intermediate P104 concentrations an associative phase separation was found, where a concentrated phase separated out from a dilute one on adding PAA. The corresponding phase separation region appeared in the phase diagram as a closed, droplet-shaped miscibility gap that was significantly larger for the longer PAA. Neither of the coexisting phases contained any long-range ordered structures. At higher concentrations of P104 (above *ca.* 25 wt%) no miscibility gap appeared but, remarkably, the various ordered liquid crystalline phases observed in binary P104/H_2O mixtures were eventually destroyed upon the replacement of H_2O by PAA. A similar effect was found when propionic acid (PrA), corresponding to the repeating unit of the PAA chain, was added to aqueous P104. A decrease in the PAA length, in the series PAA_{6000} - PAA_{25} - PrA, increased the efficiency to destroy the structured phases. NMR self-diffusion measurements showed that the self-assembled P104 aggregates dissolved on replacing water with PrA. The same mechanism was found to be responsible for the effect of added PAA, that is, PAA (or PrA) acts as less selective "solvent" for the PEO and PPO blocks compared to water.

Introduction

There is an increasing interest in the behaviour of associating polymer–surfactant or polymer–polymer mixtures in water, that is, combinations of individually water-soluble entities that associate to form water-insoluble materials on mixing in water. This interest is largely motivated by two recent breakthroughs, each having huge implications for material science. One is the development of the layer-by-layer deposition technique to create, in a simple and controlled fashion, water-insoluble surface coatings by repeatedly exposing a surface in an alternating fashion to individual solutions of the two polymers (often oppositely charged polyions) of an associating pair.[1] The other development involves the use of self-assembling block copolymers, or surfactants, to produce nano-structured "templates" around which a mesoporous hard or soft material may be built by inorganic or organic polymerisation.[2–4] Here one uses as templates the multitude of organized structures of different geometries that can be built by self-assembling amphiphilic molecules in water. It is notable that the successful creation of an *ordered* mesoporous structure on polymerisation normally requires that the template and the polymerised compound constitute an *associating* pair.[5] When there is only a repulsive depletion interaction between polymer molecules and surfactant aggregates, the ordered structures are typically destroyed by the polymerisation reaction.[3] Associating mixtures of polymers and surfactants are also used in everyday products such as shampoos or fabric detergents to create beneficial surface layers on hair or fabric by surface deposition.[6,7] Also here, the size and long-range organization of the surfactant aggregates in the concentrated surface layer is of interest, since it may have important consequences for both molecular transport and mechanical properties of the layer.

The most widely studied associating polymer–surfactant pairs contain charges of opposite sign.[5,8–10] However, there are other examples of associating mixtures in water, which have received much less attention. Poly(acrylic acid) (PAA) is known to associate with poly(ethylene oxide) (PEO) in water[11] and, similarly, PAA and nonionic surfactants containing hydrophilic segments of ethylene oxide (EO) form associating pairs in water.[12] The only previous systematic study of the phase behaviour of such a system that we are aware of is that by Galatanu and co-workers on mixtures of Triton X-100 and PAA in water.[13] As expected, an associative phase separation was observed in these mixtures at low concentrations of polymer and surfactant. At higher overall concentrations a variety of single-phase regions of different liquid crystalline or disordered structures was found.

In the present work, we study PAA of two very different chain lengths (25 and 6000 repeating units) in aqueous mixtures with a triblock copolymer of the poloxamer type, which contains two hydrophilic blocks of EO groups separated by a hydrophobic middle block of polymerised propylene oxide (PO). Poloxamers

Division of Physical Chemistry, Center for Chemistry and Chemical Engineering, Lund University, P.O.Box 124, SE-22100 Lund, Sweden. E-mail: Salome.Santos@fkem1.lu.se; Lennart.Piculell@fkem1.lu.se.
† Current address: Van't Hoff Laboratory for Physical and Colloid Chemistry, Debye Institute for Nanomaterials Science, Utrecht University, P. O. Box 80.051, 3508 TB, Utrecht, The Netherlands.

have surfactant properties and are very commonly used for templating mesoporous silica materials.[14–17] Here we have chosen to study a copolymer with the average composition $(EO)_{27}(PO)_{61}(EO)_{27}$, commercially available under the trade name Pluronic® P104. The P104 poloxamer forms a rich variety of structures upon increasing the concentration in binary mixtures with water, ranging from disordered micellar solutions to cubic micellar, hexagonal and lamellar liquid crystals.[18,19]

It is well-known that poloxamers and polymerised silica are associating mixtures, since mesoporous structures with long-range order separate out on polymerising silica in dilute solutions of poloxamers.[14–17] It is also known that an association is present between poloxamers and PAA, in some cases resulting in precipitation, but the published studies have been restricted to the dilute regime.[20–23] To look for ordered structures in concentrated aqueous mixtures has never been an objective. Some studies of dry binary mixtures of poloxamers and PAA have been performed, however, and very recently, Watkins and coworkers showed that the addition of PAA in the melt could induce the formation of ordered cubic, lamellar, or hexagonal structures in poloxamers of varying compositions.[24,25] Our study thus fills the gap between the previously studied dilute aqueous mixtures, on the one hand, and the blends in the melt state, on the other.

The objective of the present study is to address the following questions. What does the miscibility gap, caused by an associative phase separation, look like at low overall concentrations of P104 and PAA? In particular, what is the nature (structure and composition) of the concentrated phase that separates out from dilute mixtures of P104 and PAA? How does the addition of PAA affect the liquid crystalline phases formed in concentrated aqueous P104? How does the PAA chain length influence the phase behaviour, and how can we understand such an influence? What can we learn about the interactions between PAA and the different blocks, PEO or PPO, of the poloxamer? In order to answer the last questions, aqueous mixtures of P104 with propionic acid (PrA), corresponding to a single repeating unit of PAA, were also investigated. The methods we have used are visual inspection, SAXS and NMR self-diffusion. A novel conclusion that emerges from our study is that PAA actually displays considerably less selectivity than water for the different blocks of the poloxamer molecule.

Experimental

Materials

Pluronic® P104, henceforth referred to simply as P104, was obtained from BASF Corp., New Jersey. The molecular weight is approximately 5900 g mol^{-1}, the PEO content approximately 40 wt% and the density 1.04 g mL^{-1}, according to the manufacturer. The resulting composition is $(EO)_{27}(PO)_{61}(EO)_{27}$. Propionic acid (PrA), 99+%, was obtained from Aldrich. The density of PrA is 0.992 g mL^{-1}. Millipore water with a resistivity of 18.2MΩ was used throughout the study. D_2O (99.80 atom% D) for the NMR experiments was purchased from ARMAR, Switzerland. Poly(acrylic acids) with molecular weights of 450 000 g mol^{-1}, PAA_{6000}, and 1800 g mol^{-1}, PAA_{25}, were obtained from Aldrich. PAA_{6000} and PAA_{25} were purified by dialysis against Millipore water for 5 and 3 days, respectively, using cellulose membranes from Spectrum Laboratories, Inc. with molecular weight cut-offs of 10 000 and 500, respectively, and subsequently freeze-dried. Other chemicals were used without further purification.

Phase diagram determinations

For investigating the phase behaviour of P104/H_2O/PAA the following strategy was employed. Since the phase behaviour of P104 in H_2O is known,[18,19] samples were prepared along the P104/H_2O axis of the phase diagram, choosing points in the proximity of the expected phase boundaries. Subsequently, sets of ternary samples were prepared where the samples in each set had the same P104-to-H_2O ratio and increasing PAA contents, hence moving from the P104/H_2O axis towards the PAA corner in the ternary phase diagram.

Samples of about 0.5 g were prepared in glass tubes with the appropriate amounts of the respective components. The contribution from the H_2O content (0.2 wt%) in P104 to the overall sample compositions was considered; the water content of the freeze-dried PAA was found to be negligible (<0.1 wt%). Each sample was prepared by filling a glass tube with the desired amount of PAA, after which the P104 could be added. Lastly, the desired amount of H_2O was added. This order of addition was chosen since the P104 was very sticky and tended to remain at the top of the tube. For the same reason the samples were centrifuged in order to get the P104 sufficiently far down in the tube to enable flame-sealing of the tubes. After flame-sealing the tubes, samples were mixed by centrifuging the tubes alternatively right-side-up and up-side-down at least twice. Subsequently they were centrifuged for a long time (more than a week) to accelerate the equilibration, after which the samples were stored at 25 °C. Centrifugation was generally done at 4000 rpm (3416.5 *g*) and 25 °C.

Structural characterization

Samples were visually inspected for determination of the number of phases present, both under normal light and between crossed polarizers to detect birefringence revealing the presence of optically anisotropic phases (hexagonal and lamellar structures). The structures were determined by SAXS. A Kratky compact small-angle system was used, with a Seifert ID-3000 X-ray generator, operating at 55 kV and 40 mA, providing radiation with a wavelength of 1.54 Å. A position sensitive detector from MBraun with 1024 channels was used, with a sample-to-detector distance of 277 mm and a long slit geometry collimation system. Stiff samples were measured in a cell with mica windows and liquid samples in a capillary. All samples were measured for at least several hours. For other samples, the SAXS beamline (I711) with synchrotron radiation at Max II in Lund was used.[26] The experimental setup involved the use of X-rays at the wavelength of 1.1 Å and a sample-to-detector distance of 1241 mm or 1404 mm. The cell with mica windows was used. Typical acquisition times were 300 and 600 s. The volume between the sample and the detector was kept under vacuum during data collection in order to minimize the background scattering. The temperature of the sample in the cell was kept at 25 °C. The analysis of the 2D SAXS scattering patterns was conducted by the software Fit2D. The size of a cubic unit cell, α, can be obtained by plotting

$(q/2\pi)^2$, where q is the scattering vector, *versus* the Miller indices $(h^2 + k^2 + l^2)$ of the cubic structures, according to eqn (1).

$$(q/2\pi)^2 = (1/\alpha)^2(h^2 + k^2 + l^2) \quad (1)$$

It follows from the geometry of the hexagonal structure that the center-to-center distance between the adjacent rods (and the unit cell size), d, can be obtained from the first diffraction peak using eqn (2).

$$d = (2/3^{1/2})(2\pi/q_1) \quad (2)$$

For the lamellar structures the distance between the planes, D, is given by eqn (3).

$$D = 2\pi/q_1 \quad (3)$$

In eqn (2) and 3, q_1 is the position of the first diffraction peak.

Assuming that the density of all the components is $\sim$1g cm^{-3}, eqn (4) below was used to calculate the aggregation number, N_{agg}, of the micelles for the two micellar cubic structures found in the studied systems.

$$N_{agg} = w_{P104}\alpha^3/n_{mic}v_{P104} \quad (4)$$

Here w_{P104} is the poloxamer mass fraction, n_{mic} the number of micelles in the cubic cell (four for the face-centered space group and two for the body-centered space group), and v_{P104} is the volume of one copolymer molecule (9400 Å^3).[19]

NMR self-diffusion measurements

Samples of approximately 0.5 g for NMR were prepared by weight in test tubes. The samples contained 20 wt% of P104 and varying proportions of D_2O and PrA. The tubes were carefully closed, centrifuged for several hours and left to equilibrate for 5 days. Subsequently the samples were transferred to 5 mm tubes and sealed to avoid evaporation of PrA or water.

The NMR method used to measure self-diffusion coefficients, D, relies on the application of two pulsed field gradients (PFGs) in the dephasing and refocusing periods of a spin-echo (SE), 90°-τ-180°-τ-echo pulse sequence. A detailed description of the methods can be found elsewhere.[27] The intensity of the echo, I, is given by eqn (5).

$$I = I_0\exp[-(\gamma g\delta)^2(\Delta - \delta/3)D] \quad (5)$$

In eqn (5), I_0 is the intensity of the signal following a single 90° pulse, γ is the magnetogyric ratio of the studied nucleus and Δ is the separation between the leading edges of the PFGs with duration δ and strength g. The experiment is performed by acquiring the signal for a series of values of g. Eqn (6) below was used to evaluate the apparently bi-exponential decays obtained in the measurements. Here D_f and D_s are the fast and the slow diffusion coefficients obtained for the two apparent classes of poloxamer molecules with the fractions p and (*1-p*), respectively.

$$I = I_0\{p\exp[-(\gamma g\delta)^2(\Delta - \delta/3)D_f] + (1 - p)\exp[-(\gamma g\delta)^2(\Delta - \delta/3)D_s]\} \quad (6)$$

The PFG SE method is used for species with fast diffusion and long T_2. Here we assume that T_2 is similar for both P104 unimers and micelles. The NMR measurements were performed on a Bruker DMX 200 spectrometer operating at 200.13 MHz proton resonance frequency. Pulsed field gradients were generated in a Bruker DIFF-25 gradient probe driven by a BAFPA-40 unit. The self-diffusion was studied using the PFG SE pulse sequence with the parameters δ = 1 ms and Δ = 100 ms. The measurements were performed at 25 °C.

Results

Mixing and equilibration

A first observation on studying the phase behaviour of the P104/H_2O/PAA systems was the long time required for samples to mix and equilibrate. Mixing the samples by turning the flame-sealed tubes alternatively right-side-up and up-side-down in the centrifuge took hours, or sometimes days, of centrifugation. It was found to be important to equilibrate the samples for long periods of time to obtain the equilibrium structure. Especially samples with low water contents kept changing over long times. Samples with a high polymer content generally took months to equilibrate. The equilibration time for the samples containing PAA_{25} was generally not more than a couple of months. For the system P104/H_2O/PAA_{6000}, and especially samples with low amounts of P104, the concentrated phases in the miscibility gap remained turbid over long periods of time, sometimes more than 2 years. Some of the samples remained translucent or turbid in appearance. Generally, the scattering contrast was low even after long equilibration times, and difficulties in obtaining a sufficient number of diffraction peaks to resolve the structure of some samples remained. This was the reason for the use of synchrotron radiation.

The time for equilibration of the concentrated samples from the P104/H_2O/PrA system was of the order of days and hence much shorter compared to the systems containing PAA_{6000} or PAA_{25}.

Ternary phase diagrams with PAA

The ternary phase diagrams for P104/H_2O/PAA_{6000} and P104/H_2O/PAA_{25}, obtained at 25 °C, are shown in Fig. 1. The sample compositions investigated are indicated by different symbols in the phase diagrams according to the phase structure(s) that they contain. The boundaries to the various regions are indicated by solid lines. The presence of narrow two-phase regions between one-phase regions of different symmetries, required by the Gibbs phase rule, is indicated by double lines, although none of the prepared samples were actually located in these regions. In addition to these narrow biphasic regions, one extended two-phase area, separating samples of widely different compositions, is present in each of the phase diagrams. We will occasionally refer to this two-phase region as a miscibility gap, since the phase separation here is caused by a net attraction between the two polymeric solutes, P104 and PAA.

We note that both poloxamers and PAAs have a considerable degree of polydispersity. Hence, the present systems are not strictly three-component systems. Nevertheless, regions with more than three coexisting phases were not detected.

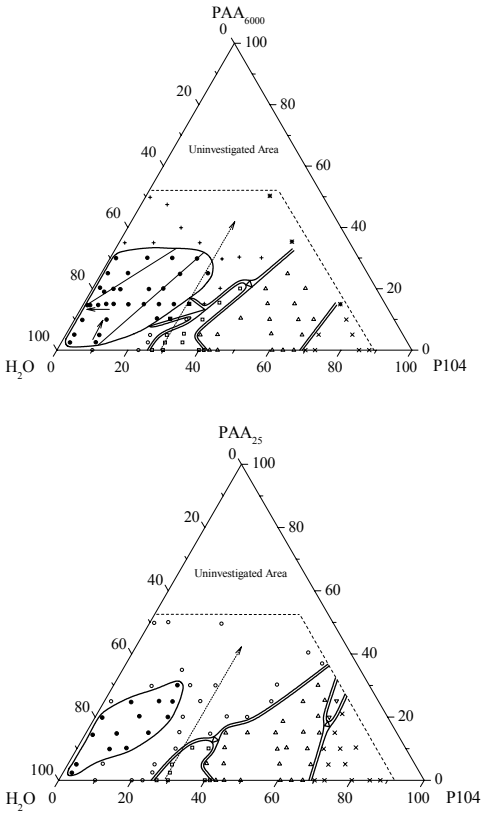

Fig. 1 Experimental P104/H_2O/PAA_{6000} (top) and P104/H_2O/PAA_{25} (bottom) phase diagrams at 25 °C. Concentrations are in wt%. Open circles – disordered solutions or gels, filled circles – 2 phases, open squares – micellar cubic, filled squares – 3 phases, open triangles – hexagonal, diagonal crosses (×) – lamellar, inverted triangles – bicontinuous cubic and crosses (+) – disordered gels. Samples indicated by stars remained macroscopically heterogeneous, presumably because of insufficient mixing (see text). Curved solid lines represent phase boundaries. Straight lines in the miscibility gap in the P104/H_2O/PAA_{6000} phase diagram are tielines. Solid arrows in the two-phase region of the P104/H_2O/PAA_{6000} system show the directions of increasing viscosity of the top phase. Dotted arrow shows the direction of replacing H_2O by PAA. Dashed lines show the limits of the investigated composition range.

The binary mixtures (P104/H_2O)

Our study includes a number of samples along the binary P104/H_2O axis, and the results confirm, with some modifications noted below, the phase behaviour reported by previous researchers.[18,19] At low P104 contents a region of optically isotropic transparent solutions was found with a viscosity that increased upon increasing the poloxamer concentration. On increasing the P104 concentration, a very stiff, isotropic phase appeared between 26 wt% and 42 wt% of P104. In Fig. 2, the SAXS profile of this phase is shown and the seven reflections $3^{1/2}$:$4^{1/2}$:$8^{1/2}$:$11^{1/2}$:$19^{1/2}$:$24^{1/2}$:$27^{1/2}$ could be indexed to the face-centred cubic (FCC) structure with the space group *Fm3m*. This cubic structure is composed of globular micelles in a face-centered cubic arrangement, with four micelles per unit cell. This assignment is different to that of Svensson *et al.* who, based on SAXS results obtained with a less advanced instrument, assigned the structure to the *Pm3n* space.[19] Table 1 contains information on unit cell sizes and micellar aggregation numbers of the cubic structures.

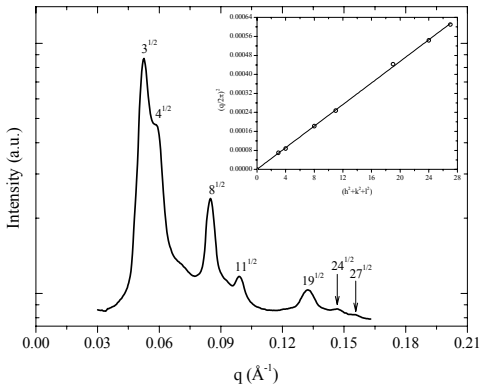

Fig. 2 SAXS pattern of a sample containing 40 wt% P104 in the P104/H_2O binary system with a FCC structure of the space group F*m3m* featuring peaks at the relative positions $3^{1/2}$:$4^{1/2}$:$8^{1/2}$:$11^{1/2}$:$19^{1/2}$:$24^{1/2}$:$27^{1/2}$. Inset: $(q/2\pi)^2$ *versus* $(h^2 + k^2 + l^2)$.

For higher P104 contents than 43 wt% optically anisotropic phases where found and SAXS patterns showed the presence of the hexagonal phase up to approximately 70 wt% of P104 and above this content the lamellar phase was found.

General trends on addition of PAA

Upon addition of PAA, miscibility gaps were observed for both the P104/H_2O/PAA_{6000} and the P104/H_2O/PAA_{25} systems, starting already at very low P104 poloxamer and PAA concentrations. The miscibility gap was larger for P104/H_2O/PAA_{6000} than for P104/H_2O/PAA_{25}. There was an asymmetry in the sense that even very small additions of P104 to PAA solutions resulted in phase separation, whereas a significant amount of PAA could be incorporated in P104 solutions before phase separation occurred.

On increasing the PAA concentration, starting from the liquid crystalline P104/H_2O mixtures, similar changes occurred for both PAA lengths. The cubic phase shrunk in extension and was finally replaced by a disordered isotropic mixture. The anisotropic phases were also eventually destroyed on adding PAA, giving place to disordered liquids or stiff gels. A small growth of the hexagonal phase, at the expense of the cubic phase, was initially seen for small additions of PAA. Otherwise, the boundaries of the anisotropic phases were found to be more-or-less straight lines pointing in the general direction of the P104/PAA axis.

We will now describe specific observations for each one of the two P104/H_2O/PAA systems.

Table 1 Characteristic parameters obtained from SAXS results

Composition (wt%)	Structure	Space group	a/Å	N_{agg}
30 P104, 70 H_2O	FCC	*Fm3m*	207	71
40 P104, 60 H_2O	FCC	*Fm3m*	208	96
34.1 P104, 63.4 H_2O, 2.4 PAA_{6000}	FCC	*Fm3m*	214	89
33.1 P104, 61.6 H_2O, 5.3 PAA_{6000}	FCC + BCC+ 2 extra peaks	*Fm3m*	212	84
		Im3m	167	82
36 P104, 54 H_2O,10 PAA_{25}	BCC	*Im3m*	154	70
64 P104, 16 H_2O, 20 PAA_{25}	Gyr	*Ia3d*	178	-
29.2 P104, 67.4 H_2O, 3.4 PrA	FCC + BCC	*Fm3m*	208	70
		Im3m	167	72
29.9 P104, 63.3 H_2O, 6.8 PrA	FCC + BCC+ 2 extra peaks	*Fm3m*	209	73
		Im3m	164	70
		d(Å)	l/n_{P104}(Å)	
45.3 P104, 54.7 H_2O	Hex	129	1.44	
49.8 P104, 50.2 H_2O	Hex	131	1.27	
60.7 P104, 39.3 H_2O	Hex	124	1.16	
63.7 P104, 36.3 H_2O	Hex	126	1.07	
49 P104, 31 H_2O, 20 PAA_{6000}	Hex	119	1.56	
67.3 P104, 22.7 H_2O, 10 PAA_{6000}	Hex	123	1.07	
42.7 P104, 52.2 H_2O, 5.1 PAA_{6000}	Hex	127	1.58	
57.8 P104, 36.9 H_2O, 5.3 PAA_{6000}	Hex	128	1.15	
51.8 P104, 33.2 H_2O, 15 PAA_{25}	Hex	116	1.56	
52 P104, 29.3 H_2O, 18.7 PAA_{25}	Hex	113	1.63	
54.4 P104, 20.7 H_2O, 24.9 PAA_{25}	Hex	109	1.68	
42.5 P104, 52.2 H_2O, 5.3 PAA_{25}	Hex	126	1.61	
40.3 P104, 49.4 H_2O, 10.3 PAA_{25}	Hex	119	1.9	
57.9 P104, 37 H_2O, 5.1 PAA_{25}	Hex	123	1.24	
54.9 P104, 35.2 H_2O, 9.9 PAA_{25}	Hex	118	1.42	
40.1 P104, 56.7 H_2O, 3.2 PrA	Hex	125	1.73	
		D (Å)		
80.2 P104, 19.8 H_2O	Lam	97		
80.7 P104, 14.3 H_2O, 5 PAA_{6000}	Lam	103		
76.5 P104, 13.5 H_2O, 10 PAA_{6000}	Lam	103		
72 P104, 18 H_2O, 10 PAA_{25}	Lam	97		
67.5 P104, 22.5 H_2O, 10 PAA_{25}	Lam	105		

P104/H_2O/PAA_{6000}

Samples found in the miscibility gap in this system were of three types: a clear liquid on top of a clear stiff gel, a clear liquid on top of a turbid (or tanslucent) stiff gel, or a viscous turbid liquid on top of a turbid stiff gel. The stiffest concentrated phases were obtained at the highest amounts of P104. From the boundaries of the miscibility gap we infer that the most concentrated phase (*i.e.*, the phase with the lowest water content) that could separate out from a two-phase sample in this system had a composition of, approximately, 29 wt% P104, 42 wt% H_2O, and 29 wt% PAA_{6000}. Using 51.4 g mol^{-1} as a number average molar mass of the repeating EO and PO units in P104, we calculate that this composition corresponds to a stoichiometry of 4.2 H_2O molecules and 0.7 repeating units of PAA per repeating unit of P104. The gel-like phases found in biphasic samples did not flow and presented a stiff, elastic consistency. The clear liquids were low-viscous, some with a very low viscosity. The viscosity of the top phase increased on changing the overall compositions in the directions indicated by the solid arrows in the miscibility gap in Fig. 1.

When samples of different overall compositions showed the same viscosities of their top phases, they were taken to belong to the same tieline. The approximate tielines drawn in Fig. 1 are based on these observations. SAXS measurements were performed to determine the nature of the phases in this two-phase region and the results indicated no long-range ordered structure for either phase (see Fig. 3).

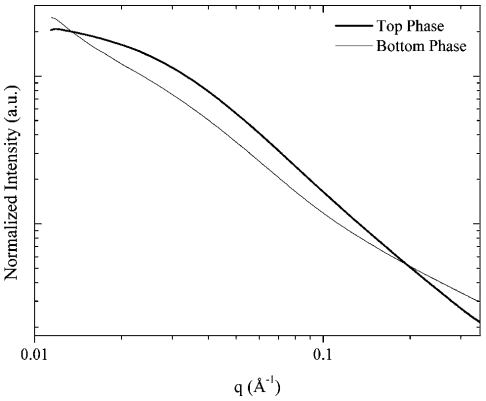

Fig. 3 SAXS scattering patterns from the clear top phase and the translucent bottom phase from a sample with the global composition 4.3 wt% P104, 81 wt% H_2O and 14.7 wt% PAA_{6000} located in the miscibility gap. Subtraction of the capillary background and the detector background was made and the normalization carried out for the transmitted beam intensity.

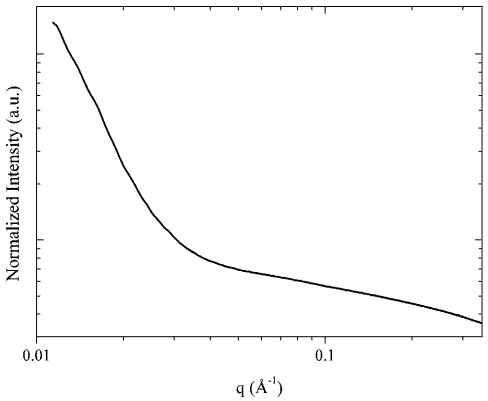

Fig. 4 SAXS scattering pattern from a translucent sample containing 9.8 wt% P104, 55.2 wt% H_2O and 35 wt% PAA_{6000}. Subtraction of the capillary background and of the detector background was made and the normalization carried out for the transmitted beam intensity.

Between the miscibility gap and the cubic phase, a three-phase region was discovered, in addition to the isotropic solution region. When the stiff bottom phase was turbid (which could be achieved by simply heating the sample slightly by holding it in the hand) one could observe two additional clear layers of liquid phases, differing in viscosity, upon tilting the sample. Attempts to mix the liquids by vortex mixing clearly showed an immiscibility of the two liquid phases. Hence, it can be concluded that these samples were indeed part of a three-phase region. At high concentrations of PAA_{6000} a very viscous, isotropic liquid was found. Upon entering this region the viscosity of the sample increased strongly with increasing PAA_{6000} content and at very high proportions of PAA_{6000}, a very stiff gel phase was found. SAXS measurements revealed that these samples did not present any long-range ordered structure (Fig. 4). A stiff gel could be distinguished from a very viscous liquid by looking at its interface with the air. If a meniscus was present at this interface the sample was most likely liquid, whereas a flat interface implied a stiff gel. Stiff samples did not flow in the gravitational field during an observation time of weeks. The micellar cubic phase extended in a narrow tongue pointing towards the P104/PAA axis, and persisted until approximately 20 wt% of PAA_{6000}.

Scattering patterns from one hexagonal and one lamellar sample are presented in Fig. 5. The scattering patterns with peaks occurring at the relative ratios $1 : 3^{1/2}:4^{1/2}:7^{1/2}:9^{1/2}$ confirmed the presence of the hexagonal structure and the $1 : 4^{1/2}:9^{1/2}$ pattern confirmed the lamellar structure. More information about the hexagonal and lamellar structures is shown in Table 1, regarding the distances between rod centers and consecutive planes, respectively.

Three samples with low water contents and high contents (>15 wt%) of PAA_{6000}, indicated by stars in Fig. 1, did not give homogeneous mixtures by our mixing procedure, but contained white solid-like material surrounded by an anisotropic phase. We doubt that these comparatively dry samples reached equilibrium through our mixing procedure. Hence, the equilibrium phase compositions in this region were not established.

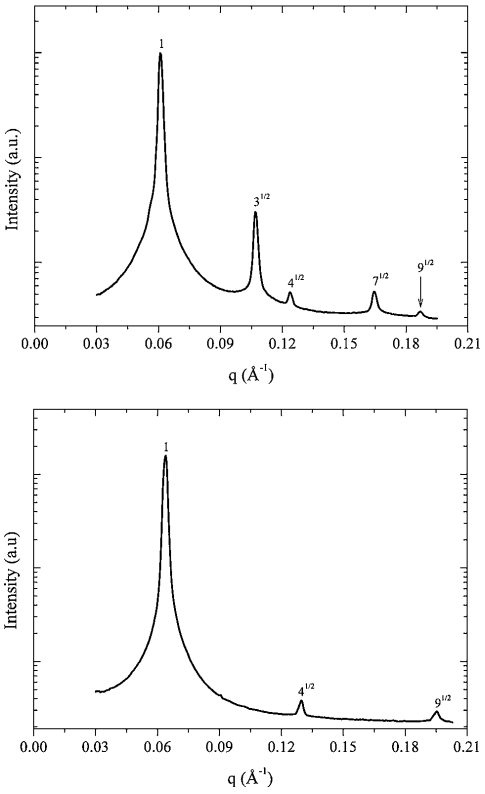

Fig. 5 SAXS patterns from anisotropic samples of the $P104/H_2O/PAA_{6000}$ system. The sample with the composition 49 wt% of P104, 31 wt% of H_2O and 20 wt% of PAA_{6000} (top) was hexagonal showing diffraction peaks at the relative positions $1 : 3^{1/2}:4^{1/2}:7^{1/2}:9^{1/2}$. The sample with 80.7 wt% P104, 14.3 wt% H_2O and 5 wt% PAA_{6000} (bottom) was lamellar with diffraction peaks at the relative positions $1 : 4^{1/2}: 9^{1/2}$.

$P104/H_2O/PAA_{25}$

In this system, the two coexisting phases in the miscibility gap were clear liquids with different viscosities. Surrounding the miscibility gap, a continuous liquid solution was found; the three-phase region found with the longer PAA was absent. The concentrated phases in the miscibility gap with PAA_{25} had higher water content than the corresponding mixtures with PAA_{6000}. The most concentrated composition at the boundary to the miscibility gap had a composition of, approximately, 19 wt% of P104, 51 wt% of H_2O, and 30 wt% of PAA_{6000}. This composition corresponds to a stoichiometry of 7.7 H_2O molecules and 1.1 repeating unit of PAA per repeating unit of P104.

The micellar cubic region was smaller for this system compared to the system with the longer polymer. An example of a SAXS pattern from this region is given in Fig. 6 for a sample with 10 wt% of PAA_{25}. The relative positions of the reflections are $2^{1/2}:4^{1/2}:6^{1/2}:8^{1/2}:12^{1/2}:14^{1/2}$. The corresponding structure was

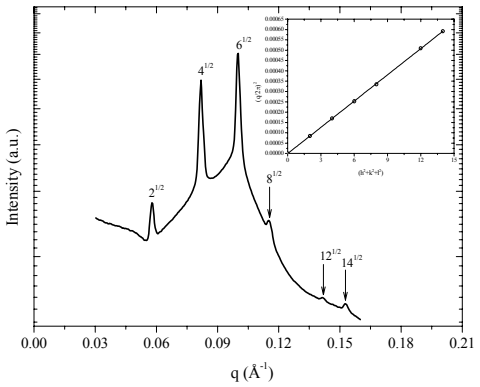

Fig. 6 SAXS pattern of a sample with the composition 36 wt% P104, 54 wt% H_2O and 10 wt% PAA_{25}, having a BCC structure of the space group *Im*3*m* featuring peaks at the relative positions $2^{1/2}$:$4^{1/2}$:$6^{1/2}$:$8^{1/2}$:$12^{1/2}$:$14^{1/2}$. Inset: $(q/2\pi)^2$ *versus* $(h^2 + k^2 + l^2)$.

body-centered cubic (BCC) with the space group *Im*3*m*. This structure is composed of globular micelles in a body-centered cubic arrangement, with two micelles per unit cell. More information about this structure is given in Table 1.

The scattering patterns obtained for the hexagonal and lamellar structures were similar to those of the P104/H_2O/PAA_{6000} system and all the results are summarized in Table 1. The lamellar phase region for the system with PAA_{25} was larger than that with the longer polymer. Moreover, an additional single-phase region was found between the hexagonal and the lamellar phases for higher amounts of PAA_{25}. The samples in this intermediate region were very stiff and optically isotropic, and the SAXS pattern is shown in Fig. 7. The eleven reflections observed, $3^{1/2}$:$4^{1/2}$:$7^{1/2}$:$8^{1/2}$:$10^{1/2}$:$11^{1/2}$:$20^{1/2}$:$22^{1/2}$:$24^{1/2}$:$26^{1/2}$:$29^{1/2}$,

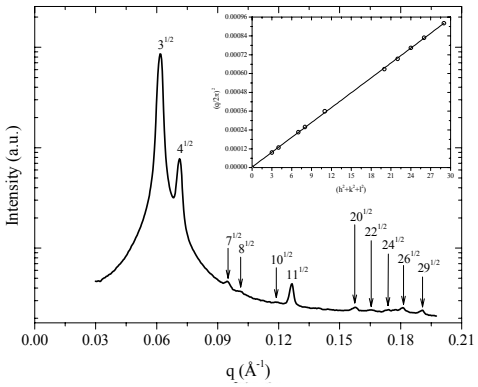

Fig. 7 SAXS pattern for an isotropic sample with the composition 64 wt% P104, 16 wt% H_2O and 20 wt% PAA_{25}. The structure was bicontinuous cubic with the space group *Ia*3*d*, featuring reflections at the relative positions $3^{1/2}$:$4^{1/2}$:$7^{1/2}$:$8^{1/2}$:$10^{1/2}$:$11^{1/2}$:$20^{1/2}$:$22^{1/2}$:$24^{1/2}$:$26^{1/2}$:$29^{1/2}$. Inset: $(q/2\pi)^2$ *versus* $(h^2 + k^2 + l^2)$.

represent the *Ia*3*d* space group of the bicontinuous cubic phase. The structure of the *Ia*3*d* cubic phase is related to the gyroid minimal surface and it is the most commonly encountered space group for bicontinuous cubic phases with surfactants and surfactant-like lipids and also in block copolymer systems. See Table 1 for the size of the unit cell.

P104/H_2O/PrA

We have seen above that the phase diagrams for the ternary mixtures with added PAA have important common features, but also show clear trends on changing the PAA length. In an attempt to separate effects of molecular interactions from effects of the degree of polymerisation of PAA, we decided to study mixtures of P104 with the compound that corresponds to a single repeating unit of PAA, that is, PrA. A partial ternary phase diagram for the P104/H_2O/PrA system is shown in Fig. 8. For low amounts of poloxamer, there was a continuous liquid region without a miscibility gap. Interestingly, as in the mixtures with PAA, the cubic region present in the binary P104/H_2O system gradually disappeared on addition of increasing amounts of PrA. Indeed, the cubic phase in this system was smaller, when compared with the same region in the systems with PAA_{6000} and PAA_{25}, thus continuing the trend on decreasing PAA chain length seen in the latter mixtures. The hexagonal phase region also disappeared more rapidly with addition of PrA, compared to the hexagonal regions with added PAA_{6000} or PAA_{25}. Samples were also prepared along the P104/PrA binary axis, and these samples, where the highest amount of poloxamer was 30 wt%, were clear isotropic liquids. Note that in the P104/H_2O mixtures, the sample with 30 wt% of P104 was cubic.

The P104/H_2O/PrA system is essentially a system of a poloxamer in a mixture of two good, miscible solvents. However, the phase diagram suggests that the self-assembly of P104 molecules into larger aggregates gradually disappears when H_2O is replaced by PrA. Owing to the low viscosity of the mixtures, NMR

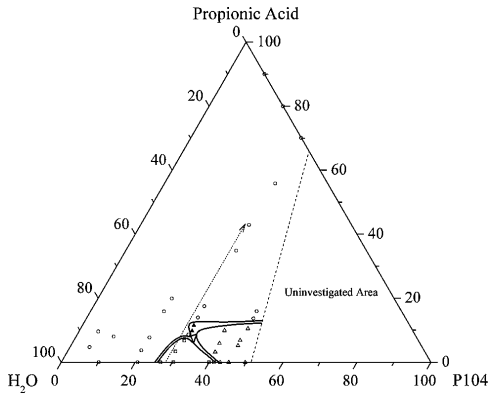

Fig. 8 Experimental P104/H_2O/PrA phase diagram at 25 °C. Open circles – disordered solutions, open squares – micellar cubic, open triangles – hexagonal and filled triangles – 2 phases. Solid lines represent phase boundaries. The dotted arrow shows the direction of replacing H_2O by PrA.

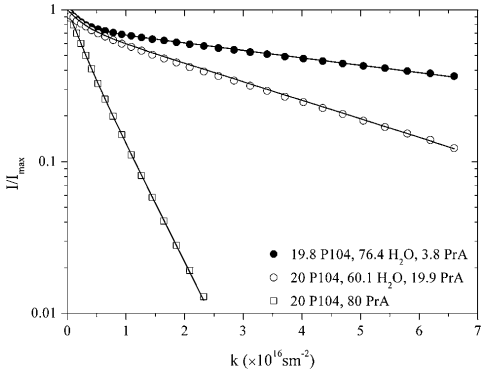

Fig. 9 NMR echo decays for P104/water/PrA samples containing 20 wt% P104 and varying proportions of PrA and water.

Table 2 Self-diffusion coefficients for samples with 20 wt% of P104 and different water weight fractions (w_{water})

w_{water}	D_f/m^{2}s^{-1}	D_s/m^{2}s^{-1}	p
0.764	4.0×10^{-11}	1.1×10^{-12}	0.247
0.601	3.5×10^{-11}	2.8×10^{-12}	0.223
0	4.1×10^{-11}	1.8×10^{-11}	0.253

self-diffusion measurements can conveniently be used to test this possibility. In Fig. 9, we present the results from the self-diffusion measurements in a series of samples, containing 20 wt% P104, where water was gradually replaced by PrA. All the curves could be satisfactorily fitted to a bi-exponential decay (eqn (5)), yielding two diffusion coefficients. A previous careful analysis of NMR self-diffusion data for similar poloxamer solutions in water has shown that the two diffusion coefficients reflect the diffusion of non-aggregated unimers (D_f) and self-assembled micelles (D_s) of the polydisperse poloxamer. The diffusion coefficients obtained for the micelles and unimers are presented in Table 2. The reason that two distinct populations, rather than an average, are observed is due to the polydispersity of the poloxamer; the unimer and the micelle populations are enriched in the more hydrophilic and the more hydrophobic components, respectively.[28] The essential feature for our purposes, however, is that the results clearly show that the slow-diffusing micelles, with an effective diffusion coefficient of the order of 10^{-12} m^2 s^{-1}, disappear on replacing water by PrA. The decay from the solution of 20 wt% of P104 in 80 wt% of PrA was also well reproduced by a bi-exponential, but here the fit gave two very similar diffusion coefficients, $D_s = 1.8 \times 10^{-11}$ m^2 s^{-1} and $D_f = 4.1 \times 10^{-11}$ m^2 s^{-1}, most probability reflecting the polydispersity of the P104 unimers. A single exponential fit to this curve gave an average diffusion coefficient of 2.2×10^{-11} m^2 s^{-1}.

Discussion

General considerations

The two most striking features of the phase behaviour of aqueous mixtures of P104 and PAA are the associative phase separation at high H_2O contents and the disappearance of the liquid crystalline structures at high PAA contents and intermediate concentrations of P104. The appearance of an effective attraction between poloxamers and PAA in H_2O was known before, but full phase diagrams describing the miscibility gap and the general directions of the tielines (confirming the association) have not been reported, to the best of our knowledge. As expected from the difference in the entropy of mixing between the systems, the phase separation becomes stronger with increasing molecular weight of the PAA polymer. Accordingly, in mixtures with the monomeric PrA, no phase separation is seen.

The disappearance of the liquid crystalline phases when H_2O is replaced by PAA at intermediate concentrations of P104 is a novel feature found in the present investigation. The experiments with PrA shed lights on the origin of this effect. Clearly, PrA acts as a non-selective solvent for the PEO and PPO blocks of the poloxamer and, hence, the self-assembly of the poloxamer molecules into large aggregates is gradually destroyed when H_2O is replaced by PrA as a solvent. In previous investigations of the effect of a number of other water-miscible cosolvents on poloxamer self-assembly, Ivanova *et al.* found a similar disappearance of the PEO-PPO segregation on replacing H_2O by, in particular, ethanol.[29,30] It is, in fact, well-known that H_2O *induces* segregation of the PEO and PPO blocks; solvent-free melts of short poloxamers, or solutions of poloxamers in xylene, do not contain self-assembled aggregates.[25,31–33] The striking similarities between the effects of PrA and PAA leave little doubt that a similar decrease in selectivity on replacing H_2O with PAA is responsible for the disappearance of the self-assembly of P104—clearly evident from the featureless SAXS patterns (Fig. 4)—in the latter mixtures. While understandable in principle, this seems to be a novel phenomenon; we are not aware of previous observations where the replacement of a low-molecular weight solvent (here H_2O) with a *polymer* (here PAA) results in a less selective environment and, hence, a vanishing segregation between the blocks of a block-copolymer system.

The quantitative differences between PrA, PAA_{25} and PAA_{6000} in their abilities to dissolve the P104 aggregates can be understood as a consequence of the balance between entropy of mixing and preferential interactions. Thus, while PAA is clearly a less selective environment for poloxamers than water, there should nevertheless be a weak preference for a PAA unit to reside in the PEO-rich corona of the poloxamer aggregate, as shown by recent studies of dry melts.[24,25] On the other hand, the entropy of mixing favours a uniform distribution of PAA repeating units throughout the polyoxamer aggregate. Hence, the monomeric PrA is most efficient, and PAA_{6000} least efficient, in breaking up the PPO aggregates.

For the specific systems and conditions that we have investigated, the much weaker selectivity of PAA, compared to water, apparently prevents the formation of long-range ordered structures in the concentrated phases that separate out from dilute mixtures of poloxamer and PAA. It seems that when the proportion of PAA is sufficiently high to induce an associative phase separation, it is also sufficiently high to prevent the formation of long-range ordered self-assembled structures in the concentrated phase that separates out. This implies that the self-assembly of the poloxamer, which occurs in pure H_2O, is largely irrelevant for the associative phase separation that occurs in

aqueous poloxamer/PAA mixtures; the latter phase separation seems to involve individual poloxamer chains rather than aggregates of chains. It is interesting to compare this situation with that found in mixtures of polymerised silica and poloxamers, including P104: on polymerising silica in dilute solutions of poloxamers, the poloxamer molecules remain aggregated, and a concentrated *ordered* phase separates out.[14–16] This seems to suggest a selectivity of the silica environment for the PEO blocks. This conclusion is indeed supported by the detailed studies of the initial formation of poloxamer-templated mesoporous silica by Goldfarb and coworkers.[34] Interestingly, the latter authors found that while the non-hydrolyzed hydrophobic silica source, tetramethoxy orthosilane, initially rapidly penetrated into the PPO cores of the poloxamer micelles, the polymerising silica network later partitioned to the PEO coronas of the micelles.

The micellar cubic systems

We will now discuss some of the trends observed within the various liquid crystalline regions on replacing water with PAA or PrA. Inside the micellar cubic region, both FCC and the BCC structures were found. The binary P104/H_2O mixtures showed pure FCC structures. We note that the cubic structures for the P104 concentrations of 30 and 40wt% in the binary mixtures had the same unit cell size, meaning that the number of P104 molecules in each micelle increased (see Table 1). A pure BCC structure was found for a P104/H2O/PAA_{25} system with 10 wt% of PAA_{25} (Fig. 6). Of the other four samples analysed, three showed SAXS patterns that could not be interpreted as single distinct structures. A mixture of the FCC and BCC structures and, sometimes, some other reflections that could not be assigned were found. Micellar aggregation numbers calculated from eqn (4) based on our assignments are presented in Table 1, and we found that in systems with mixed cubic structures, the aggregation numbers were the same for the coexisting structures. This implies, as would be expected, that in a mixed system, the different coexisting structures contain micelles with the same aggregation numbers, but arranged in different close-packed arrangements.

We note in this context that previous investigations of other block copolymer systems have shown that small changes may affect the symmetry of micellar cubic structures. FCC, BCC and the hexagonally close-packed (HCP) micellar arrangement can coexist for a single block copolymer system.[35] Changes in the external conditions, such as temperature or shear, can produce an interchange between these arrangements. In poloxamers, the presence or absence of diblock impurities have been found to affect the preference for BCC *versus* FCC structures.[36]

The hexagonal phase

The SAXS results revealed that the rod-rod distance d (Table 1) varies significantly with the composition of the hexagonal phase. We shall now to try to understand the molecular background to this variation. From simple geometrical considerations (see the Appendix) we obtain, for a two-dimensional hexagonal array of rodlike poloxamer aggregates, the relation

$$d^2 = (2/3^{1/2})v_{P104}n_{P104}/l\phi_{P104} \quad (7)$$

Here v_{P104} is the partial volume of the poloxamer molecule, n_{P104}/l is the number of poloxamer molecules per unit length of the poloxamer rod, and ϕ_{P104} is the volume fraction of poloxamer chains in the system. The composite quantity n_{P104}/l reflects the packing of polyxamer molecules in the rod, and is affected by the extent of penetration of water, PAA and/or PrA molecules into the PEO-rich corona and/or the PPO-rich core of a rod.

Let us first consider a hypothetical situation where both v_{P104} and n_{P104}/l are independent of the composition of the system. This would be the case, for instance, if water molecules, PAA repeating units or PrA molecules all penetrated the rod in the same way and to the same extent. Then the rod-rod distance would only depend on ϕ_{P104}, irrespectively of the proportions of water and PAA or PrA in the system. We can test this possibility by plotting d *versus* w_{P104}, where w_{P104} is the weight fraction of poloxamer, for all our systems. We then make, as in deriving eqn (4), the approximation $\phi_{P104} \approx w_{P104}$ since the partial specific volumes of all components are close to 1g cm^{-3}. The result is shown in Fig. 10 (top panel). The large scatter in this plot clearly shows that this analysis is too simplistic; there is no universal dependence on the variable w_{P104}.

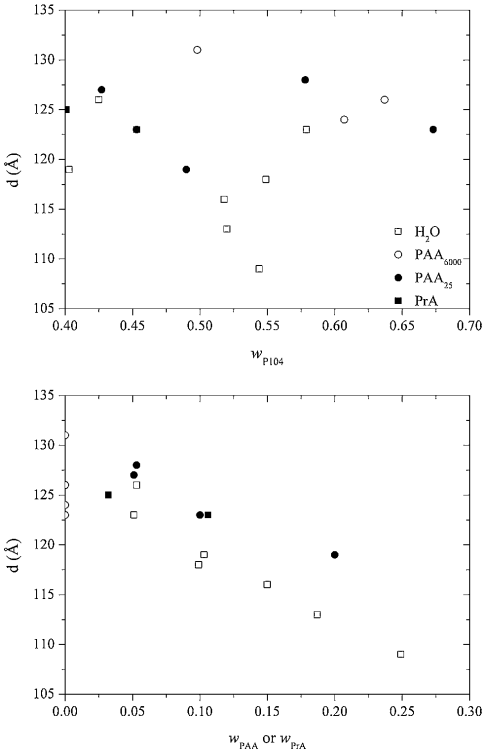

Fig. 10 Rod-rod distance (d) in the hexagonal phases as a function of the P104 weight fraction (top) and the PAA or PrA weight fraction (bottom). The rod-rod distance was calculated using eqn (2).

An alternative possibility, suggested by our general conclusion that PAA and PrA are less selective "solvents" than water, is that the PAA and PrA molecules penetrate into the poloxamer rods to a larger extent than the water molecules. Such a penetration should dilute the rod and thus result in a decrease in the number of poloxamer molecules per unit length, n_{P104}/l. To test for the latter possibility, we again plot, in Fig. 10 (bottom panel), all values of d, but this time *versus* the weight fraction of PrA or PAA in the system. Here, a very clear trend is seen, that is, a monotonic decrease in d with increasing content of the added carboxylic acid. Moreover, the data for PAA_{25} consistently lie below those for PAA_{6000}, supporting our previous conclusion that PAA_{25} more efficiently penetrates into the rods.

The bicontinuous cubic phase

At higher concentrations of P104 and PAA_{25}, the bicontinous cubic *Ia*3*d* structure was found, increasing the richness of the phase behaviour. The location of the bicontinuous cubic phase, between the water-continuous hexagonal phase and the lamellar phase, is where a so-called normal bicontinuous cubic phase is sometimes found in surfactant systems, notably also for certain poloxamers in water,[32,37] in formamide[37] or in water mixed with cosolvents.[29] To our knowledge, however, the Pluronic P104 has not been found to form a normal bicontinuous cubic phase in any other solvent environment before. It has been noted that bicontinuous structures often appear near the order–disorder transitions, that is, under conditions where the ordered structures are nearly lost.[32] This could apply to the present situation, since the bicontinuous cubic phase appears at compositions near those where the poloxamer self-assembly is ultimately lost, judging from the rapid shrinking of the hexagonal phase on approaching the P104/PAA_{25} axis.

Comparisons with previous phase studies

As stated in the introduction, we have found only one previously published study showing phase diagrams of aqueous mixtures of PAA with a surfactant, or block copolymer, featuring a hydrophilic block of EO units. The phase diagram of Triton X-100 with H_2O and PAA obtained by Galatanu *et al.* has many similarities with the diagrams for the P104/PAA/H_2O systems studied here.[13] Galatanu *et al.* used one sample of PAA, with a nominal molecular weight of 150 000 g mol^{-1}, and studied the mixtures at different temperatures. A closed miscibility gap was found inside the disordered liquid region, just as in the P104/PAA/H_2O systems. Moreover, the boundaries of the concentrated liquid crystalline regions (hexagonal and lamellar) ran more or less parallel to the binary PAA/H_2O axis, and both the latter phases disappeared at high contents of PAA, depending on temperature. This would suggest that PAA is a less selective solvent than water also for Triton X-100. In this context it is interesting to note that in mixtures of the "complex salt" $C_{16}TAPA_{6000}$ with H_2O and PAA_{6000}, the cubic phase, which occupies a large region of the phase diagram, eventually disappears when water is replaced by PAA_{6000}.[38] ($C_{16}TAPA_{6000}$ is the hexadecyltrimethylammonium surfactant neutralised by polyacrylate counterions.) This effect could again indicate that PAA is a less selective environment than water for the surfactant molecules.

Very recently, studies of binary PAA/poloxamer blends have been published by Watkins *et al.*[24,25] Interestingly, these studies showed that in such solvent-free blends, PAA *induces* a segregation between the blocks and a concomitant ordering. Superficially, the latter results could be taken to contradict our findings; we will therefore discuss them in some detail, to conclude that they are indeed consistent with our results. Watkins *et al.* studied, by SAXS, films of a thickness of the order of a millimetre, produced by solvent evaporation from mixed ethanolic solutions of various combinations of the Pluronics® L92, P105 and F108 with a number of PAAs of different molecular weights, in the interval 1000–88 000 g mol^{-1}. They also studied PAA mixed with a deuterated poloxamer using small angle neutron scattering (SANS) on a 0.5μm thin film. Most films were annealed and studied at 80 °C, but the SANS study revealed ordered structures also at 25 °C. Already PAA fractions as low as 4.5 wt% induced some order, but scattering patterns with two or more sharp peaks required *ca.* 20 wt% PAA. The highest PAA content in the mixtures was 50 wt%. The most detailed study was performed on P105,[25] with PAAs of molecular weights 8500–88 000g mol^{-1}, where a lamellar phase was found in the interval 20–30 wt% PAA, and additional peaks corresponding to a hexagonal structure were found in samples containing 40 and 50 wt% PAA. Significantly, Watkins *et al.* noted—in agreement with our findings here—that no ordered poloxamer structures were induced if PrA, rather than PAA, was added to P105. This also supports the trend, found in the present study, that the poloxamer aggregates are less efficiently destroyed by polymeric PAA, rather than monomeric PrA.

The focus of our studies is on aqueous mixtures and, as mentioned previously, we believe that our method of sample preparation (direct mixing and centrifugation) is not suitable for blending and studying very dry mixtures. Nevertheless, it seems that our results for aqueous P104/PAA mixtures are in good qualitative agreement with the results of Watkins *et al.* on dry P105/PAA mixtures, if we assume that the hexagonal and lamellar phases in Fig. 1 extend all the way out to the binary P104/PAA axis. Quantitative agreement with the phase boundaries should not be expected, since Watkins *et al.* studied a different poloxamer (P105) at a different temperature (80 °C). From this comparison, we would predict that a disordered phase should appear at sufficiently high contents of PAA in the binary system studied by Watkins *et al.*; unfortunately, however, they gave no results for samples containing more than 50 wt% PAA.

Molecular interactions

All binary interactions in the mixtures studied here are highly orientation dependent. Water in itself is a structured solvent. Moreover, the repeating units EO, PO and AA are all amphiphilic, featuring both hydrophobic and hydrophilic functionalities. Thus, we should not expect to reproduce the features of this system in any model that only considers isotropic binary interactions. Even in the considerably simpler mixtures of the homopolymer PEO with PAA in H_2O, there is a long-standing debate on the origin of the observed net attraction between PEO and PAA. Our understanding of the latter issue, summarized

below, is closely analogous the explanation given by Evans and Wennerström[39] for the formation of a stable DNA double helix, with complementary base pairing, in water.

The amphiphilic PEO and PAA polymers both contain important hydrophobic characteristics, and their individual H_2O solubilities are essentially due to the fact that these polymers can hydrogen bond to water. A phase separation from water, driven by hydrophobic interactions, of PEO on its own, or PAA on its own, would thus lead to a loss in the number of hydrogen bonds involving the polymer, which is unfavourable. However, since PAA is a hydrogen bond donor and PEO is a hydrogen bond acceptor, a hydrophobically driven phase separation of the PAA-PEO *pair* can occur without a net loss in the number of hydrogen bonds in the mixture, since hydrogen bonds with the solvent are now replaced by hydrogen bonds between AA and EO residues. The lack of association between PAA and PEO that is observed in certain non-aqueous solvent such as dioxane[40] and dimethylsulfoxide[41] is, from this perspective, not due to a competing hydrogen bonding between solvent molecules and PAA—as is sometimes proposed[41]—but, rather, to a lack of a strong solvophobic interaction in these other solvents.

Returning to the interactions in aqueous poloxamer/PAA mixtures, available phase studies, including the present one, imply that there is a net attraction between PAA and PPO in water (otherwise, PAA would not penetrate the PPO core of the poloxamer aggregates, as is observed here at high PAA contents), but at the same time, this net attraction is less strong than the net attraction between PAA and PEO (since there seems to be a preference of PAA for the PEO corona). We have found few studies of aqueous mixtures of PAA and PPO. However, Satio concluded, based on cloud-point measurements, that there was a weak complexation between PAA and PPO in water.[42] He found a much stronger complexation between PPO and the more hydrophobic poly(methacrylic acid). A complexation of the latter pair in water was also found by Shenkov *et al.*[43] As regards the inferred preference of PAA for PEO over PPO, Costa *et al.* indeed concluded, in their recent fluorescence studies on dilute aqueous mixtures of pyrene-labeled PAA with Pluronic® P123, that there was a preference of the PAA chain to reside in the PEO corona of the aqueous P123 micelles.[44]

Conclusions

The influence of the polymer PAA on the phase behaviour of the poloxamer P104 has been investigated, using two different PAA chain lengths. Two main trends were found: an associative phase separation between P104 and PAA, and a destruction of long-range order and of poloxamer self-assembly. As expected, the phase separation was stronger for the higher molecular weight of PAA. Owing to the destruction of the ordered structures, the concentrated phase that separates out from water-rich PAA–P104 mixtures has no long-range order. This is different from the situation when silica is polymerised in water-rich poloxamer solutions, where ordered concentrated phases typically separate out.

We are not aware of any previous studies where the replacement of a solvent by a polymer has been found to lead to a *weaker* segregation between the blocks of a block copolymer. We conclude that PAA is a less selective environment than water, but there is still a preference for PEO, confirmed by the persistence of the structure in the drier mixtures. The destruction of order was weaker for a higher molecular weight of PAA. Owing to a larger entropy of mixing, PrA destroys the structure even more effectively also in the dry region as was confirmed by previously published studies.

A bicontinuous cubic phase, previously not seen for P104 at any temperature in any environment, was found with short PAA, close to the order-disorder boundary.

Appendix

Derivation of eqn (7)

Fig. A1 shows a cross-section of a hexagonal array of poloxamer rods of infinite length. Surrounding the PPO core of a rod is a corona of PEO chains. Added PAA or H_2O molecules may, in general, reside anywhere in the system: in the core or the corona. We will now consider a repeating unit of the hexagonal structure, with a cross-sectional area given by the rhomb in the Fig. A1, and a height (perpendicular to the plane of the figure) of l. The repeating unit contains n_{P104} poloxamer molecules, n_{AA} repeating units of PAA, and n_{H2O} water molecules. The center-to-center distance between two neighbouring cylinders is d. When we add water or PAA, both d and l may, in general, vary. The total volume of the repeating unit, V_{ru}, may be expressed in terms of l and d

$$V_{ru} = (3^{1/2}/2)d^2 l \tag{A1}$$

and, also, in terms of the numbers of molecules or PAA units it contains and their molecular volumes,

$$V_{ru} = n_{P104}v_{P104} + n_{H2O}v_{H2O} + n_{AA}v_{AA} \tag{A2}$$

Here v_{P104}, v_{H2O} and v_{AA} are the partial molecular volumes of the poloxamer, the water molecule and the repeating unit of PAA, respectively. The volume fraction of poloxamer in the system, ϕ_{P104}, may be written as

$$\phi_{P104} = n_{P104}v_{P104}/(n_{P104}v_{P104} + n_{H2O}v_{H2O} + n_{AA}v_{AA}) = n_{P104}v_{P104}/V_{ru} \tag{A3}$$

From eqn (A1)–(A3), we obtain

$$d^2 = (2/3^{1/2})V_{ru}/l = (2/3^{1/2})n_{P104}v_{P104}/l\phi_{P104} \tag{A4}$$

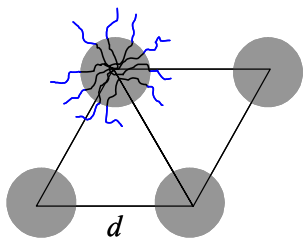

Fig. A1 A cross-sectional rhomb-shaped area of a hexagonal structure.

Acknowledgements

This study was funded by Fundação para a Ciência e a Tecnologia (SS, SFRH/BD/30929/2006) and by the Swedish Research council. We want to thank Jens Norrman for valuable discussions. We thank Mehran Asad Ayoubi and Tomás Plivelic for help with the SAXS measurements at the Max II Laboratory in Lund and Ingrid Åslund for help with the NMR measurements.

References

1 G. Decher, *Science*, 1997, **277**, 1232–1237.
2 K. Edler, *Aust. J. Chem.*, 2005, **58**, 627–643.
3 H.-P. Hentze and M. Antonietti, *Curr. Opin. Solid State Mater. Sci.*, 2001, **5**, 343–353.
4 A. Thomas, F. Goettmann and M. Antonietti, *Chem. Mater.*, 2008, **20**, 738–755.
5 L. Piculell, A. Svensson, J. Norrman, J. S. Bernardes, L. Karlsson and W. Loh, *Pure Appl. Chem.*, 2007, **79**, 1419–1434.
6 S. Marchioretto and J. Blakely, *SOFW Journal*, 1997, **123**, 811–812, 814–816, 818.
7 Y. Hiwatari, K. Yoshida, T. Akutsu, M. Yabu and S. Iwai, *Int. J. Cosmet. Sci.*, 2004, **26**, 316.
8 J. C. T. Kwak, *Polymer-Surfactant Systems*, Marcel Dekker, New York, 1998.
9 P. M. Claesson, A. Dedinaite, R. Meszaros and I. Varga, *Colloids and Interface Science Series*, 2007, **3**(Colloid Stability and Application in Pharmacy), 337–395.
10 D. Langevin, *Adv. Colloid Interface Sci.*, 2009, **147–148**, 170–177.
11 R. J. Hefford, *Polymer*, 1984, **25**, 979–984.
12 D. F. Anghel and Sjuji Saito, *Recent Res. Devel. Surface & Colloids*, 2004, **1**, 301–322.
13 A. N. Galatanu, I. S. Chronakis, D. F. Anghel and A. Khan, *Langmuir*, 2000, **16**, 4922–4928.
14 D. Y. Zhao, J. L. Feng, Q. S. Huo, N. Melosh, G. H. Fredrickson, B. F. Chmelka and G. D. Stucky, *Science*, 1998, **279**, 548–552.
15 K. Flodström and V. Alfredsson, *Microporous Mesoporous Mater.*, 2003, **59**, 167–176.
16 P. Linton and V. Alfredsson, *Chem. Mater.*, 2008, **20**, 2878–2880.
17 D. Zhao, Q. Huo, J. Feng, B. F. Chmelka and G. D. Stucky, *J. Am. Chem. Soc.*, 1998, **120**, 6024–6036.
18 G. Wanka, H. Hoffmann and W. Ulbricht, *Macromolecules*, 1994, **27**, 4145–4159.
19 B. Svensson, P. Alexandridis and U. Olsson, *J. Phys. Chem. B*, 1998, **102**, 7541–7548.
20 M. L. Cole and T. L. Whateley, *J. Colloid Interface Sci.*, 1996, **180**, 421–427.
21 R. Barreiro-Iglesias, C. Alvarez-Lorenzo and A. Concheiro, *Int. J. Pharm.*, 2003, **258**, 165–177.
22 Y. Wang, E. J. Goethals and F. E. Du Prez, *Macromol. Chem. Phys.*, 2004, **205**, 1774–1781.
23 M. K. Chun, C. S. Cho and H. K. Choi, *J. Appl. Polym. Sci.*, 2001, **79**, 1525–1530.
24 V. R. Tirumala, A. Ronang, S. Agarwal, E. K. Lin and J. J. Watkins, *Adv. Mater.*, 2008, **20**, 1603–1608.
25 V. R. Tirumala, V. Daga, A. W. Bosse, A. Romang, J. Ilavsky, E. K. Lin and J. J. Watkins, *Macromolecules*, 2008, **41**, 7978–7985.
26 M. Knaapila, C. Svensson, J. Barauskas, M. Zackrisson, S. S. Nielsen, K. N. Toft, B. Vestergaard, L. Arleth, U. Olsson, J. S. Pedersen and Y. Cerenius, *J. Synchrotron Radiat.*, 2009, **16**, 498–504.
27 E. O. Stejskal and J. E. Tanner, *J. Chem. Phys.*, 1965, **42**, 288–292.
28 M. Nilsson, B. Hakansson, O. Soderman and D. Topgaard, *Macromolecules*, 2007, **40**, 8250–8258.
29 R. Ivanova, B. Lindman and P. Alexandridis, *Langmuir*, 2000, **16**, 3660–3775.
30 R. Ivanova, P. Alexandridis and B. Lindman, *Colloids Surf., A*, 2001, **183–185**, 41–53.
31 P. Alexandridis, U. Olsson and B. Lindman, *Macromolecules*, 1995, **28**, 7700.
32 P. Alexandridis, U. Olsson and B. Lindman, *Langmuir*, 1998, **14**, 2627–2638.
33 B. Chu, *Langmuir*, 1995, **11**, 414–421.
34 S. Ruthstein, V. Frydman and D. Goldfarb, *J. Phys. Chem. B*, 2004, **108**, 9016–9022.
35 M. J. Park, J. Bang, T. Harada, K. Char and T. P. Lodge, *Macromolecules*, 2004, **37**, 9064–9075.
36 K. Mortensen, W. Batsberg and S. Hvidt, *Macromolecules*, 2008, **41**, 1720–1727.
37 P. Alexandridis, *Macromolecules*, 1998, **31**, 6935–6942.
38 J. Norrman, I. Lynch and L. Piculell, *J. Phys. Chem. B*, 2007, **111**, 8402–8410.
39 *Colloidal Domain: where physics, chemistry, biology and technology meet*, Wiley-VCH, 1999, ed. D. F. Evans and H. Wennerström, pp. 383–386.
40 Y. Cohen and V. Prevysh, *Acta Polym.*, 1998, **49**, 539–543.
41 Pradip, C. Maltesh, P. Somasundaran, R. A. Kulkarni and S. Gundiah, *Langmuir*, 1991, **7**, 2108–2111.
42 S. Saito, *Colloids and Surfaces*, 1986, **19**, 351–357.
43 S. Shenkov and V. Y. Baranovski, *J. Polym. Sci., Part A: Polym. Chem.*, 1994, **32**, 1385–1387.
44 T. Costa, K. Schillén, M. G. Miguel, B. Lindman and J. Seixas de Melo, *J. Phys. Chem. B*, 2009, **113**, 6194–6204.

Paper II

CREATED USING THE RSC ARTICLE TEMPLATE (VER. 3.1) - SEE WWW.RSC.ORG/ELECTRONICFILES FOR DETAILS

ARTICLE TYPE www.rsc.org/xxxxxx | XXXXXXXX

Phase behaviour and rheological properties of DNA-cationic polysaccharide mixtures: formation of highly viscolelastic solutions

Salomé dos Santos[a], Lennart Piculell[a], Bruno Medronho[a,b], M. Graça Miguel[b] and Björn Lindman[a,b]

Received (in XXX, XXX) Xth XXXXXXXXX 200X, Accepted Xth XXXXXXXXX 200X
First published on the web Xth XXXXXXXXX 200X
DOI: 10.1039/b000000x

Associative aqueous mixtures of double- (ds) or single- (ss) stranded DNA with dilute or semidilute solutions of two cationic derivatives of hydroxyethyl cellulose (cat-HEC and cat-HMHEC, the latter carrying hydrophobic groups), were studied. The phase behaviour showed an interesting asymmetry: phase separation occurred immediately when only small substoichiometric amounts of cationic polyelectrolyte were added to the DNA solution, but with a modest charge excess of the cationic polyelectrolyte, a redissolution into a single cat-(HM)HEC/DNA phase occurred at a charge ratio that was approximately independent of the overall polyelectrolyte concentration. Cat-HEC/dsDNA/H_2O and cat-HEC/ssDNA/H_2O systems presented a considerable difference in the extension of the phase separation region. The one-phase samples with excess cationic polyelectrolyte were studied by rheology. The presence of DNA strengthened the viscoelastic behaviour of the solutions of the cationic polyelectrolytes, reflected in an increase in storage modulus (G') and viscosity (η). Differences in phase behaviour and rheology were observed, particularly between systems containing cat-HEC or cat-HMHEC, but also between ssDNA and dsDNA. An interesting non-monotonic rheological behaviour on increasing the cat-HEC concentration was found for single-phase cat-HEC/dsDNA/H_2O mixtures containing excess cat-HEC.

Introduction

Interactions between DNA and positively charged macromolecules have been studied both theoretically and experimentally for several years[1-7] due to the important role played by these interactions in native cells as well as in strategies to purify DNA, formulate DNA for gene therapy and drug delivery, immobilize DNA onto solid supports and design DNA-templated nano-materials, among others[1,2,8]. There is also a strong fundamental interest in understanding the behaviour of mixtures of oppositely charged polyelectrolytes, and for such purposes DNA represents an interesting case where both the charge density and the stiffness of the polyion can be varied by varying the strandedness (double stranded, ds, or single stranded, ss) of DNA.

The strong electrostatic interaction between the oppositely charged entities leads to a strong association that, typically, generates an associative phase separation where a concentrated mixed polyion phase separates out from a more dilute solution. However, the extension of the phase-separation region can vary considerably, depending on the studied system. Often in cases involving DNA, a redissolution of the complexes is seen when a sufficient excess charge from the positive polyelectrolyte and/or the negative DNA is present in the mixture[8,9]. In other cases, however, some of which involve cationic surfactant aggregates (behaving as cationic "polyelectrolytes"), a redissolution is not seen even for a very large excess of charge[9,10,11]. Clearly, strategies to reversibly bring DNA complexes out of solution, and to formulate such complexes in redissolved single-phase solutions, are of interest.

In the present study, we have mixed double- or single-stranded DNA with two common cationic hydroxyethyl cellulose derivatives, one of which also contains hydrophobic side chains attached to the cationic substituents. The behaviours of these cationic polymers (here referred to individually as cat-HEC or cat-HMHEC, and collectively as cat-(HM)HEC) in mixtures with other negatively charged polyelectrolytes[12,13] and surfactants[14] have been well studied and serve as useful references for the present study. We extended the previous research[15] by thoroughly studying the phase behaviour and the rheology of single-phase mixtures, in a range of concentrations extending to the semidilute range of the cat-(HM)HECs.

Experimental

Materials

DNA type XIV from herring testes, in the salt form (Sigma), was used as received. In a previous study[10], gel electrophoresis showed this type of DNA to be polydisperse, with a range between 400 and 1000 base pairs (bp) and a centre of the distribution at *ca*. 700bp. The molecular weight corresponding to 700 bp is 462000 g/mol. The two cationic cellulose derivatives JR400 (cat-HEC) and Quatrisoft LM200 (cat-HMHEC) (Union Carbide Chemicals and Plastics Company, Inc.) are *N,N,N*-trimethylammonium and *N,N*-dimethyl-*N*-dodecylammonium derivatives of hydroxyethyl cellulose, respectively. The characteristics of the polyelectrolytes used are collected in Table 1. Note that both

Table 1 Structural parameters for the polymers.

	cat-HEC	cat-HMHEC	dsDNA	ssDNA
Mw (g/mol)	500 000 [a]	100 000 [b]	462 000[c]	231 000[c]
Contour length (nm)	1000[a]	200[a]		
Mean contour length between charge (nm)	2[a]	10[a]		
Charge/chain	(+)500[d]	(+)20[d]	(-)1400[e]	(-)700[e]
Persistence length (nm)			30-50[f]	0.75-8.5[f]
Charge concentration in a 1wt % solution (mM)	11.25[g]	2.88 or 2.52[g]		
Overlap concentration (wt%)		2[h]		
Water content	5.1%[i]	4.8%[i]		
Salt content	1.5%NaCl[i] + 1.5%Na acetate[i]	1.5%NaCl[i] + 1.5%Na acetate[i]		

[a] Reference 12 and 25

[b] Reference 23

[c] 1 base pair=2 nucleotides; ds: 700 base pairs × 2 × 330g/mol; ss: 700 nucleotides × 330g/mol

[d] Charge/chain≅Contour length/Mean contour length between charge

[e] One charge per nucleotide

[f] Reference 1 (page 29-31 and 51-52)

[g] Determined by nitrogen elemental analysis using gas-liquid chromatography and a thermal conductivity detector. Two cat-HMHEC batches were used.

[h] Reference 26

[i] From the supplier

charge density and molecular weight were higher for cat-HEC than for cat-HMHEC, and that cat-HMHEC is hydrophobically modified through the dodecyl groups attached to the nitrogen in the charged quaternary ammonium substituent. Millipore filtered water was used throughout the study. Sample preparations and all experiments were performed at room temperature.

Methods

DNA solutions

Stock solutions of DNA were prepared and their concentrations in mM of nucleotide (which equals the equivalent concentration of charged units) were determined by ultraviolet absorption at 260 nm using a molar extinction coefficient of 6600 $M^{-1}cm^{-1}$ for double-stranded and 8700 $M^{-1}cm^{-1}$ for single-stranded DNA[16]. The ratioA_{260}/A_{280} was determined to be higher than 1.8, which suggests that DNA solutions are protein-free[16].

Weight percent concentrations of DNA were calculated from the equivalent concentrations assuming an average molecular weight of 330 g/mol for the nucleotides. Single-stranded DNA stock solutions were prepared by thermal denaturation of a dsDNA stock solution at 75ºC for 20 minutes, which was then immediately immersed into ice for fast cooling, in order to prevent renaturation. With this procedure it is possible to obtain stable ssDNA solutions as reported elsewhere[11]. The thermal stability of DNA was investigated by UV absorbance at 260 nm in thermal denaturation experiments. The inflection point of the sigmoidal temperature curve is denoted as the melting temperature.

Phase behaviour

Each of the two cat-(HM)HECs was mixed with either single- or double- stranded DNA. Several samples were individually prepared by mixing DNA stock solutions with the desired amount of cat-(HM)HEC added as a powder, unless otherwise stated. (Alternative preparation methods were used to test for a possible history-dependence, see below.) The equivalent charge concentration of cat-(HM)HEC was calculated from the weight percent values using equivalent molar masses of 889g/eq for cat-HEC and 3472g/eq and 3968g/eq for cat-HMHEC (two different batches were used). After approximately 5 minutes in the vortex mixer, the samples were placed in a platform stirrer and after 24 hours they were centrifuged at 4000 rpm for about 2 hours. This procedure was repeated a second time in order to ensure complete mixing. The samples were then stored at room temperature and left to equilibrate for several weeks. After this period, samples showing no visible turbidity or macroscopic phase separation were considered monophasic. The phase behaviour observed was reproducible and the samples did not change (periodic visual inspection) for more than a year. Weight measurements of both top and bottom phases in the phase separation region were made for samples containing 2.66 mM of DNA and different amounts of cat-(HM)HEC. Measurements of DNA concentration in the top phase were done for samples containing 2.64 mM of DNA and different amounts of cat-(HM)HEC.

Rheology Measurements

Linear (oscillatory) and nonlinear (rotational) experiments on monophasic samples were conducted at 25ºC in a Rheologica StressTech rheometer with an automatic gap setting. A cone-and-plate measuring geometry (1º, 50 mm diameter) was used for all measurements. The frequency dependences of the storage (G') and loss (G'') moduli and the complex viscosity ($\eta^* = (G'^2 + G''^2)^{1/2}/2\pi f$, where f is the frequency of oscillation) were recorded in the oscillatory measurements. All measurements were performed within the viscoelastic linear regime previously investigated by stress sweep experiments over a range of shear stresses from 0.2 to 10Pa.

The shear viscosity (η) of the samples was determined in nonlinear rotational measurements.

Results

Stability of the DNA conformation

Since one aspect of the present work concerns comparisons between ssDNA and dsDNA in their mixtures with cat-(HM)HECs, we investigated whether the addition of cat-HEC in any way influenced the DNA conformation. Recordings of the UV absorption at 260 nm with increasing temperature (not shown) for selected mixtures confirmed that the DNA kept its original conformation when mixed with the cat-HEC: no change in absorption on heating up to 90°C was observed for the mixtures with ssDNA, whereas a sigmoidal increase at elevated temperatures, indicating DNA melting, was seen for dsDNA. Notably, the presence of the cationic polyelectrolyte stabilised the dsDNA helix, as manifested by an increased melting temperature. The stabilization of the dsDNA by the interaction with polycations has been reported in the work of Kabanov et al[8].

Phase behaviour

General features

Quasi-ternary phase maps are presented in Figure 1 for three of the studied mixtures. The full three-dimensional phase diagrams, giving also the full ionic compositions of the coexisting phases in the regions of phase separation, are outside the scope of the present study. The system cat-HMHEC/ssDNA/H_2O system is not shown, since it was studied in less detail. However, for the compositions studied, its phase behaviour closely resembled that of the corresponding system with dsDNA. Two alternative representations of each diagram are presented, using either the weight percent or the equivalent charge concentration of the polyelectrolytes as concentration units - both being of fundamental interest. Note that the mass per unit charge is much smaller for DNA than for cat-HEC or cat-HMHEC. The highest DNA concentration used was 4.5 mM (0.14 wt%). The lowest cationic polyelectrolyte and DNA concentrations used were 0.213 mM (0.0189 wt%) for cat-HEC, 0.274 mM (0.0951 wt%) for cat-HMHEC and 0.5 mM (0.016 wt%) for DNA. At concentrations below 0.5 mM, DNA is single-stranded in the absence of added salt[11].

Each polyelectrolyte alone was soluble in water, but all mixed systems presented wide regions of associative phase separation in the phase maps. In these regions, denser concentrated phases, enriched in both DNA and in cat-(HM)HEC, settled from more dilute solutions. Notably, all phase maps showed an asymmetry with respect to charge stoichiometry. Accordingly, we saw that only very minor additions of cat-(HM)HEC to DNA solutions lead to phase separation, while mixtures dominated by the cationic polyelectrolytes did not phase separate on addition of DNA until some distinct global stoichiometry (charge ratio) of the mixture was reached. Hence, the boundary separating the phase-separation region from the single-phase region rich in cat-(HM)HEC generally appeared as an almost straight line for all systems, in the range of compositions studied. For reference, charge equivalence lines, denoting systems containing equal amounts of DNA and cat-(HM)HEC charges, are shown in all phase maps.

To ensure that the observed phase behaviour was not influenced by the preparation procedure, we performed various control experiments. For cat-HEC/dsDNA/H_2O, we used samples in the phase separation region, prepared following the procedure described above, and added an amount of salt sufficient to dissolve the complex. This mixture was then placed in a dialysis bag and left for dialysis against pure water for some days. After some minutes it was possible to see the re-formation of the concentrated phase. Another approach was to add a solution of cat-HEC, rather than the dry powder (see the Experimental section), to the solution of DNA. Regardless of the preparation method, the observed phase behaviour was always in accordance with the diagrams shown in Figure 1. Lastly, we made control experiments using different batches of cat-HMHEC and using dialysed cationic polyelectrolytes for the phase maps. Indeed, such changes gave rise to measurable shifts in the positions of the phase boundary separating the phase separation region from the one-phase region rich in the cationic polyelectrolyte. However, these shifts were small when compared to the quantitative differences observed between the four different mixtures.

Mixtures with cat-HEC

The two systems containing cat-HEC had much in common apart from the general features presented above. Figure 2 shows a partial characterisation of the compositions of phases found for two series of samples, all containing 2.656 mM (for weight measurements) and 2.64 mM (for determination of DNA concentration) of ds- or ss-DNA but varying concentrations of cat-(HM)HEC, in the regions of phase separation. The x-axis shows the charge ratio, r, of the samples, defined as

r = equivalent concentration of cat-(HM)HEC/equivalent concentration of DNA

The DNA concentration in the dilute phase of two-phase samples was determined by UV absorption measurements at the wavelength of 260 nm and is shown in the left-hand graph of Figure 2. The results show that DNA was present in the dilute phase at charge ratios below unity, i.e., below charge equivalence, and that the concentration of DNA in the dilute phase decreased with increasing charge ratio. Around charge equivalence almost all DNA was removed from the dilute phase. The right-hand graph of Figure 2 shows the percentage of the total mass that was contained in the concentrated phase. Clearly, the relative mass of the concentrated phase was very small at low charge ratios, but the concentrated phase started to swell slightly as the composition approached charge equivalence for both DNA systems. On increasing the cat-HEC content further above charge equivalence, the viscosity of the dilute phase was seen to increase and the concentrated phase became clearer. On increasing the cat-HEC content still

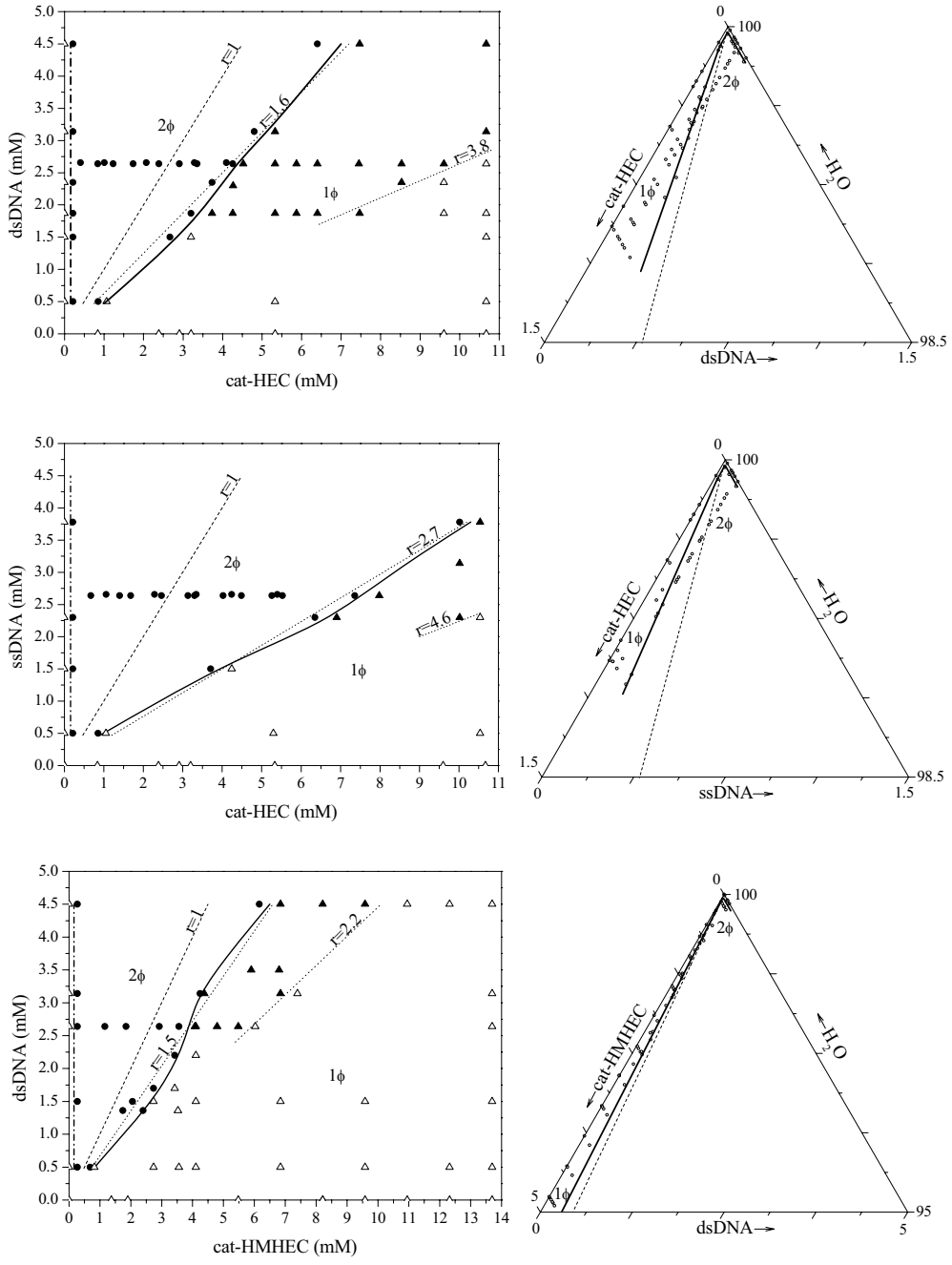

Fig. 1 Experimental phase maps of the cat-(HM)HEC/DNA/H_2O systems. On the left phase maps, the axes give the concentration of charges and, on the right, the ternary phase maps are expressed in weight percent. Triangles – one single phase, filled triangles – bluish samples, filled circles – area of phase separation. The thick solid lines are phase boundaries, the dashed line is the charge equivalence line and the dotted lines are guide-lines for certain charge ratios.

further, two coexisting transparent viscoelastic phases were obtained. These phases were difficult to separate because the interface separating the phases was not sharp even after centrifugation and their viscosities were similar, although the concentrated bottom phase always had a higher viscosity compared to the more dilute top phase. The weight fraction of the concentrated phase was always very low, maximally 12% of the total weight of the sample (see in Figure 2). Further addition of cat-HEC to the system eventually gave rise to an abrupt transition into a one-phase, transparent, viscoelastic solution. At the lowest charge ratios, this one-phase solution was bluish in appearance, but the phase became clear upon further addition of cat-HEC. Some highly viscous bluish solutions were centrifuged for long times (approximately one week) but no sedimentation was observed.

The most obvious difference in phase behaviour between the systems with dsDNA and ssDNA was that the phase separation region was much more extended in the cat-HEC/ssDNA/H_2O system (see Figure 1). The phase separation region ended at a charge ratio r = 1.6 (one dsDNA molecule to 4.4 cat-HEC molecules) for dsDNA but persisted until r = 2.7 (one ssDNA molecule to 3.8 cat-HEC molecules) for ssDNA. The wider phase separation region for ssDNA allowed us to follow the separated phases over a wider range of charge ratios. In addition, Figure 2 shows that the DNA concentration in the dilute phase of the phase-separated ssDNA mixtures increased at charge ratios above charge equivalence.

The transition from bluish to clear one-phase samples did not move as much as the phase boundary with a change of the strandedness of DNA. For dsDNA, the transition occurred at r = 3.8 (one dsDNA molecule to 10.6 cat-HEC molecules) compared to r = 4.6 (one ssDNA to 6.4 cat-HEC molecules) for ssDNA.

Mixtures with cat-HMHEC

The two systems containing cat-HMHEC also presented similar features within the investigated concentration range. The extension of the phase separation region was similar for dsDNA and ssDNA systems. However, the DNA mixtures with cat-HMHEC showed some notable differences compared to the mixtures with cat-HEC. Figure 1 shows that on a weight basis, cat-HMHEC was less effective than cat-HEC to redissolve DNA, whereas, on a charge basis, the trend was the opposite. The formation of a single cat-HMHEC-rich phase in mixtures with ssDNA or dsDNA was seen already a at charge ratio around 1.5 (one dsDNA to 105 cat-HMHEC molecules and one ssDNA to 52.5 cat-HMHEC molecules).

The largest difference between the cat-HMHEC and cat-HEC systems was observed in the features of the phases formed in the phase separation region (see Figure 2). For cat-HMHEC, the DNA concentration in the dilute phase decreased to an almost constant value already at charge ratios far below charge equivalence, where it remained until the one-phase region was reached. Interestingly, for cat-HMHEC the concentrated phase swelled very much as the concentration of cat-HMHEC was increased, particularly above charge neutrality, where a roughly linear increase was seen with increasing charge ratio until the concentrated phase finally "absorbed" all of the dilute phase. In parts of the phase-separation region above r = 1 the concentrated phase(s) seemed to split into one turbid and one transparent layer. It is difficult to know whether this layering represented a true equilibrium behaviour; if so, it could possibly reflect a considerable polydispersity in the degree of substitution of the cat-HMHEC molecules. In any case, at high degrees of swelling, the layering disappeared and the concentrated phase was uniform and clear. The dilute phase was always very dilute, judging from its low viscosity.

Rheology

General features

In Table 2 we present results for rheological measurements for the cat-(HM)HEC in water. For the compositions studied the differences between the two polymers arose for large contents of polymer. For the mixtures with DNA, rheological measurements were conducted on homogeneous samples from the one-phase region rich in cat-(HM)HEC. The linear viscoelastic regime was typically found to extend over the entire shear stress range between 0.2 and 10 Pa. The results from oscillatory measurements generally showed the classical features that have previously been observed for cat-HEC and cat-HMHEC in mixtures with ionic surfactants[14,17] or sodium polyacrylate[12], that is, monotonic increases of G' and G'' with increasing frequency showing a point of intersection at some critical frequency f^* within the accessible frequency range. Figure 3 shows two mechanical spectra for a constant cat-HEC concentration (two different DNA concentrations). An simple but convenient characteristic of the polymer dynamics is the effective relaxation time τ^*, defined as the inverse of the angular frequency ($\tau^* = 1/(2\pi f^*)$) where G' and G'' intersect. At times shorter than τ^*, a solution has a response which is mainly elastic, while at longer times viscous behaviour prevails. While τ^* is not expected to correspond to any simple process on the molecular level for a polydisperse polymer solution[18], it can still be used to indicate differences between samples of different compositions.

We want to note here that for all the experiments the viscosity follows the exact same trend as the G', but for simplicity we decide to plot only the G' (1Hz).

Mixtures with cat-HEC

As mentioned, Figure 3 shows the results from oscillatory measurements on two mixtures containing the same concentration of cat-HEC but different concentrations of dsDNA. The figure illustrates the general trend that both G' (at some fixed frequency) and τ^* increased with increasing DNA concentration at a constant concentration of cat-HEC. Figure 4 summarizes the variations of G' (1Hz) and τ^* with

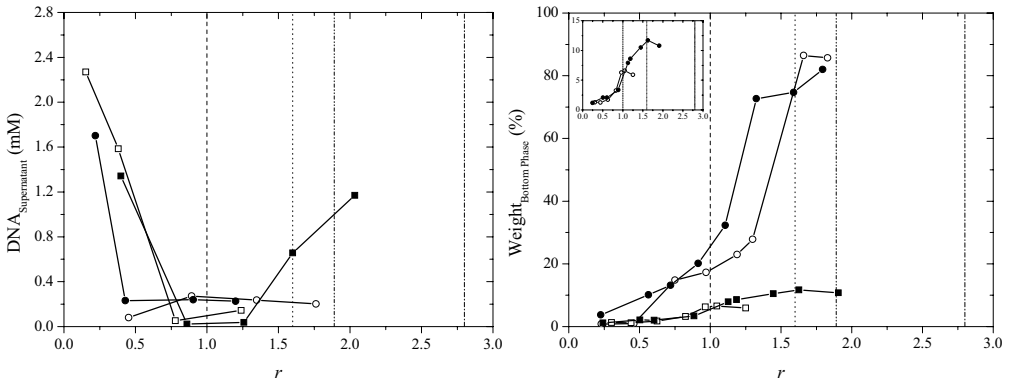

Fig. 2 Weight fraction of the concentrated phase (left) and DNA concentration in the dilute phase (right), within the phase separation region, expressed as a function of the r. Open squares – cat-HEC/dsDNA/H_2O, filled squares – cat-HEC/ssDNA/H_2O, open circles – cat-HMHEC/dsDNA/H_2O and filled circles – cat-HMHEC/ssDNA/H_2O. The vertical lines show the charge equivalence (dash) and other lines show roughly where the redissolution occurs for cat-HEC/dsDNA/H_2O (dot), cat-HEC/ssDNA/H_2O (dash-dot) and cat-HMHEC/DNA/H_2O (dash-dot-dot).

the charge ratio *r* for different compositions of cat-HEC/dsDNA/H_2O mixtures. The left-hand graphs represent systems at three different constant concentrations of dsDNA but varying concentrations of cat-HEC, whereas the right-hand graphs are for constant cat-HEC concentrations and varying dsDNA concentrations. Note that the total polyelectrolyte concentration thus increases with increasing *r* in the left-hand graphs, but decreases with increasing *r* in the right-hand graphs. We recall that the one-phase region for the cat-HEC/dsDNA/H_2O system appeared above a charge ratio equal to 1.6, and the transition from bluish to clear samples at a charge ratio of 3.8; these charge ratios are indicated as dotted lines in Figure 4.

Starting with the right-hand graphs, one can see that the trend in Figure 3 was indeed general in the investigated range of compositions, that is, at a constant cat-HEC concentration, both G' and τ* increased with increasing dsDNA concentration (decreasing *r*). Interestingly, the left-hand set of graphs shows a more complex pattern. The storage modulus showed a pronounced maximum, roughly coinciding with the transition from bluish to clear samples, for all series of samples where the cat-HEC concentration was increased at constant dsDNA concentration. The G' maximum did not change significantly with the total polyelectrolyte concentration. When the charge ratio was increased further in the latter series of samples, G' eventually increased again as can be seen from the results for the highest dsDNA concentration in Figure 3, top left graph, but we did not investigate this further. The relaxation time also showed a maximum with increasing cat-HEC concentration at constant dsDNA concentration (bottom left graph). However, the position of the τ* maximum varied with the total polyelectrolyte concentration as can be clearly observed in Figure 4 (bottom left). At high charge ratios the relaxation time values were very small, but still far enough from the detection limit (*ca* 0.002 s).

In Figure 5 the complex viscosity, η*, as a function of frequency is presented for the series of samples with a constant dsDNA concentration (1.87mM) and varying cat-HEC amounts. All samples showed pronounced shear-thinning but with a frequency-independent plateau at low frequencies within the accessible range. As observed for G', the value of the viscosity plateau went through a maximum with increasing cat-HEC concentration. A wide variety of shear-thinning or shear-thickening fluids can be adequately described by a power law constitutive equation of the form: $\eta^* = k f^{b}$. The three systems corresponding to lower cat-HEC content showed the same slope (b = -0.65) of logη* versus log*f* in the shear-thinning regime at high frequencies. For the samples at higher cat-HEC concentrations, above the viscosity maximum, the high-frequency slope slightly decreased with increasing cat-HEC concentration. The same features described here for the complex viscosity were seen for the apparent viscosity as a function of the shear rate measured in nonlinear rotation experiments (see Figure 6).

We also performed a limited amount of rheology measurements on one-phase mixtures of cat-HEC with ssDNA (not shown), from which the following trends could be established. As for the mixtures with dsDNA, the relaxation time decreased with increasing charge ratios, reaching very low values at high charge ratios. However, for the same global compositions, the ssDNA-containing systems presented generally lower values for G', viscosity and τ*, when compared to the mixtures with dsDNA.

Mixtures with cat-HMHEC

Linear oscillatory measurements were performed on a large set of samples, all found to be viscoelastic, in the cat-

Table 2 Measured G' and viscosity for the aqueous solutions of the cationic polymers alone.

	Composition (wt%-mM)	G'_{1Hz} (Pa)	$Viscosity_{0.1Hz}$ (η*) Pa.s	Shear Viscosity (η) Pa.s
cat-HEC	0.95-10.7	0.03	0.03	
	1.9-21.4	0.15	0.2	0.2
	2.8-31.5	1.2	1	1
	4.7-53.4	9.19	5.9	7.8
cat-HMHEC	1.9-5.5	0.09	0.18	0.18
	2.9-8.4	0.7	0.79	0.8
	4.8-13.8	18.6	11.11	13.16

HMHEC/dsDNA/H_2O system. An overview of our findings is presented in Figure 7, which has the same layout as Figure 4 above, and thus shows G' (1 Hz) and τ* values plotted against *r* for different series of one-phase samples where either the cat-HMHEC concentration was varied at constant dsDNA concentration (left-hand graphs), or the dsDNA concentration was varied at a constant cat-HMHEC concentration (right-hand graphs). In the investigated range of compositions the trends found were simpler for the mixtures with cat-HMHEC than for the mixtures with cat-HEC. Thus, regardless of whether the cat-HEC concentration was varied at constant dsDNA concentration or *vice versa*, τ* increased with increasing *r*, that is, as the sample compositions moved further away from the region of phase separation. The values of G', on the other hand, seemed more sensitive to the total concentration of polyelectrolyte, since G' increased monotonically, in each individual series of measurements, when either more cat-HMHEC or more dsDNA was added at a constant concentration of the other polyelectrolyte.

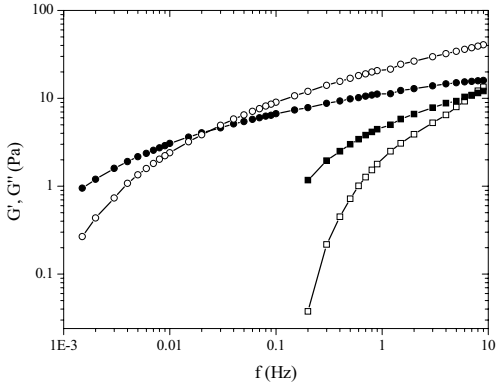

Fig. 3 G' (open symbols) and G'' (filled symbols) as a function of frequency for the samples with constant 10.67mM (0.95 wt%) of cat-HEC and 1.87mM (0.061 wt%) (squares) and 3.14mM of dsDNA (0.0103 wt%) (circles).

Comparing samples composed of cat-HMHEC with samples composed of cat-HEC, the most striking difference is that only the latter mixtures showed a pronounced maximum in G' with increasing concentration of cat-(HM)HEC at a constant concentration of dsDNA. We also observed that at the same dsDNA concentration and for the same value of *r*, both the G' and the τ* values were much higher in the cat-HMHEC systems. However, one must note that the weight per cent concentration of cationic polyelectrolyte was also much higher in the latter systems, owing to the much lower charge density of cat-HMHEC (Table 1).

Again, a more limited set of mixtures of ssDNA with cat-HMHEC were investigated. These showed no significant differences, compared to the corresponding mixtures with dsDNA, as regards G' or viscosity. However, there were some quantitative differences in the effective relaxation times. In both systems, τ* decreased with increasing *r*, but at higher cat-HMHEC concentrations, the values of τ* were significantly smaller for the mixtures with ssDNA.

Discussion

Formulating DNA in mixtures with cationic cellulose derivatives

We have shown in this investigation that it is possible to make formulations of double- or single-stranded DNA with widely different properties by mixing the aqueous DNA with appropriate amounts of the common cationic cellulose derivatives cat-HEC or cat-HMHEC. While phase separation was observed at substoichiometric and intermediate charge ratios of cat-(HM)HEC to DNA, a modest and approximately concentration-independent excess of the cat-(HM)HEC (a charge ratio of 1.5 - 2.7, depending on the system) was sufficient to produce redissolved, highly viscoelastic one-phase mixtures. Previous studies by other groups have found a similar redissolution of DNA by excess cationic polyelectrolyte, but the latter studies were limited to dilute solutions[8,9,19]. Thus, we are not aware of any previous studies reporting highly viscoelastic, almost gel-like mixtures of DNA with cationic polyelectrolytes of the type that we have found here. We have, furthermore, shown that the rheological properties of redissolved mixtures of DNA and the cationic cellulose derivatives can be varied within wide ranges by varying the overall polyelectrolyte concentration and/or the charge ratio. In particular, a non-trivial maximum in the storage modulus and the complex viscosity was observed when increasing the concentration of cat-HEC at a constant concentration of dsDNA.

Turning to the phase separated mixtures, those containing cat-HMHEC at charge ratios in the interval $1 \leq r < 1.5$ seem particularly interesting. In this region, the concentrated phase seems to contain almost all of both the DNA and the cat-HMHEC, but the degree of swelling, that is, the equilibrium water uptake, of this phase can be tuned within wide ranges simply by changing the charge stoichiometry. The highly viscolelastic mixtures containing DNA can be very useful in applications which demand a sustainable release (due to the reduction of the convection effects) of DNA.

In the remaining part of the discussion, our main aim is to

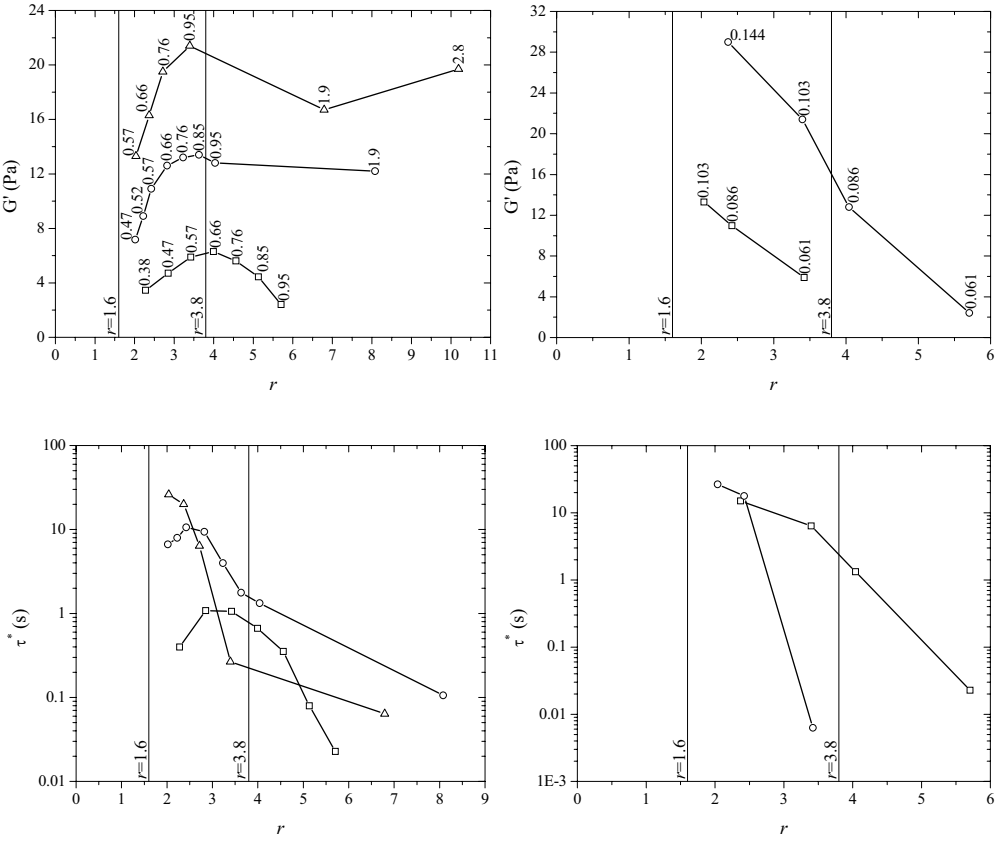

Fig. 4 G' at 1Hz and τ* as a function of r for the cat-HEC/dsDNA/H_2O system. On the left: 1.87 mM (0.061 wt%) (squares), 2.64 mM (0.086 wt%) (circles) and 3.14 mM (0.0103 wt%) (triangles) of dsDNA. On the right: the plots correspond to change of dsDNA concentration for the fixed 6.4 mM (0.57 wt%) (squares) and 10.67 mM (0.95 wt%) (circles) of cat-HEC. The numbers on top of the points are the wt% of the variable component.

identify possible molecular mechanisms that can explain the observed behaviour. For this purpose we will also make more detailed comparisons with previous studies of related systems.

Phase Behaviour

The phase maps established in this work all have the following features in common: the charge stoichiometry is of obvious importance, and at charge equivalence, both polyions separate out from the dilute solution more or less quantitatively into a concentrated phase. On the DNA-rich side of charge equivalence, phase separation occurs in the entire mixing range, even for systems containing very small substoichiometric amounts of cationic polyelectrolyte. On the cat-(HM)HEC rich side, however, a redissolution occurs at a distinct and concentration-independent charge excess of cat-(HM)HEC. It seems clear that the asymmetry in the phase behaviour in aqueous mixtures of DNA and cat-(HM)HEC must have its origin in some difference between the polyions, other than the sign of the charge. A mixture of two polyions differing only in the sign of their charge must necessarily give rise to a symmetric phase diagram (neglecting effects of counterions or the asymmetry of the water molecule).

A well-established cause of asymmetry in phase behaviour is a pronounced difference in the number of charges per molecule of the two polyions. Extensive work by Kabanov and co-workers has shown that mixtures of "host" polyions, containing many charged units, with "guest" polyions, containing much fewer charges, display an asymmetry of the phase behaviour such that soluble complexes are formed when the "host" polymer is in excess, but not when the "guest" polymer is in excess relative to charge equivalence[20]. However, this simple model does not predict the behaviour

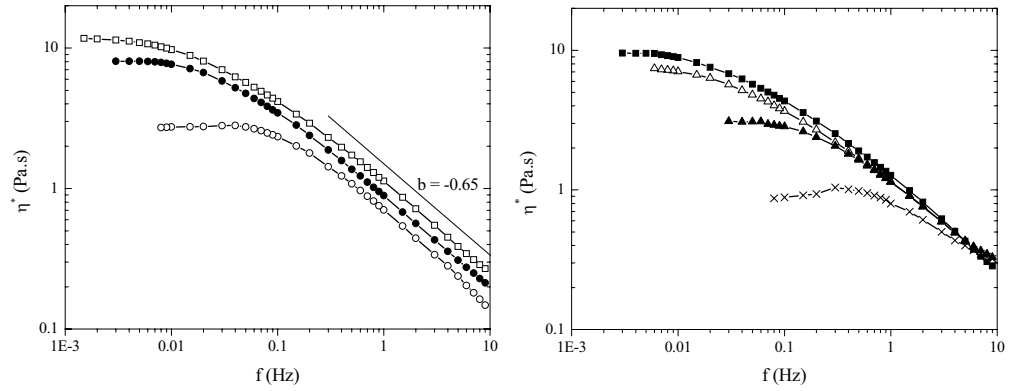

Fig. 5 Complex viscosity as a function of frequency for seven different samples with 1.87mM (0.061wt%) of dsDNA with on the left: 4.26mM (0.38wt%) (open circles), 5.33mM (0.47wt%) (filled circles), 6.4mM (0.57wt%) (open squares) of cat-HEC, and on the right: 7.45mM (0.66wt%) (filled squares), 8.53mM (0.76wt%) (open triangles), 9.6mM (0.85wt%) (filled triangles) and 10.67mM (0.95wt%) (crosses) of cat-HEC.

observed here. Since the ds and ssDNA molecules carry more charges (Table 1), DNA should act as the host polyion, but the observed asymmetry of the phase map is the opposite of that predicted by the guest-host model. Two other obvious molecular asymmetries that could give rise to an asymmetric phase map in the present system are a mismatch in charge density (for all mixtures) and the presence of hydrophobic side groups (for mixtures with cat-HMHEC). Another candidate could be a difference in intrinsic stiffness, but the role of this factor seems less obvious here, since quite similar phase behaviour was observed for ssDNA and dsDNA.

The role of hydrophobic modification of the polyion(s) has been thoroughly investigated for other associating mixtures of polycations with cat-HMHEC, and we believe that this is the key to understanding the mixtures of cat-HMHEC with DNA. Of particular relevance here is the investigation by Thuresson et al of mixtures of cat-HMHEC with poly(acrylate) (PA) or hydrophobically modified poly(acrylate) (HMPA), both with a molecular weight of 150 000 g/mol[12]. The phase map for the mixtures with PA was very similar to that observed here for the mixtures with DNA: a phase separation was observed over most of the PA-rich side of the mixing range. By contrast, highly viscoelastic one-phase mixtures were obtained for only a small charge excess of cat-HMHEC (above $r = 1.1$). The redissolution behaviour on the cat-HMHEC rich side of charge equivalence changed only marginally when PA was replaced by HMPA, but a dramatic difference was observed for HMPA-rich mixtures: the hydrophobic modification of PA led to an efficient redissolution also here.

Mixtures of cat-HMHEC with the anionic surfactant sodium dodecylsulfate (SDS) also shows important analogies with the corresponding mixtures with PA, HMPA or DNA. A thorough phase separation study has shown that on the cat-HMHEC-rich side of charge equivalence, these mixtures redissolve at a fixed stoichiometry of $r = 1.4$ for a range of global concentrations, that is, the boundary between the two-phase region and the cat-HMHEC-rich one-phase region is linear, analogously to what was found here for mixtures with DNA (Figure 1)[14]. Like the mixtures with HMPA, but unlike the mixtures with PA or DNA, the mixtures of cat-HMHEC redissolve at a sufficient excess of SDS (sodium dodecyl sulfate).

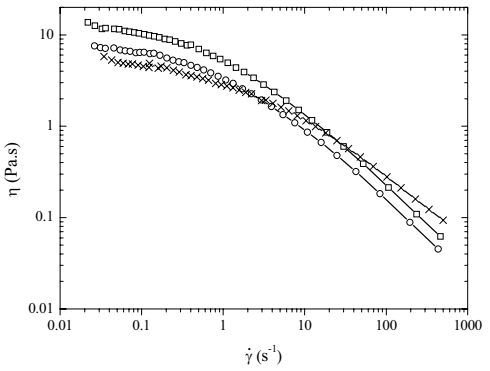

Fig. 6 Shear viscosity as a function of shear rate for three different samples with: 1.87mM (0.061wt%) of dsDNA and 4.26mM (0.38wt%) (open circles), 6.4mM (0.57wt%) (open squares) and 10.67mM (0.95wt%) (crosses) of cat-HEC.

The consistent physical picture that has emerged from the previous studies just mentioned is that, owing to the association between the hydrophobic groups of the cat-HMHEC molecules, this component has a strong tendency to reside almost quantitatively in one and the same phase: if it phase-separates, it does so quantitatively. Thus, when negatively charged polyions are added to a solution of cat-HMHEC, they distribute over the entire network of cat-HMHEC molecules. As charge equivalence is approached by further addition of polyanions, the network contracts and eventually phase separates from a dilute supernatant

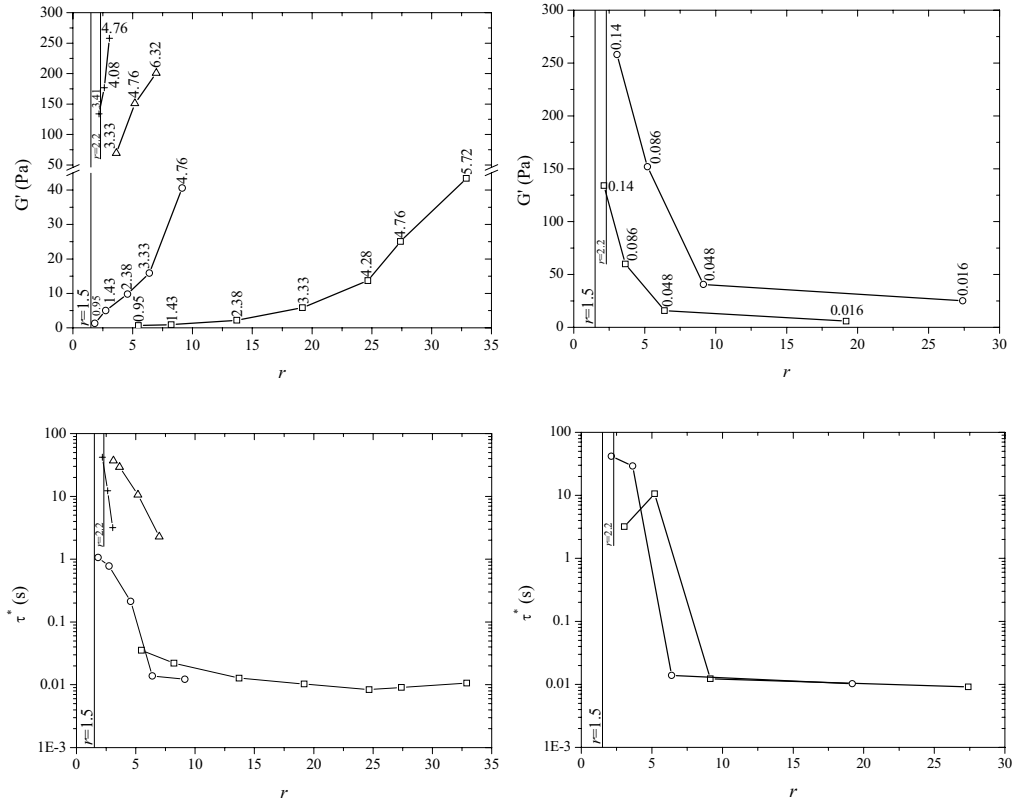

Fig. 7 G' at 1Hz and τ* as a function of the charge ratio (r) for the cat-HMHEC/dsDNA/H_2O system. On the left: filled squares – 0.5mM (0.016wt%), filled circles – 1.5mM (0.048wt%), filled triangles – 2.64mM (0.086wt%) and crosses – 4.5mM (0.14wt%) of dsDNA. On the right, the plots correspond to the change of dsDNA concentration for 9.58mM (3.33wt%) of cat-HMHEC (open squares) and 13.7mM (4.76wt%) of cat-HMHEC (open circles). The bluish samples are located in between the vertical dotted lines. The numbers on top of the points are the wt% of the variable component.

containing, as solutes, essentially only a combination of the original simple counterions of the polyelectrolytes. The concentrated phase then continues to shrink, by eliminating water, until charge equivalence is reached. Here, the osmotic pressure of the mixed network is at a minimum, since the net charge is zero and no excess of small counterions are required to maintain electroneutrality in the concentrated phase. In our study, the scenario just described corresponds to moving from high r to r = 1 for the cat-HMHEC systems in Figure 2. Available experiments show that for this cat-HMHEC-rich part of the phase map, it is unimportant whether or not the polyanion contains hydrophobic moieties; electrostatic interactions alone are sufficient to make the polyanion partition quantitatively to the concentrated phase. Thus, this part of the phase map is very similar regardless of whether the anionic component is PA, HMPA, dsDNA, ssDNA or DS (dodecyl sulfate).

The situation becomes different in the polyanion-rich part of the phase map. Polyanions that contain hydrophobic moieties, such as DS and HMPA, continue to partition strongly to the concentrated phase, associating into mixed hydrophobic aggregates with the cat-HMHEC hydrophobes. The scenario for $r < 1$ then becomes the reverse of that for $r > 1$: both polyions reside in a single mixed polyion network, with an equilibrium water uptake that varies with the net charge of the network. By contrast, if the polyanions do not associate hydrophobically with the cat-HMHEC molecules, they can simply distribute between the dilute and the concentrated phases. Unless this distribution for some reason is very uneven, the concentration of small counterions becomes similar in the two phases, and an osmotic balance is maintained without any transfer of water from the dilute to the concentrated phase. Hence, a phase separation can be maintained even at a very high global excess of polyanions.

This scenario would seem to give a reasonable explanation of the phase behaviour for cat-HMHEC mixed with an excess of DNA or PA.

The interpretation of the phase behaviour for mixtures with cat-HEC is much less clear. While the scenario in the DNA-rich part of the phase map could be the same as that just described for the mixtures with cat-HMHEC, resulting in phase separation over the studied mixing range for $r < 1$, the mechanism for redissolution at $r > 1$ must be different for cat-HEC. This follows not only from the absence of strongly associating hydrophobic side-chains in cat-HEC, but also from the significant differences in the observed redissolution behaviour for cat-HEC, as compared to cat-HMHEC. The recorded phase volumes in Figure 2 (right panel), as well as our observations of a significantly increasing viscosity of the dilute phase, shows that excess cat-HEC does *not* partition quantitatively to the concentrated phase, resulting in a concomitant gradual swelling of that phase. Instead, soluble complexes of cat-HEC and DNA start to form in the dilute phase at $r > 1$. At least close to the one-phase region, the stoichiometry of those soluble complexes should be close to that given by the boundary to the cat-HEC rich one-phase region (r = 1. 6 or r = 2.7 for dsDNA and ssDNA, respectively, independently of concentration). The bluish appearance of the one-phase solutions at the lowest excess of cat-HEC suggests that the redissolved semidilute cat-HEC solutions were still rather inhomogeneous in this region, whereas more homogeneous solutions formed at a larger excess of cat-HEC (above r = 3.8 or r = 4.6 for dsDNA or ssDNA, respectively).

Why such soluble complexes are formed in the cat-HEC-rich part of the phase map, and not in the DNA-rich part, is not clear to us, and relevant previous studies give us little guidance. Many previous studies of mixtures of DNA with polycations deal with very dilute mixtures (10^{-6} - 10^{-3} M DNA). Often the studied mixtures also contained much larger concentrations (10^{-2} M) of neutral salt, and then the phase separation may not be immediately comparable to the behaviour found in the present system. Nevertheless, Raspaud et al found for mixtures of 150 bp DNA with basic protamines or histones an associative phase separation in a narrow region of charge ratios close (but not exactly equal) to charge equivalence. Similar results were found for the same polycations added to dilute solutions of poly(styrene sulphonate)[9]. Thus, in these systems and under these conditions, redissolution occurred both at the polycation-rich side and at the DNA-rich side of charge equivalence. By contrast, measurable phase separation occurred more or less over the entire investigated mixing range ($0.4 \leq r \leq 3.8$) for mixtures of the same polycations with 48 500bp lambda DNA. Izmrudov et al investigated dilute solutions of "highly polymerized" DNA from calf thymus in mixtures with highly charged aliphatic ionene bromides, poly(N,N'-dimethyldiallyammonium chloride) or poly(N-ethyl-4-vinylpyridinium bromide). Without addition of salt, they found insoluble complexes in the range $0.7 < r < 2$ for the mixtures with poly(N,N'-dimethyldiallyammonium chloride) and a broader range of phase separation in the mixtures of DNA with the other two referred above[19]. In mixtures of DNA with cationic surfactants, the immediate phase separation with addition of surfactant was also observed and redissolution was never seen in excess of surfactant[10].

From the previous studies of DNA mixed with polycations we thus conclude that redissolution of water-insoluble DNA-polycation complexes sometimes, but not always, occurs with a sufficient excess of either DNA or polycation. However, we are unable to find any underlying trends correlating with the properties of either the DNA or the polycation.

We should also ask how cat-HEC behaves with other polyanions than DNA. Indeed, cat-HEC has been shown to redissolve phase-separated mixtures with DS micelles at an excess of $r = 2$[21]. However, in the latter case a hydrophobic association between DS micelles and cat-HEC has been established, resulting also in a redissolution in DS-rich mixture - unlike what is here observed for DNA-rich mixtures.

Rheology

To the best of our knowledge, no other rheological study has been performed on semidilute DNA-containing physical networks of the type studied here. However, analogous mixtures of cat-(HM)HECs with other polyanions have been studied[12,13]. On increasing the DNA concentration at constant cat-(HM)HEC concentration, G' and the viscosity increase dramatically, as shown for G' in the right-hand graphs of Figures 4 and 7. Similar effects have been observed for cat-(HM)HECs mixed with SDS,[14,17,22,23], for mixtures of cat-HMHEC with catanionic vesicles,[24] and for mixtures of cat-HMHEC with PA and HMPA[12]. Semi-dilute networks of cat-(HM)HEC molecules are clearly strengthened by electrostatic interactions with the anionic components. We note in this context that at least for mixtures of cat-HMHEC with PA, no additional increase in viscosity was seen for the hydrophobically modified HMPA compared to the unmodified PA[12].

The non-monotonic effect on increasing the cat-HEC concentration at constant dsDNA concentration that we demonstrated here is unusual. This shows that the stoichiometry is important, not just the overall concentration, even in the one-phase region. We recall also that the charge ratio at the maximum was independent on the total concentration of the polyelectrolytes. We can speculate about the origin of this effect. We imagine a dynamic mixed network of cat-HEC and dsDNA molecules, partially swollen by the excess charge of the cat-HEC chains. The decrease in effective relaxation time with increasing cat-HEC concentration signifies that individual cat-HEC chains become less arrested in the network as the excess of cat-HEC (relative to DNA) increases. On the other hand, the value of G' initially increases. The latter effect may be due to an increased swelling and entanglement among the increasing excess of cat-HEC chains. This is supported by the observation that the system becomes more homogeneous (changes from bluish to clear) with increasing cat-HEC concentration. Eventually, however, the crosslinking of DNA molecules by cat-HEC chains diminishes as the concentration of cat-HEC increases. At some point, each DNA molecule becomes saturated by cat-

HEC chains, so that no bridging from one DNA molecule to another by cat-HEC occurs. We are thus making an analogy with polymer bridging in colloidal dispersions; the bridging is not effective at a large excess of the adsorbing polymer. In the limit of high cat-HEC concentrations we can imagine a system with centipede-like complexes, each containing one central DNA molecule with attached cat-HEC chains extending in long tails, dispersed in an entangled solution of excess cat-HEC chains.

The situation is different in mixtures of cat-HMHEC and DNA, since there will always be a continuous associated network of cat-HMHEC molecules through their hydrophobic association. Presumably, this effect is sufficient to give a continuously increasing viscosity with increasing cat-HMHEC concentration also in the presence of a constant concentration of DNA (Figure 7, top left panel – we recall that viscosity follows the trend of G'). We note, however, that also in these mixtures, the effective relaxation time decreases with increasing cat-HMHEC concentration.

Conclusions

From the mixtures of DNA with cat-(HM)HEC we learned that we efficiently redissolve DNA and form strong viscoelastic solutions when cat-(HM)HEC is added to the DNA solutions. Another way to see it is to have DNA in a matrix of cationic polymer. Differences in between ssDNA and dsDNA were found both in phase behaviour and rheology, but the biggest difference between the systems relied on the molecular difference between the cationic polymers. The rheology showed us important differences between the systems which can find applications when controlled rheological properties are required as in DNA release.

Acknowledgments

We thank Fundação para a Ciência e a Tecnologia (&POPH/FSE) for the funding of this project (SS, SRFH/DB/30929). LP acknowledges grants (personal and via the Linnaeus Center of Excellence "Organizing Molecular Matter") from the Swedish Research Council.

References

1 *DNA interactions with polymers and surfactants*, Wiley-Interscience, 2008, ed. R. S. Dias and B. Lindman.
2 L. Zonghua, Z. Ziyong, Z. Changren and J. Yanpeng, *Progress in Polymer Science*, 2010 (in press).
3 M. Carmen Morán, M. Graça Miguel and Björn Lindman, *Soft Matter*, **2010,** 6, 3143 - 3156
4 F. J. Solis and M. Olvera de la Cruz, Eur. Phys. J. E, 2001, 4, 143–152.
5 F. J. Solis, J. Chem. Phys., 2002, 117, 9009–9015.
6 R. Zhang and B. I. Shklovskii, Phys. A, 2005, 352, 216–238.
7 Dan Lundberg, Anna M. Carnerup, Karin Schillén, Maria da Graça Miguel, and Bjorn Lindman, Langmuir, 2010, 26, 2986–2988.
8 A. V. Kabanov and V. A. Kabanov *Bioconjugate Chem.*, 1995, 6, 7-20.
9 E. Raspaud, J. Pelta, M. De Frutos, and F. Livolant, *Physical Review Letters* 2006, PRL 97, 068103.
10 Rita Dias, Sergey Mel'nikov, Björn Lindman and Maria G. Miguel, *Langmuir*, 2000, 16, 9577-9583)
11 Mónica Rosa, Rita Dias, Maria da Graça Miguel and Björn Lindman, *Biomacromolecules* 2005, 6, 2164-2171.
12 K. Thuresson, S. Nilsson and B. Lindman, *Langmuir*, 1996, 12, 530-537.
13 M. Tsianou, A.-L. Kjöniksen, K. Thuresson and B. Nyström, Macromolecules, 1999, 32, 2974-2982.
14 F. Guillemet, and L. Piculell, *J. Phys. Chem.*, 1995, 99, 9201-9209.
15 Diana Costa, Salomé dos Santos, Filipe E. Antunes , Maria G. Miguel, and Björn Lindman Issue in Honor of Prof. Armand Lattes ARKIVOC 2006 (iv) 161-172.
16 Sambrook, J., Russell, D. W. Molecular cloning: a laboratory manual, 3rd ed., Cold Spring Harbor Laboratory Press: New York, 2001, Vol. 1.
17 M. Tsianou and P. Alexandridis, *Langmuir*, 1999, 15, 8105-8112.
18 Larson R. G., *The structure and rheology of complex fluids*, Oxford University Press: New York, 1999.
19 V. A. Izumrudov, P.-O. Wahlund, P.-E. Gustavsson, P.-O Larsson, and I. Yu. Galaev Langmuir 2003, 19, 4733-4739.
20 A. V. Kabanov and A. B. Zezin, Makromol. Chem. Suppl. 1984 6, 259-276.
21 A. Svensson, J. Sjöström, T. Scheel, and L. Piculell *Colloids and surfaces A: Physcochem. Eng Aspects*, 2003, 228, 91-106.
22 P. S. Leung and E. D. Goddard, *Langmuir*, 1991, 7, 608-609.
23 E. D. Goddard and P. S. Leung, *Colloids and Surfaces*, 1992, 65, 211-219.
24 Antunes, F. E., Lindman, B. and Miguel, M. G., *Langmuir* 2005, 21, 10188-10196.
25 S. Dhoot, E. D. Goddard, D.S. Murphy and M. Tirrel, *Colloids Surf*, 1992, 66, 91.
26 C. Alvarez-Lorenzo, R. Duro, J. L. Goméz-Amoza, R. Mertínez-Pacheco and C. C. A. Souto, *Colloid Polym Sci*, 2001, 279, 1045.

Notes

[a] *Division of Physical Chemistry, Center for Chemistry and Chemical Engineering, Lund University, P.O.Box 124, SE-22100 Lund, Sweden. E-mails: Salome.Santos@fkem1.lu.se , Lennart.Piculell@fkem1.lu.se & Bjorn.Lindman@fkem1.lu.se*
[b] *Chemistry Department, Coimbra University, 3004-535 Coimbra, Portugal. E-mail: mgmiguel@ci.uc.pt, bfmedronho@portugalmail.pt*

Paper III

When do Water-Insoluble Polyion-Surfactant Ion Complex Salts "Redissolve" by Added Excess Surfactant?

Salomé dos Santos, Charlotte Gustavsson, Christian Gudmundsson, Per Linse and Lennart Piculell*

*Corresponding author

Division of Physical Chemistry, Center for Chemistry and Chemical Engineering, Lund University, P.O. Box 124, SE-22100 Lund, Sweden

Abstract

The redissolution of water-insoluble polyion-surfactant ion complexes by added excess of surfactant have systematically been investigated by experimental and theoretical phase equilibrium studies. A number of stoichiometric polyion-surfactant ion "complex salts" were synthesized, consisting of akyltrimethylammonium surfactant ions of two different alkyl chain lengths ($C_{12}TA^+$ and $C_{16}TA^+$) combined with homopolyions of polyacrylate of two different lengths (PA^-_{25} and PA^-_{6000}) or copolyions of acrylate and the slightly hydrophobic nonionic comonomers *N*-isopropylacrylamide (PA^--co-NIPAM) or *N*,*N*-dimethylacrylamide (PA^--co-DAM). The complex salts were mixed with water and excess alkyltrimethylammonium surfactant with either bromide or acetate counterions (C_nTABr or C_nTAAc). Factors promoting efficent redissolution were (i) very short polyions, (ii) a large fraction of NIPAM or DAM co-monomers and (iii) acetate, rather than bromide, as the surfactant counterion. Added C_{12}TAAc gave an efficient redissolution of $C_{12}TAPA_{25}$ but virtually no redissolution of $C_{12}TAPA_{6000}$. A very efficient redissolution by added C_{12}TAAc was obtained for PA^--co-NIPAM with 82 mol% of NIPAM. The C_{12}TAPA-co-NIPAM/C_{12}TAAc/H_2O ternary phase diagram closely resembled the corresponding diagram for the much-studied pair cationic hydroxyethyl cellulose – (sodium) dodecyl sulfate. The simple Flory-Huggins theory adopted for polyelectrolyte systems successfully reproduced the main features of the experimental phase diagrams for the homopolyion systems, including the effect of the surfactant counterion. The efficient redissolution found for certain copolyion systems was explained by the formation of soluble polyion–surfactant ion complexes carrying an excess of surfactant ions through an additional hydrophobic attraction.

1. Introduction

Oppositely charged polymer-surfactant systems are used as rheology modifiers, gelling agents, colloidal stabilizers and surface deposition agents in a wide range of applied contexts, including pharmaceutics, foods, personal care products and waste water treatment [1-7]. The fundamental feature of the system that is utilized in all these contexts is the strong attraction between the charged polyions and the oppositely charged surfactant ion aggregates, both containing multiple charges leading to extensive association in the system. Obviously, an essential property to control is the phase behavior of the mixture. Typically, a concentrated polyion-surfactant ion phase separates out under mixing conditions when a stoichiometric and neutral polyion-surfactant ion complex is formed. However, the situation for off-stoichiometric mixtures may vary widely, depending on the system, as will be amply exemplified below. Certain off-stoichiometric systems produce single-phase solutions, whereas other systems remain phase separated at practically all mixing ratios. These differences are widely utilized. In some applications off-stoichiometric single-phase solutions are desired, for instance in the form of highly viscous physical networks. Under other circumstances one may want a complex that remains insoluble, for instance as a surface coating at wide variations of the system composition. Indeed, important applications, such as hair care products or laundry detergents, use formulations that effectively switch from one-phase mixtures to phase-separated mixtures by a simple operation such as a dilution of the system [6]. Typically, the initial one-phase formulation in the latter applications contains a large excess of surfactant.

The above background serves to justify why the present study focuses on the phenomenon that we will refer to as "surfactant redissolution", i.e., when the addition an excess of surfactant to an associatively phase-separated stoichiometric polyion-surfactant ion complex leads to its transformation into a single-phase solution. As we have indicated, the capability for the surfactant to redissolve the complex varies greatly from system to system and the underlying physics is poorly understood. The ability to understand and control this variation is of considerable interest for applications, such as those mentioned above. The phase behavior of polymer-surfactant mixtures is also a problem of fundamental importance in polymer and colloid science.

Experimentally, the redissolution phenomenon is also insufficiently characterized. Many studies of phase separation and redissolution phenomena of oppositely charged polymer-surfactant mixtures have dealt with dilute systems, where the surfactant concentration has been varied at some constant low concentration of the polyelectrolyte [8-11]. Turbidity, light scattering and/or zeta potential measurements in such studies typically show re-entrant phenomena, where soluble or colloidally stable complexes bearing a net charge are formed for

strongly non-stoichiometric mixtures, whereas turbid dispersions of large aggregates or even macroscopically phase separated systems result under mixing conditions where net neutral complexes are formed. In some cases it seems clear that truly redissolved complexes form at high surfactant concentrations; in particular, it has been demonstrated that an additional hydrophobic interaction between the polyion and the surfactant ion aggregate can facilitate an excess binding and a redissolution of the polyion [10-12]. Additional evidence for a true redissolution has come from gel swelling experiments, where a re-entrant compaction and re-swelling of gels immersed in surfactant solutions of increasing concentration have demonstrated an additional surfactant binding step above charge neutralization, leading to a strong effective repulsion between "overcharged" polyion-surfactant ion complexes [13-15]. In other cases, however, investigators of dilute mixtures have concluded that apparently redissolved complexes were, in reality, non-equilibrium dispersions of particles of the concentrated phase, stabilized by a surface covered with excess surfactant [9]. In addition to the difficulties to distinguish between equilibrium and non-equilibrium systems, a weakness with studies on dilute systems is that the composition of the separated phase is typically not determined. While zeta potential measurements detect excesses of polyions or surfactant ions that often arise at the surfaces of dispersed particles of the concentrated phase, no information is obtained about the polyion-surfactant ion stoichiometry in the interior of the particles. The interior must clearly be electroneutral, but this can be achieved by a large set of combinations of surfactant ions, polyions and small ions.

One of the best studied cases where a true surfactant redissolution in water has been firmly established concerns cationically modified hydroxyethyl cellulose (cat-HEC) mixed with sodium dodecyl sulfate (NaDS). A consistent picture of the redissolution behavior of this system comes from a number of phase equilibrium studies in solution and from gel swelling experiments [10,13,16,17]. For cat-HEC and NaDS, a particularly simple phase diagram was established by an approach, introduced by our group, where the so-called complex salt (a neutral salt containing the surfactant ion neutralised by the polymeric counterion) is mixed with the surfactant (the surfactant ion neutralised by a simple counterion) and water [17]. The resulting ternary phase diagram of the cat-HECDS/NaDS/H_2O system is reproduced here as Figure 1a. The virtue of the simplified approach to the study of polyion-surfactant ion phase behavior is that it involves a minimum number of components, so that the entire phase diagram becomes a two-dimensional surface. Here one can access the tie-lines that describe the equilibrium compositions of coexisting phases and thus show the partitioning of the excess surfactant between the coexisting phases.

We note, for the cat-HECDS/NaDS/H_2O system, that the region of associative phase separation into two phases of widely different concentrations (here referred to as the miscibility gap) is limited to a region close to the binary complex salt/water axis. In the dilute part of the miscibility gap the "redissolution boundary", which separates the miscibility gap from the disordered micellar solution at higher surfactant contents, is approximately a straight line that intersects the binary surfactant/water at a low but finite surfactant concentration.

Another oppositely charged combination with a very well-studied phase behavior involves anionic polyacrylate (PA) mixed with cationic alkyltrimethylammonium surfactants of the type C_nTAX, where *n* signifies the number of carbons in the surfactant alkyl chain and X is a simple anion, such as bromide (Br) or acetate (Ac) [18-21]. For this type of system, a number of ternary mixtures of complex salts $C_{16}TAPA$ with added $C_{16}TAX$ surfactant have been established by our group and are reproduced in Figure 1b-d [22-24]. We immediately note that the three latter phase diagrams, referring to complex salts with short (30 repeating units) or long (6000 repeating units) polyacrylate polyions, and two different simple surfactant counterions, are all very different. Moreover, all three-phase diagrams are quite different from the phase diagram of the cat-HECDS/NaDS/H_2O system. An efficient surfactant redissolution of $C_{16}TAPA$ by added $C_{16}TAAc$ is observed when the PA^- chain is very short (Figure 1b). However, if instead a very long PA^- chain is used in $C_{16}TAPA$ (Figure 1c), or if $C_{16}TABr$ is used instead of $C_{16}TAAc$ (Figure 1d), a wide two-phase region results, which extends practically all the way across the phase triangle with an almost constant low water content of the concentrated phase - even when the latter phase is dominated by the added surfactant.

The physical interpretation of these previously recorded effects of the surfactant counterion or the polyion length are complicated by the fact that both these changes result in a change of the structure of the surfactant ion aggregates in the concentrated phase: The concentrated phases in both Figures 1c and 1d consist of hexagonal phases of very long rod-like aggregates, rather than small spherical micelles as in Figure 1b. Bromide ions are known to associate strongly to the cationic surfactant ion aggregates, giving rise to a decreased curvature and micellar growth [20,21,25]. One may therefore ask if the wide miscibility gaps found in Figures 1c and d are, in fact, secondary effects caused by a strong growth of the surfactant ion aggregate. A long rodlike aggregate should be more prone to separate out of solution than a small spherical micelle.

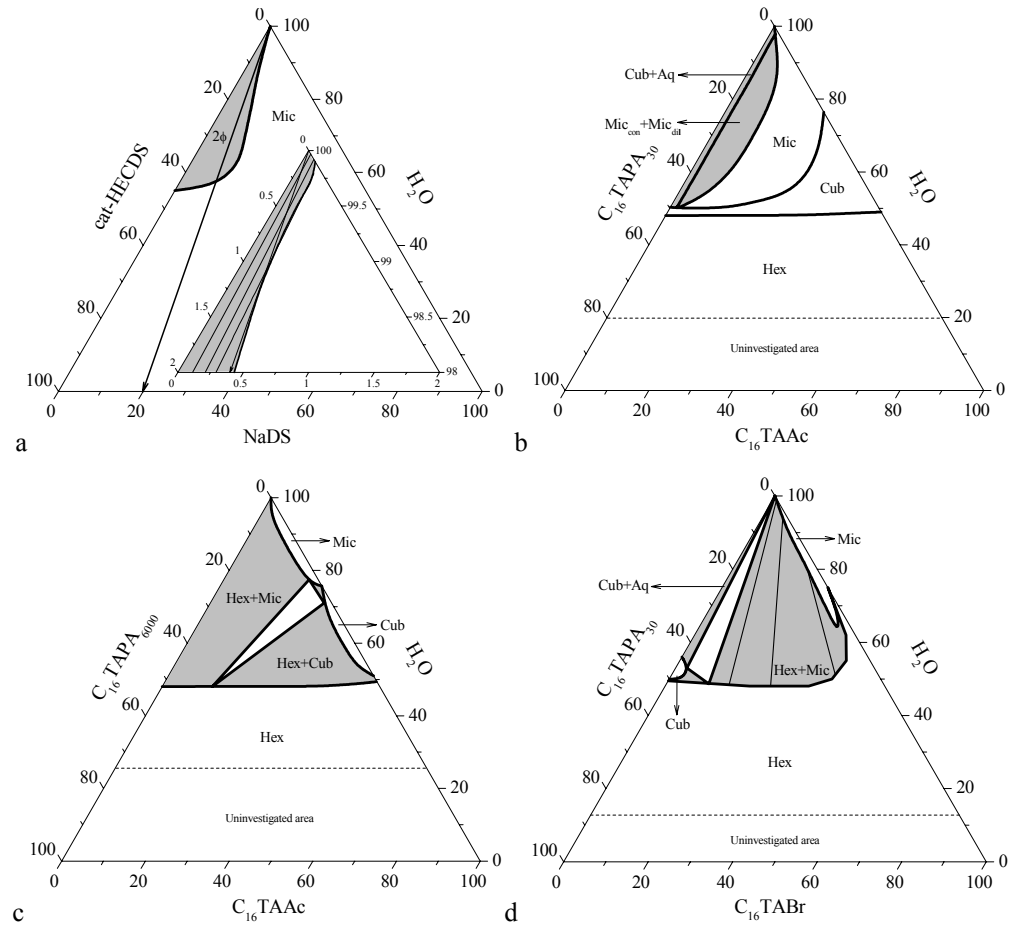

Figure 1. Equilibrium phase diagrams for ternary mixtures of surfactant, complex salt and water. Phase diagrams were reproduced from (a) ref 17, (b) ref 19, (c) ref 20 and (d) ref 18. Estimated phase boundaries (solid curves) and tie-lines (straight lines) are given. In (a), also the 1:1 molar ratio (arrow) is shown. Single phase regions are disordered micellar (Mic), micellar cubic (Cub) or hexagonal (Hex).

The purpose of the work presented here is to gain further insight in the phenomenology and the mechanism of surfactant redissolution. Some specific questions concern the differences observed in Figure 1: (i) is the poor redissolution in Figures 1c and 1d caused by aggregate growth and (ii) are the differences between the cat-HECDS/NaDS/H_2O (Figure 1a) and the C_{16}TAPA/C_{16}TAAc/H_2O (Figure 1c) systems, which both involve long polyions, due to the fact that the two systems are chemically very different? To address these and other questions we have in this study determined additional phase diagrams for mixtures of complex salt containing linear polyions based on polyacrylate that are either very long or very

short homopolyions, or long copolyions (PA^--co-NIPAM or PA^--co-DAM, containing *N*-isopropylacrylamide or *N*,*N*-dimethylacrylamide comonomers, respectively), in mixtures with C_nTAX surfactants of different alkyl chain lengths and with either bromide or acetate counterions. We have also compared the results obtained experimentally with the outcome of calculations using a simple Flory-Huggins model for polyelectrolytes introduced previously [26-28].

2. Materials and Methods

2.1. Materials. *N*-Isopropylacrylamide (NIPAM) (purity >99%) (Phase Separations Ltd.) was recrystallized from hexane. *N*,*N*-dimethylacrylamide (DAM) (Fluka) and acrylic acid (AA) (Alfa Aeser) stabilized with 200 ppm hydroquinone monomethyl ether were passed through a column containing aluminium oxide to remove the inhibitor. Azobisisobutyronitrile initiator (AIBN) (purity 98%+) (Aldrich), ammonium persulfate (APS) (Sigma-Aldrich), cetyltrimethylammonium bromide ($C_{16}TABr$) (purity 98.5%) (Merck) and dodecyltrimethylammonium bromide ($C_{12}TABr$) (TCI Europe) were used without further purification. Polyacrylic acids (Aldrich) with nominal molar masses of 1800 g/mol (PAA_{25}) and 450 000 g/mol (PAA_{6000}) were purified by dialysis against Millipore water for 5 and 3 days, respectively, using cellulose membranes (Spectrum Laboratories, Inc.) with molecular weight cut-offs of 10 000 and 500, respectively, and subsequently freeze-dried. The water uptake of the PAAs after freeze drying was found to be negligible (< 0.1 wt%). The water used was of Millipore quality.

2.2. Copolymers. Most of the copolymers used in this work were the same batches as used and described in the work of Norrman et al. [29].

Two additional copolymers were prepared based on the procedure described in ref [27] by free radical polymerization in a toluene/ethanol (60:40) mixed solvent at 65ºC or 60ºC with AIBN as the initiator. For the synthesis of PAA-co-NIPAM(18:82), 8.69 g (0.077 mol) of NIPAM and 1.35 mL (0.019 mol) of AA were dissolved in a mixture of 125 mL toluene and 80 mL ethanol. For the synthesis of PAA-co-DAM(39:61), 7.0 mL (0.068 mol) of DAM and 3.10 mL (0.045 mol) of AA were added to a mixture of 138 mL toluene and 92 mL ethanol. The reaction was performed in a 250 mL round-bottom flask. The solutions were degassed by bubbling nitrogen gas for 1-2 h. AIBN (0.5 mol%) was dissolved in 20-50 mL of the degassed toluene/ethanol mixture and added to the reaction flask that was degassed for another 0.4-1 hours. The reaction was initiated by immersing the reaction flask into a 60-65°C water bath while stirring. After 4 h the reaction was terminated by exposure to air and cooling in an ice bath for 30-40 minutes. Then the solvent was evaporated off and the copolymer was gradually

dissolved in 70-250 mL of water before it was purified by dialysis for several weeks with daily changes of water. Finally the copolymer was freeze-dried and then appeared as white, very light "cotton". The AA content in the copolymers was determined by titration of a 1 wt% copolymer solution with 0.01 M sodium hydroxide using phenolphthalein as indicator.

The molecular weight of PAA-co-DAM(39:61) was determined by SEC-MALLS with a Dawn-DSP Multi-Angle Laser Light Scattering photometer (Wyatt Technology Corporation) coupled with Size Exclusion Chromatography using an Ultrahydrogel Linear 7.8×300 mm column (Serial Number: T02351A 13, Part no. WAT011545) designed for separation of water-soluble polymers. The molecular weight of PAA-co-NIPAM(18:82) was done with an asymmetrical flow FFF instrument, 3+Separation system (Wyatt technology Europe, Dernbach, Germany) connect with a Dawn Heleos II Multi-Angle Laser Light Scattering detector (Wyatt Technology). Both systems were connected to an Optilab DSP differential refractive index (RI detector). The flow rate was 0.3 mL/min. The polymer was dissolved in a solution of 0.1 M $NaNO_3$ and 0.02 wt% of sodium azide (NaN_3). The latter solution was also used as the mobile phase, which was degassed by a degasser connected to the water pump. The data was analyzed using the Wyatt's ASTRA software. The performance of the SEC-MALLS setup was checked using monodisperse pullulan standards.

The molecular weights determined for PAA-o-DAM(39:61) and PAA-o-NIPAM(18:82) were 146 500 g/mol and 163 000 g/mol, with polydispersity indices of 1.4 and 1.7, respectively.

2.3. Preparation of Complex Salts and Acetate or Acrylate Surfactants. Complex salts and surfactants with acetate or acrylate counterions were prepared by titrating the acid forms of the (poly)carboxylates with the hydroxide forms of the surfactants as described elsewhere [22,24]. The pH values at the equivalence points were separately determined to be 8.6, 8.7, 8.5, 9, 8.0 and 8.9 for C_{12}TAAc, C_{16}TAAc, $C_{12}TAPA_{6000}$, $C_{12}TAPA_{25}$, C_{12}TAPA-co-NIPAM(18:82) and C_{12}TAPA-co-DAM(39:61), respectively. For the preparation of C_{16}TAPA-co-NIPAM(37:63) and C_{16}TAPA-co-NIPAM(20:80) we used the equivalence points 9.33 and 8.1, respectively, determined in ref [27]. After titration the components were left in the fridge overnight and freeze-dried. It was found by thermogravimetric analysis (TGA) and weight measurements that the freeze-dried surfactants and complex salts had a water content of 0.01 – 3.5 wt%. The water contents were taken into account in the calculations.

2.4. Phase Behavior. Appropriate amounts of complex salt, surfactant and water were weighed and put in glass tubes. The tubes were centrifuged for a couple of hours to ensure that all the material was far down in the tube, flame-sealed and further mixing proceeded by centrifuging the tubes alternating right-side-up and up-side-down at least twice at 4000 rpm

(3416.5 g). The samples were then stored at 25°C. As in refs 20 and 21 samples containing C_{16}TAPA-co-NIPAM, C_{16}TABr and water were centrifuged and stored at 40°C, owing to the high Krafft temperature of C_{16}TABr.

All samples were investigated by visual inspection in normal light and between crossed polarizers to detect the number of coexisting phases and the presence of optically anisotropic phases (in the present case, the hexagonal phase). Many samples were further analyzed by SAXS, as described below.

Tie-lines in wide miscibility gaps were established for certain systems where the dilute phase was found to contain essentially pure surfactant in water, i.e., even the slightest addition of complex salt resulted in phase separation. For such samples, the two phases were separated, individually weighed and analyzed by TGA to determine the water content. From this information, together with the known global composition of the samples and the experimental observation that the dilute phase contained no complex salt, the tie-lines could be determined.

2.5. SAXS. Small angle X-ray scattering (SAXS) measurements were performed at the I711 line in Max-lab in Lund, Sweden [30]. The experimental setup involved the use of X-rays at the wavelength of 1.1 Å and a sample-to-detector distance around 1250 mm. A cell with mica windows was used and was maintained at the desired temperature (25 or 40°C). Typical acquisition times were 300 and 600 seconds. The volume between the sample and the detector was kept under vacuum during data collection to minimize the background scattering. The analysis of the 2D SAXS scattering data was conducted by the software Fit2D [31].

The size of a cubic unit cell, α, can be obtained by plotting $(q/2\pi)^2$ versus the Miller indices $(h^2+k^2+l^2)$ of the structures according to

$$\alpha = (2\pi/q)(h^2 + k^2 + l^2)^{1/2} \quad (1)$$

It follows from geometry that the center-to-center distance between adjacent rods, d, of the hexagonal structure can be obtained from the first diffraction peak (q_1) using

$$d_{hex} = (2/(3)^{1/2})(2\pi/q_1) \quad (2)$$

3. Results

3.1. Homopolyion Complex Salts Mixed with Surfactant and Water. The purpose of this part of the study was to investigate the effect of the polyion length on the surfactant redissolution behavior in systems where the surfactant ion aggregates remained as small micelles with a size independent on the polyion length throughout the composition range of interest. For this purpose we chose the complex salts $C_{12}TAPA_{25}$ and $C_{12}TAPA_{6000}$, which both form micellar cubic phases in equilibrium with excess water [22], and C_{12}TAAc as the added surfactant. The resulting phase diagrams at 25°C, shown in Figure 2, contain disordered

micellar, micellar cubic (*Pm3n*) and hexagonal phases. SAXS results for representative samples are available as Supporting Information. For brevity, we will henceforth use the terms "micellar" and "cubic" to denote disordered micellar and (micellar) cubic phases, respectively.

As anticipated, the water-rich top parts of the phase diagrams (above 40 wt% water) in Figures 2a and 2b feature phases with small spherical or nearly spherical micelles. Cubic one-phase regions stretch across the phase triangles for both short and long polyions, covering all complex salt/surfactant mixing ratios from the complex salt/water axis to the surfactant/water axis. Table 1 summarizes the unit cell size α of the *Pm*3*n* structure and the aggregation number N_{agg} of the micelles for cubic samples as obtained from the SAXS results. The micellar aggregation number was found to decrease with increasing water content but, importantly, there was no significant dependence on the proportions of polymeric/simple counterions or the length of the polyion.

At water contents above the cubic one-phase region striking differences in the phase behavior for short and long polyions were observed. In the $C_{12}TAPA_{25}/C_{12}TAAc/H_2O$ system a micellar phase covers most of the top part of the phase diagram. For this system, addition of less than 2 wt% of $C_{12}TAAc$ transforms the cubic-micellar coexistence region, found for binary $C_{12}TAPA_{25}/H_2O$ mixtures, into a micellar-micellar coexistence region. Above 7 wt% of added surfactant, the latter two-phase region changes into a single micellar region. By contrast, for the $C_{12}TAPA_{6000}/C_{12}TAAc/H_2O$ system the top part of the phase diagram is dominated by a wide micellar-cubic miscibility gap and the micellar phase is limited to a very narrow region along the $C_{12}TAAc/H_2O$ axis. The tie-lines of the wide miscibility gap run approximately parallel to the $C_{12}TAPA_{6000}/H_2O$ axis, showing that the $C_{12}TAAc$ component partitions almost equally between the cubic and micellar phases.

There are other significant, if less striking, differences between the phase diagrams for short and long polyions. As found previously [22], the two pure complex salts took up different amounts of water when equilibrated against excess water; the maximum water uptakes of the cubic phases were here found to be ca. 56 and 42 wt% for the $C_{12}TAPA_{25}/H_2O$ and $C_{12}TAPA_{6000}/H_2O$ systems, respectively. This difference persisted also with added $C_{12}TAAc$, e.g., Figure 2 shows the cubic phase generally spanned a larger range of water contents for the system with the short polyion.

At less than ca. 40 wt% water, a hexagonal phase was found for both short and long polyions at all complex salt/surfactant mixing ratios. As shown in Table 1, the rod-to-rod distance in the hexagonal phase did not vary very much with the nature or composition of the counter(poly)ions. Unexpectedly, a wide cubic-hexagonal two-phase region was found in the interior of the phase diagram for the $C_{12}TAPA_{6000}/C_{12}TAAc/H_2O$ system. For some of these

samples, the two phases were macroscopically separated with one phase on top of the other, indicating a significant concentration difference. In other samples the presence of two phases was only detected by the SAXS results, which exhibited a mixture of the cubic and hexagonal patterns.

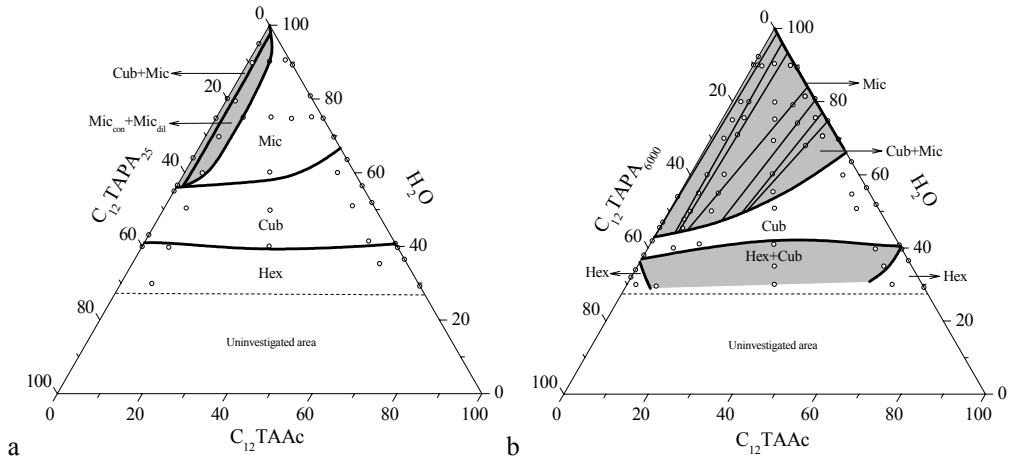

Figure 2. (a) $C_{12}TAPA_{25}/C_{12}TAAc/H_2O$ and (b) $C_{12}TAPA_{6000}/C_{12}TAAc/H_2O$ phase diagrams at 25ºC containing disordered micellar (Mic), micellar cubic (Cub) and hexagonal (Hex) phases. Estimated phase boundaries (solid curves) and tie-lines (straight lines) are given.

Table 1. Structural Parameters of Liquid Crystalline Phases Obtained from SAXS Results

$C_{12}TAAc$ (wt%)	$C_{12}TAPA_{6000}$ (wt%)	$C_{12}TAPA_{25}$ (wt%)	H_2O (wt%)	α [a] (Å)	$N_{agg,theo}$ [b]	N_{agg} [c]	D [d] (Å)
0	58.1		41.9	82.3	56	81	
6.6	53.5		39.9	80.8	56	80	
24.6	24.5		50.9	81.4	56	71	
36.2	3.9		59.9	81.6	56	57	
59.2	0		40.8	79.3	56	75	
36.5	0		63.5	-	56	-	
0	68.0		32.0				38.6
2.2	67.9		29.9				38.5
7.2 [e]	63.3 [e]		29.5 [e]	80.8			36
34.6 [e]	34.4 [e]		31.0 [e]	79.5			37.8
62.0	6.9		31.1				36.9
60.4	0		39.6				37.0
0		56.0	44.0	81.2	56	77	
5.2		44.4	50.4	81.5	56	68	
30.0		30.0	40.0	80.2	56	79	
44.0		5.0	51.0	80.6	56	67	
7.3		62.8	29.9				37.8
58.1		6.4	35.5				37.9

[a] Obtained from the linear fits of eq 1 to the SAXS results for *Pm*3*n* structure.

[b] Theoretical value for a spherical micelle of a surfactant with an n carbon linear alkyl chain: $N_{agg,theo} = V_{hc}/v_{hc}$, where the volume of the micelle hydrocarbon core is $V_{hc} = 4\pi l_{hc}^3/3$, the length of the fully stretched hydrocarbon chain is $l_{hc} = 0.15 + 0.127n$ and the volume of the hydrocarbon chain is $v_{hc} = 0.027(n + 1)$ [33].

[c] Experimental value for the cubic samples, obtained as the number concentration of surfactant ions (assuming a density of 1g/cm^3 for the samples) divided by the number concentration of micelles (obtained from the unit cell dimensions, with eight micelles per unit cell).

[d] Calculated using eq 2.

[e] Two-phase samples.

A selected set of samples from the $C_{12}TAPA_{25}/C_{12}TAAc/H_2O$ and $C_{12}TAPA_{6000}/C_{12}TAAc/H_2O$ systems were investigated also at 60°C. The resulting less detailed phase diagrams are available as Supporting Information. The extensions of the wide miscibility gaps did not change on increasing the temperature to 60°C in either of the two systems, but there were some changes within the miscibility gaps. For the system with the short polyion, the narrow cubic-micellar region essentially collapsed onto the binary complex salt/water axis. For the system containing the long polyion, a new micellar-micellar two-phase region and a corresponding micellar-micellar-cubic three-phase region appeared at high surfactant contents in the wide miscibility gap.

3.2. Incorporation of Neutral Comonomers in the Polyion. In this part of the study, the main aim was to study how the presence of neutral comonomers in the polyion influenced the surfactant redissolution behavior of the corresponding complex salts. Ternary phase diagrams were established for four selected systems, chosen to represent (as will become apparent below) efficient redissolution conditions. Both the fraction and the chemical identity of the neutral comonomer in the copolyion were varied, and two different surfactants were studied.

Figure 3 shows phase diagrams for the complex salts C_{16}TAPA-co-NIPAM(64:36) and C_{16}TAPA-co-NIPAM(52:48) mixed with C_{16}TABr and water at 40°C. Actually, on lowering the temperature to 25°C no changes were detected for samples with low amounts of C_{16}TABr. For the samples closer to the surfactant/water axis, precipitation of C_{16}TABr was observed. The same phases were present and that no large changes occurred when changing the fraction of NIPAM in the complex salt from 36 to 48 mol%. Moreover, the same phases appeared in roughly the same locations as in the corresponding phase diagram for the short homopolyion depicted in Figure 1d. In all three systems, (i) the micellar phase is limited to a very narrow region of the phase diagram close to the binary $C_{16}TABr/H_2O$ axis, (ii) wide miscibility gaps, comprising a micellar-cubic two-phase area and a micellar-hexagonal two-phase area are

present and (iii) the hexagonal phase extends continuously across the entire range of complex salt/surfactant mixing ratios.

The most striking effect of the nonionic comonomers concerns the extension of the cubic phase, which is very small in the $C_{16}TAPA_{30}/C_{16}TABr/H_2O$ system (Figure 1d) but grows both along the complex salt/water axis and inwards in the phase diagram, when NIPAM comonomers are incorporated in the polyion. Significant differences are clearly visible also when comparing the two-phase diagrams in Figure 3. The one-phase cubic region formed in the ranges 32–49 wt% of water in the C_{16}TAPA-co-NIPAM(64:36)/H_2O system and 37–53 wt% of water in the C_{16}TAPA-co-NIPAM(52:48)/H_2O system. The maximum amount of $C_{16}TABr$ that could be incorporated in the cubic phase increased from 14 to 17 wt% on increasing the NIPAM content from 36 to 48 mol%. Thus, the curvature of the surfactant ion aggregate increases on increasing the nonionic monomer content in the polyion, in agreement with previous findings for binary complex salt/water mixtures [29].

Another clear effect of the NIPAM comonomer is that the hexagonal phases in the copolyion systems (Figure 3) took up more water at high $C_{16}TABr$ contents compared to the $C_{16}TAPA_{30}/C_{16}TABr/H_2O$ system (Figure 1d), despite the fact that both copolyions studied have a much higher degree of polymerization than the short homopolyion PA^-_{30}. Since the extension of the miscibility gap decreases with increasing NIPAM content, we conclude that the NIPAM comonomers favor surfactant redissolution, as was indeed found in ref [14]. Representative SAXS results for cubic and hexagonal samples of the C_{16}TAPA-co-NIPAM(64:36)/$C_{16}TABr/H_2O$ systems are available in the Supporting Information.

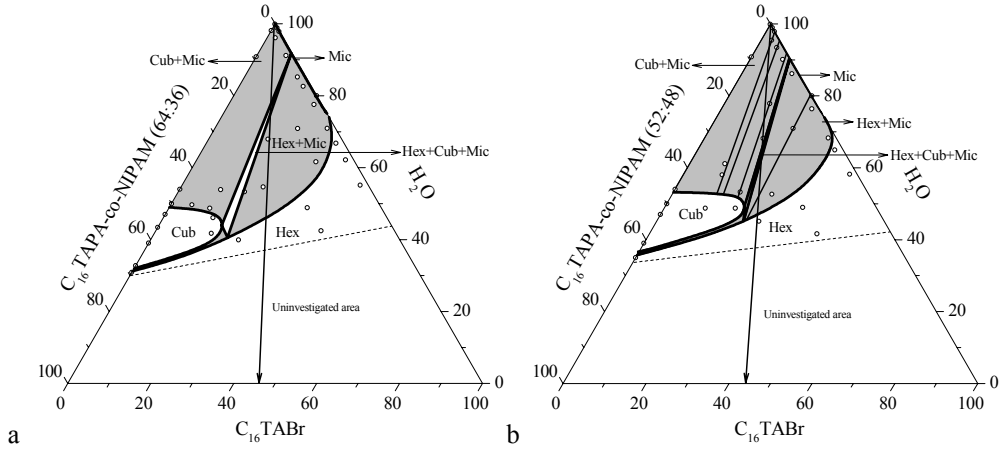

Figure 3. C_{16}TAPA-co-NIPAM/$C_{16}TABr/H_2O$ phase diagrams at 40ºC for the copolymer composition (a) 64:36 and (b) 52:48 containing disordered micellar (Mic), micellar cubic (Cub) and hexagonal (Hex) phases. Estimated phase boundaries (solid curves), tie-lines (straight lines) and the 1:1 molar ratio (arrow) are given.

To enhance the tendency for efficient surfactant redissolution we investigated two systems with an increased content of neutral comonomer in the polyion. We also used a surfactant ion with a shorter alkyl chain length and with acetate as the counterion, C_{12}TAAc. Indeed, the resulting phase diagrams shown in Figure 4 for the two ternary systems C_{12}TAPA-co-DAM(39:61)/C_{12}TAAc/H_2O and C_{12}TAPA-co-NIPAM(18:82)/C_{12}TAAc/H_2O both feature a quite efficient redissolution. Compared to other available phase diagrams for PA^--based complex salts and cationic surfactants (Figures 1b-d, 2 and 3), the most striking difference is that in both diagrams in Figure 4, the miscibility gap is quite small and completely surrounded by a (disordered) micellar phase. The shape of the miscibility gap is also noteworthy, especially in the dilute region, where the redissolution boundary separating the miscibility gap from the one-phase region at excess surfactant appears as a straight line that extrapolates to a finite surfactant concentration at the C_{12}TAAc/H_2O axis.

Some differences between the C_{12}TAPA-co-DAM(39:61)/C_{12}TAAc/H_2O and C_{12}TAPA-co-NIPAM(18:82)/C_{12}TAAc/H_2O the systems are evident in Figure 4. The miscibility gap was larger in the first system, and a cubic phase was observed at low water contents along the binary C_{12}TAPA-co-DAM(39:61)/H_2O axis.

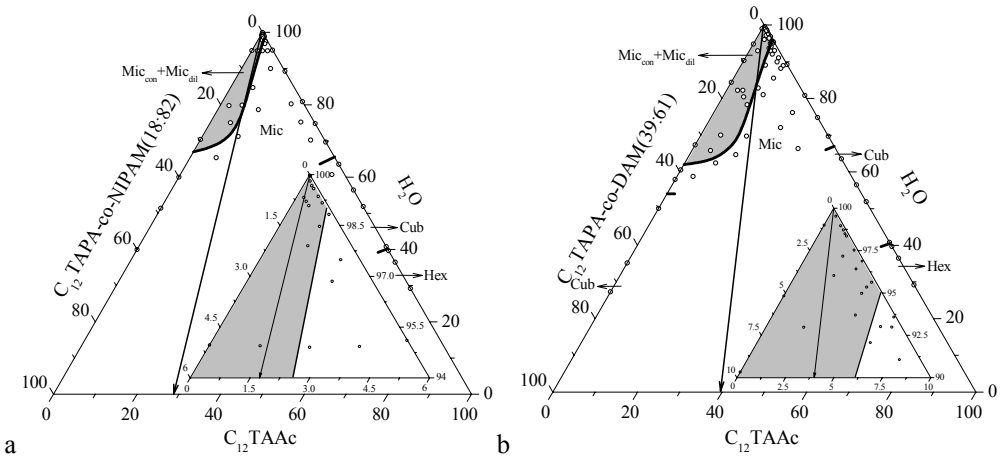

Figure 4. (a) C_{12}TAPA-co-NIPAM(18:82)/C_{12}TAAc/H_2O and (b) C_{12}TAPA-co-DAM(39:61)/C_{12}TAAc/H_2O phase diagrams at 25ºC containing micellar (Mic), cubic (Cub) and hexagonal (Hex) phases. Estimated phase boundaries (solid curves), tie-lines (straight lines) and the 1:1 molar ratio (arrow) are given.

3.3. Additional Redissolution Studies at a Constant Complex Salt Concentration. To access a more extensive set of systems, we performed limited studies on a number of additional combinations of copolyion and surfactant, where we used a single global

concentration of the complex salt but varied the concentration of the added surfactant. Figure 5 summarizes the results as one-dimensional phase maps, where we also include relevant sets of samples from the phase diagrams in Figures 3 and 4. Comparing the positions of the boundaries between phase separation and one-phase systems for the various mixtures shown in Figure 5, we conclude that a more efficient surfactant redissolution is favored by (i) increasing the comonomer content and (ii) using acetate rather than bromide surfactant.

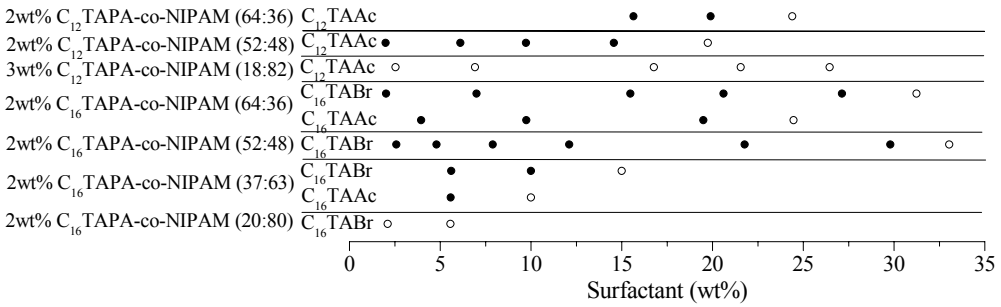

Figure 5. Phase behavior for different complex salts, at a constant overall concentration, mixed with different surfactants. Selected two-phase (filled dots) and one-phase (open dots) samples are shown.

4. Discussion

4.1. Which Factors Influence Redissolution? The new result presented in this study considerably clarifies the factors that influence the efficiency of the redissolution of a water-insoluble polyion-surfactant ion complex salt by added excess surfactant. Before proceeding with more detailed discussion of some of these factors, we will summarize and briefly discuss all of them here.

4.1.1. Polyion length. At least for homopolyions, the length of the polyion of the complex salts has a strong influence on its propensity to redissolve by added surfactant. As shown in Figure 2 and Table 1, this conclusion holds even when the surfactant ion aggregates are small, nearly spherical micelles at all complex salt-surfactant mixing ratios throughout the miscibility gap. We recall that the tie-lines in Figure 2b clearly show that a very large excess of surfactant in the concentrated complex phase is not sufficient to cause a redissolution of the complex.

4.1.2. Nonionic comonomers. The inclusion of nonionic NIPAM or DAM co-monomers in the polyion greatly increases the propensity of the complex salt to redissolve by added surfactant, and the efficiency increases (except for one case) with an increasing content of nonionic monomer (Figure 5). In fact, the phase diagram for the system C_{12}TAPA-co-NIPAM(18:82)/C_{12}TAAc/H_2O (Figure 4a) very closely resembles that previously obtained [17]

for the chemically very different system cat-HECDS/NaDS/H_2O (Figure 1a), including the size and shape of the miscibility gap, the linear redissolution boundary at high water contents and the fact that it is surrounded by a continuous micellar phase.

4.1.3. Surfactant counterion. An acetate, rather than a bromide, counterion makes a cationic surfactant more potent to redissolve a complex salt, in agreement with the previous results reproduced in Figure 1.

4.2. A Simple Lattice-Model Analysis. *4.2.1. General.* As a basis for our further discussion we have made calculations using the simple Flory-Huggins lattice model [32], adopted for polyelectrolyte systems [26-28]. The essence of this version of the Flory-Huggins theory, as applied to the present type of system, is to treat each of the solvent, the polyion, the surfactant ion aggregate, and the simple counterion of the surfactant as a separate species, but with the additional constraint that each equilibrium phase in the mixture must be electroneutral. As in the real system, the latter constraint implies that the mixture of the four species considered is reduced to a three-component system. To incorporate the electroneutrality condition we assign to each unit taken to occupy one lattice site (a polyion repeating unit, a surfactant ion, a simple ion or a water molecule) a charge z, which here may vary from -1 to +1. A non-integer value will in our model be used to represent the average charge of a co-polyion containing a mixture of charged and nonionic monomers. The Coulomb attraction between oppositely charged species is modeled by a strongly negative Flory-Huggins χ parameter. The essential features that the model captures are thus the strong attraction between oppositely charged species, the electroneutrality condition and the change in the translational entropy of mixing that accompanies a change of the degree of polymerization of an ionic species.

We will here consider the following four species: the solvent water (W), the positively charged surfactant aggregate (S^+), the negatively charged polyion (P^-) and the simple counterion to the surfactant ion (A^-). Dissociated surfactant unimers are neglected, and both the surfactant ion aggregate and the polyion are modeled as polymers occupying a large number of lattice sites. One may have objections to modeling the compact surfactant ion aggregate as a linear flexible chain, as is assumed for a polymeric component in the derivation of the Flory-Huggins expressions for the enthalpy and entropy of mixing [32,33]. However, the properties of a surfactant ion aggregate are taken to be constant in each of our systems; what is varied is the degree of polymerization of the surfactant counterion. We expect that the effects of the latter variation are largely insensitive to the detailed modeling of the surfactant ion aggregate itself.

Table 2 summarizes the parameter values used in our calculations. A repeating unit of the surfactant ion aggregate is assigned a positive charge $z_S = 1$, whereas a repeating unit of the homopolyion or a simple anion are assigned a negative charge according to $z_P = -1$ and $z_A = -1$, respectively. Since the number of charges per ionic species is a key ingredient in the model, we have chosen the number of repeating units r_A and r_P of a surfactant ion aggregate or a polyion, respectively, to represent the number of charges of the corresponding species in the real system. Both r_A and r_P are varied in our calculations, but the reference species are a surfactant ion aggregate with 60 positively charged units (corresponding to a C_{12} micelle) and a short or long homopolyion with 15 or 3000 repeating units, respectively. In choosing the latter values we have assumed that the number average degree of polymerization of a polyion, which is the relevant parameter for the translational entropy of mixing, is half of the weight average. In our reference system we have chosen the simplest possible set of pair interaction parameters, i.e., all binary exchange parameters are zero except the strongly negative parameters that describe the interaction between oppositely charged species. We note in passing that a much weaker attraction is required for associative phase separation of the SP component if it is assumed that the polyion and/or the surfactant ion aggregate are hydrophobic, which corresponds to assigning positive values to the χ_{SW} and χ_{PW} interaction parameters [34].

Table 2. Parameters Used for the Flory-Huggins Calculations [a]

Figure	line	z_P	r_P	r_S	χ_{SP}	χ_{SA}
6a	full	-1	3000	60	-3.5	-3.5
6b	dotted	-1	3000	60	-3.5	-3.5
“	full	-1	15	60	-3.5	-3.5
6c	dotted	-1	15	60	-3.5	-3.5
“	full	-1	15	500	-3.5	-3.5
6d	dotted	-1	15	60	-3.5	-3.5
“	full	-1	15	60	-3.5	-5
7a	dotted	-1	3000	60	-3.5	-3.5
“	full	-0.8	3000	60	-2.8	-3.5
“	full (thick)	-0.7	3000	60	-2.45	-3.5
7b	full	-1	3000	60	-3.15	-3.5
“	full (thick)	-0.5	6000	60	-3.5	-3.5

[a] $z_S = 1$, $z_A = -1$, $z_W = 0$ and $\chi_{SW} = \chi_{PW} = \chi_{AW} = \chi_{AP} = 0$.

4.2.2. Modeling Homopolyion Complex Salts. We will first address the effects of polyion length and the choice of surfactant counterion that were found for homopolyion complex salts. Figure 6a shows one calculated phase diagram for a system with $r_P = 3000$ and $r_S = 60$. Here we adjusted the χ_{SP} interaction parameter to obtain a water content for the binary complex salt/water mixture that was in good agreement with the experiments for the binary

$C_{12}TAPA_{6000}/H_2O$ system (Figure 2b). We then chose the same value, -3.5, for the χ_{SA} interaction parameter, since the acetate counterion and the PA^- repeating unit are chemically similar (both contain carboxylate anions). Interestingly, the model phase diagram with these parameters gives a very good reproduction of the experimental phase diagram for the $C_{12}TAPA_{6000}/C_{12}TAAc/H_2O$ system: There is a full miscibility along the SA/W axis, but a wide miscibility gap for almost all ternary compositions in the top part of the phase diagram. Both the experiment and the model feature a concentrated phase where the water content increases only slightly with increasing surfactant content and the tie-lines are approximately parallel with the complex salt/water axis. Obviously, our simple Flory-Huggins model does not capture the possible presence of a liquid crystalline order of the surfactant ion aggregates in the concentrated phase, but such features, which result from packing effects in the concentrated mixtures, will not concern us here. We note that a theoretical diagram similar to the one just discussed was published previously in [28], but for a much more complex set of interaction parameters.

Encouraged by the agreement between model and experiments, we made further calculations to see if reasonable changes of the parameter values in the model could reproduce some of the trends that we found experimentally. Indeed, changing to $r_P = 15$ (Figure 6b) gave rise to a large increase in the maximum water uptake of the concentrated complex salt phase, and a significant shrinking of the miscibility gap for mixtures with added surfactant. Interestingly, additional calculations (not shown) for $r_P = 100$ led to a miscibility gap that was only very slightly smaller than that for $r_P = 3000$ shown in Figure 6a, whereas $r_P = 25$ gave a significant shrinking of the miscibility gap. Thus, the model predicts that the sensitivity to polyion length should only be significant for short polyions ($r_P < 100$).

The experimental phase diagrams in Figure 1b and d show that complex salts with short polyions are much less efficiently redissolved by $C_{16}TABr$ than by $C_{16}TAAc$. Bromide ions are known to be more strongly attracted than acetate ions to C_nTA^+ micelles [20,21,23], and two consequences of this binding could be relevant for our results: $C_{16}TABr$ micelles grow and become non-spherical at higher concentrations, and $C_{16}TABr$ is less water soluble than $C_{16}TAAc$. In our model, we can separate these effects. Figure 6c shows that an increase of the number of units in the model surfactant ion aggregate to represent a significant micellar growth ($r_A = 500$, full lines), only gave a small increase in the calculated miscibility gap for a short polyion ($r_P = 15$, dotted lines). Thus, according to the model, an efficient redissolution of the complex salt can be obtained even if the surfactant ion aggregates are large, provided that the polyion is short.

In another calculation (Figure 6d), we increased the strength of the attraction between surfactant ion aggregates and the simple anion significantly, keeping all other parameters unchanged. Interestingly, the change from χ_{SA} = -5 (full lines) to χ_{SA} = -3.5 (dotted lines) reproduced several trends observed experimentally on replacing acetate with bromide, viz. (i) the miscibility gap became wider and (ii) the concentrated phase became enriched in the added surfactant, as shown by the direction of the tie-lines at large levels of added surfactant. The strong attraction between S^+ and A^- is responsible for the biased partitioning of the simple ions to the phase concentrated in S^+. For the same reason, the SA component also becomes significantly less water-soluble than for a weaker S^+–A^- attraction. A less soluble SA component leads to a decreased tendency of the concentrated phase to take up solvent and, hence, to a miscibility gap that stays wide even at high contents of SA in the concentrated phase.

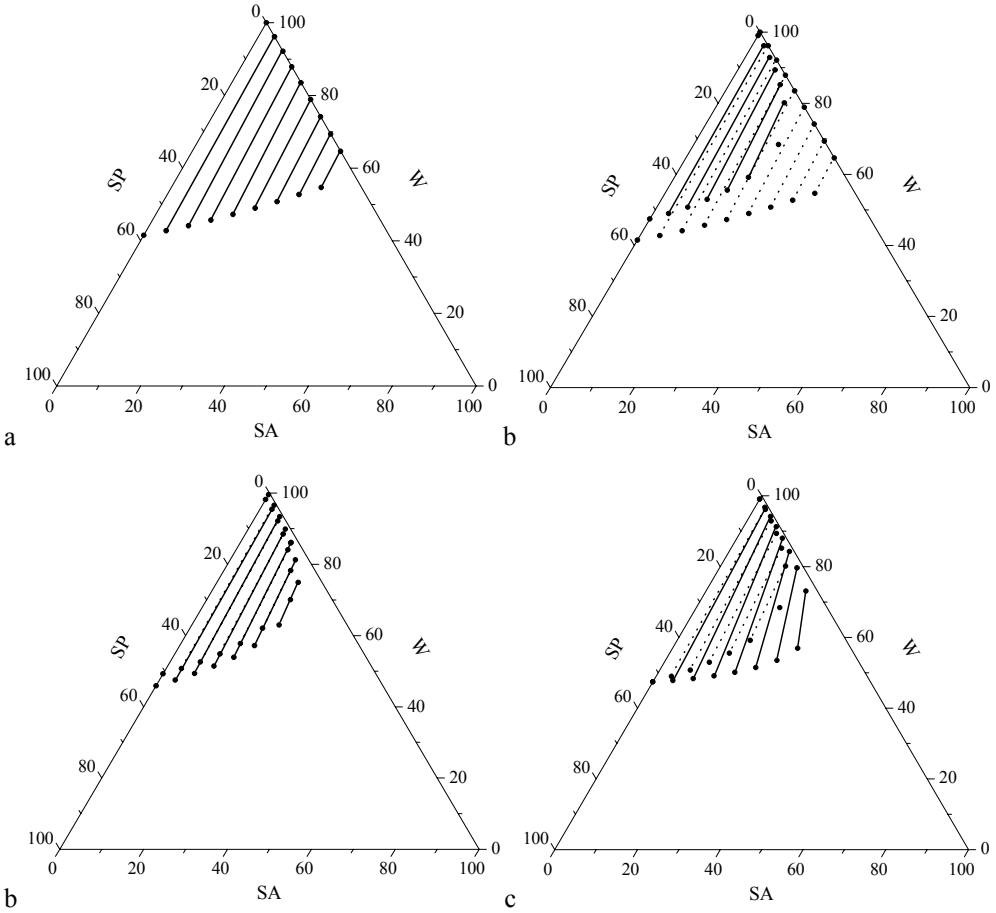

Figure 6. Phase diagrams produced by Flory-Huggins calculations for the surfactant mixing plane with parameters given in Table 2.

4.2.3. A Physical Interpretation of the Homopolyion Phase Diagrams. We believe that the success of the simple mean-field model above is not coincidental, and we will attempt to identify the main physical mechanisms explaining our results as follows. We consider a process where we gradually add surfactant to an initially phase-separated system, containing a water-swollen complex salt in equilibrium with almost pure water. In such a process, the overall composition of the system changes along a line across the phase diagram that starts in the miscibility gap and moves in the direction of the surfactant corner. The essence of our reasoning is that we in turn consider three effects of increasing the surfactant content. (A) First, we ask how the added surfactant distributes between the two phases, remembering that it is a single electroneutral component containing equal amounts of surfactant ions and counterions. (B) Then we ask how the distribution of surfactant might affect the distribution of the complex salt between the phases. (C) Lastly, we consider possible changes in the balance of the osmotic pressures of the phases, which would lead to a redistribution of water between the phases.

(A) We start by discussing the experimental and corresponding model results for the simplest $C_{12}TAPA_m/C_{12}TAAc/H_2O$ systems, Figures 2, 6a and 6b. Here the added surfactant, in the absence of any specific ion binding, partitions essentially equally to the concentrated and dilute phases. The main reason for this unbiased partitioning is the translational entropy of mixing of the simple counterions to the surfactant ion aggregates. The numerous small counterions have a tendency to distribute uniformly throughout the systems, which outweighs any enthalpic preference of the surfactant component.

(B) Next we consider the consequences of the added surfactant for the distribution of the complex salt between the phases. Here we find that the complex salt with the long polyion (Figure 2b and Figure 6a) remains in the concentrated phase essentially at all mixing ratios. This is because the translational entropy of the long polyion is small and, hence, it remains quantitatively in the concentrated phase due to a strong electrostatic preference for the later phase. For the short polyion, however, (Figure 2a and Figure 6b) the translational entropy becomes significant thermodynamic force, and a finite concentration of short polyions therefore partitions to the dilute micellar phase. Moreover, a shorter polyion has a larger water uptake even in the absence of added surfactant. This leads to a less wide miscibility gap, i.e., a smaller difference in the concentration of surfactant aggregates between the dilute and concentrated phases. As the concentration of added surfactant increases, this difference decreases further, which in turn allows for a more even distribution of short polyions.

(C) Lastly, we consider the partitioning of water between the dilute and the concentrated phases. In the initial binary complex salt/water system, the osmotic pressure is zero in both phases, since the dilute phase is essentially pure water and the concentrated phase

is in equilibrium with the water phase. As we add surfactant, the simple counterions should dominate the osmotic pressure of the dilute phase, and its osmotic pressure will therefore be of order RTc_{Adil}, where c_{Adil} is the concentration of simple counterions in the dilute phase. Similarly, the osmotic pressure of the concentrated phase will be dominated by the contribution from the simple surfactant counterions, RTc_{Aconc}, where c_{Aconc} is the concentration of simple counterions in the concentrated phase. If $c_{\mathrm{Aconc}} = c_{\mathrm{Adil}}$ as was found from the tie-lines of the phase diagrams, there will be a balance, and no transfer of water should occur between the phases. Expressed alternatively, the concentrated phase stays concentrated, despite its increasing content of simple counterions, because the coexisting phase is not pure water, but a phase that also has a similarly large concentration of small counterions and thus a large osmotic pressure. The picture is modified in the mixtures with short polyions, where a finite partitioning of short polyions to the dilute phase occurs, as pointed out above. As the proportions of polymeric/simple counterions become increasingly similar in the two phases when surfactant is added, then the distribution of water must also become more similar, and eventually a critical point is reached.

At this stage we note that none of the arguments above rely on a detailed description of the polyion or the surfactant ion aggregate. We may therefore expect that the predictions of a wide miscibility gap for long polyions should have a broad validity for oppositely charged polymer–polymer or polymer-surfactant mixtures, as long as the mean-field approximation is valid (we will return to this point below). Indeed, mixtures of DNA with cationic surfactants give phase separation at practically all mixing ratios, as shown by Dias et al. [35].

We also wish to highlight some implications of the phase diagram for the long polyion in Figure 6a that may not be generally appreciated. The phase diagram predicts that the dilute phase in a non-stoichiometric mixture of two long and oppositely charged polyions, both containing many charges, should contain only the polyion in excess (plus its counterions). Hence polyelectrolyte titration should indeed work as a method to determine polyelectrolyte concentrations, but this does not require that the complex that separates out is stoichiometric in charge at all mixing ratios, as we see from the tie-lines. Still, an investigator might find experimental "evidence" for the prevalence of a stoichiometric complex, as the following numerical example will illustrate. Let us consider a complex salt/surfactant/water system containing 1% complex salt and 5% surfactant. In our model, assuming that each charged unit occupies one lattice site, this corresponds to a charge ratio of 6 surfactant charges per polyion charge, i.e., a very large excess of surfactant ions. The phase diagram for the long P^- in Figure 6a shows that this mixture will separate in one dilute solution of 5% surfactant and one concentrated phase containing ca. 50% complex salt and 5% surfactant. Thus, despite the large

overall excess of surfactant ions in the system, the excess of surfactant ions in the concentrated phase is only 10%, which could even be difficult to detect experimentally. Faced with this experimental result, the investigator might be tempted to conclude that the polymer-surfactant complex is reluctant to bind surfactant above charge equivalence, whereas in reality the partitioning of the surfactant between the phases is taken to be completely unbiased in our example.

4.2.4. Modeling of Copolyion Complex Salts. A simple and obvious way to model the presence of uncharged comonomers in the polyion P^- is to reduce the linear charge density of the polyion. In a mean-field approach, this may be done by assigning to each repeating unit of the polyion a reduced average charge z_P of a magnitude less than one. One could then argue that one should, at the same time, reduce the magnitude of the χ_{SP} interaction parameter by the same factor, since the total electrostatic attraction between an S^+ aggregate and a P^- polyion must also decrease. In a series of calculations, the results of some of which are shown in Figure 7, we initially studied the effects of such parameter changes. The calculations were restricted to long polyions (constant r_P), since the experimentally studied polyions all contained more than 500 charged units per chain.

When examining the results in Figure 7, it is instructive to first consider the effects of the parameter changes on the extension of the miscibility gap along the binary SP/W axis. We found that reducing both the linear charge density and the interaction parameter rapidly increased the equilibrium swelling of the pure complex salt phase in the presence of excess solvent. Already a 20 % reduction of the charge content led to a shift in the maximum solvent uptake from 42 % to 63 % and with 30 % reduction of the charge the miscibility gap was strongly reduced (Figure 7a). With a 40 % charge reduction, the complex salt modeled in the described fashion was found to be fully miscible with the solvent.

To better understand the results just described, we studied the effects of the charge density and the interaction parameter separately (Figure 7b). Obviously, reducing the magnitude of the interaction parameter should make the concentrated complex salt phase take up more solvent, and this turned out to be the dominating effect in our co-polyion model. In fact, very similar results were found for a 10% reduction of the magnitude of the interaction parameter to $\chi_{SP} = -3.15$, regardless of whether the charge density was also reduced to $z_P = -0.9$ (not shown) or allowed to remain at $z_P = -1$ (Figure 7b). Reducing only the charge density with an unchanged interaction parameter also increased the miscibility, since the electroneutrality condition then requires that the complex salt contains an excess of P^- repeating units over the S^+ units. However, here a reduction to $z_P = -0.5$ is required for producing an effect as large as for the former example with $z_P = -1$ and $\chi_{SP} = -3.15$ (Figure 7b).

The above analysis indeed predicts an increased swelling in water for copolyion complex salts, compared to homopolyion complex salts, and we believe that the reasons that the model identifies are the correct ones: the excess of neutral units in the complex salt, and the decreased Coulomb interaction between the polyion and the surfactant aggregate, should give an increased water uptake.

We will now go on to consider the model effect of added surfactant SA on the miscibility gap, also illustrated in Figure 7. In calculations for long polyions, we invariably found that the P^- ion effectively remained in the concentrated phase also for very large additions of surfactant (e.g. see Figure 7). Evidently, for the long polyion and the investigated interaction parameters, the attraction of a polyion chain to the surfactant ion aggregates remained sufficiently strong to prevent a finite partitioning to the dilute phase.

One feature of the real system that the model, with the chosen parameters, does not capture is the additional hydrophobic interaction between the polyion and the surfactant aggregate. To model this additional attraction we could make the χ_{SP} more attractive, rather than less attractive as in Figure 7. However, all that such a stronger interaction does (calculations not shown) is to make the miscibility gap wider at all mixing ratios: we simply obtain the reverse of the effect that the decreased interaction strength was seen to produce in Figure 7. We thus conclude that our Flory-Huggins model fails to predict the experimentally observed redissolution of the copolyion complex salt with a miscibility gap extending along the complex salt/water axis and disappearing at high surfactant contents (Figures 1a and 4).

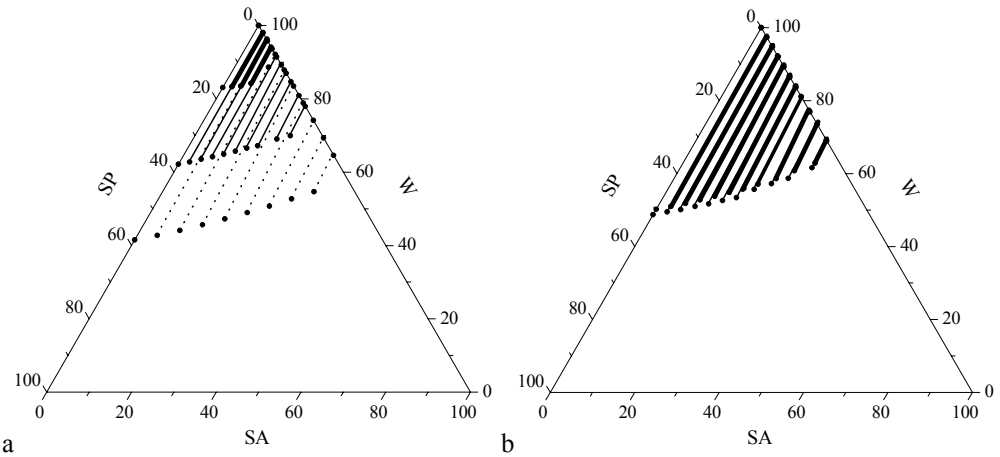

Figure 7. Phase diagrams produced by Flory-Huggins calculations for the surfactant mixing plane with parameters given in Table 2.

4.2.5. What do we Learn from the Lattice-Model Analysis? The model was found to be most successful to reproduce the experimental results for long homopolyions in the complex

salt. The model also succeeds to capture the effect of a specific binding of the simple anion to the surfactant ion aggregate, which results in a similarly wide miscibility gap, but with a biased partitioning of the surfactant to the concentrated phase. We conclude that the mean-field approach is most successful in cases when the dilute phase contains virtually no polyions. We propose that this is because the model assumption of random mixing between all species then becomes reasonable for both phases: both the homogeneous solution of the pure surfactant and the concentrated mixture of surfactant aggregates, long polyions and simple ions.

The model does not succeed in reproducing the redissolution of copolyions containing slightly hydrophobic nonionic comonomers. We believe that the key reason for this failure is that the dilute phase in the real systems contains soluble non-stoichiometric polyion-surfactant ion complexes, a situation for which the mean-field assumption of uniform concentrations of all species is clearly inappropriate. Soluble complexes feature a close contact between surfactant ion aggregates and polyions, and thus make the enthalpic penalty for partitioning P^- molecules into the dilute solution considerably less than what is predicted by the mean-field model. We will come back to the situation for complexes involving slightly hydrophobic polyions below. Before that, we note that the existence of soluble complexes in the experimental system could also account for some quantitative differences between experiment and Flory-Huggins model predictions for the surfactant redissolution of complex salts with short hydrophilic homopolyions. A comparison of Figures 2a and 6b shows that the surfactant redissolution is less efficient in the model that in the experimental system. Simulations of aqueous mixtures of short flexible polyions with oppositely charged spherical macroions interacting only via Coulomb attractions indeed predict the presence of soluble clusters, consisting of macroions connected by polyion bridges, even at a small relative excess of oppositely charged spheres [36].

4.3. Soluble Complexes Containing Slightly Hydrophobic (Co)polyions. A large body of experiments indicate that for polyions that are sufficiently hydrophobic, such as the cat-HEC and the PA^--co-NIPAM(18:82) polyions discussed here, an excess of oppositely charged surfactant ions can associate with the polyion via an additional hydrophobic attraction to produce soluble non-stoichiometric complexes [10,11,13,14,16,17]. The non-stoichiometric complexes form cooperatively at a specific free surfactant concentration, similarly to the formation of net charged complexes between certain nonionic slightly hydrophobic polymers and ionic surfactants at the so-called critical association concentration [37,38]. The following arguments, which are similar to those presented in references 10, 12 and 17, show that the existence of such a complexation should lead to a miscibility gap of the type shown in Figure

1a and 4b with a linear redissolution phase boundary at low surfactant concentrations and a finite intercept at the surfactant/water axis.

At the redissolution boundary, we can generally write the total surfactant ion concentration $c_{S,tot}^{rediss}$ in the dilute phase as a sum of concentration of non-complexed "free" surfactant ions $c_{S,f}^{rediss}$ and of surfactant ions "bound" in the soluble complexes $c_{S,b}^{rediss}$ according to

$$c_{S,tot}^{rediss} = c_{S,f}^{rediss} + c_{S,b}^{rediss} = c_{S,f}^{rediss} + \beta^{rediss} c_{P}^{rediss} \quad (3)$$

where we also have rewritten the concentration of bound surfactant ions in terms of the concentration of polyions in soluble complexes c_{P}^{rediss} and the stoichiometric surfactant ion/polyion ratio β^{rediss} in the complex. In a pseudo-phase separation model, we may treat the complex as a separate pseudo-phase, which becomes thermodynamically stable when the free surfactant concentration has reached the critical value $c_{S,f}^{rediss}$. This is analogous to the familiar pseudo-phase separation model for surfactant micellization, where a micellar pseudo-phase forms when the surfactant concentration has reached the critical micelle concentration. In the present context, the pseudo-phase approximation implies a pseudo three-phase equilibrium at the redissolution boundary with a coexistence among (i) the free surfactant solution pseudo-phase, (ii) the soluble complex pseudo-phase and (iii) the concentrated phase dominated by complex salt. In a ternary system, the compositions of all phases must stay constant at a three-phase coexistence, hence $c_{S,f}^{rediss}$, β^{rediss} and the composition of the concentrated phase must all stay constant at the redissolution boundary. From eq 3 it then follows that an incremental increase in the amount of the soluble complex pseudo-phase along the redissolution boundary, i.e., an increase in c_{P}^{rediss} requires a linear increase of the total surfactant concentration, which results in a linear redissolution boundary. The pseudo-phase separation model should be valid in water-rich systems when the concentration of surfactant ions bound in complexes is low compared to the free surfactant ion concentration.

We conclude that the above analysis predicts that for a system where a soluble complex forms at a low free surfactant concentration, the miscibility gap of the type shown in Figure 2c, featuring an unbiased partitioning of added surfactant between the phases, should become interrupted by a linear redissolution boundary with an intercept at $c_{S,f}^{rediss}$ on the surfactant/water axis and a slope β^{rediss} that gives the stoichiometry of the soluble complex.

V. Summary and Conclusions

The present study contributes a large set of new experimental results on the phase behavior of oppositely charged polyion-surfactant complexes in aqueous mixtures with excess surfactant. The strategy has been to use systematic variations of the minimum number of components required to address the problem – a complex salt, an added surfactant and water – so that the resulting isothermal phase equilibria can be represented in simple two-dimensional phase diagrams. This approach makes the results considerably easier to grasp and interpret compared to typical studies of multi-component systems.

The present phase studies confirm that the outcome of an experiment, where excess surfactant is added to a phase separated mixture of a complex salt in water, may vary widely: from a wide miscibility gap, covering practically all mixing ratios of complex salt and surfactant, to an efficient "surfactant redissolution", where a limited amount of excess surfactant is capable of closing the miscibility gap into a single-phase micellar solution. Compared to previously available complex salt/surfactant/water phase studies, the present study has succeeded to isolate various factors responsible for this transition, and to show that a range of behaviours previously encountered for chemically different systems can be covered using minimal chemical variations in a single class of experimental systems.

We have found that surfactant redissolution of polyacrylate by a cationic trimethylalkylammonium surfactant is much more efficient when the complex salt contains short, rather than long, homopolyions, even if the surfactant ion aggregates are small spherical micelles in both cases. Thus, a large excess of small spherical micellar aggregates with simple counterions is not sufficient to redissolve complexes containing long homopolyions.

We have also found that the introduction of a large fraction of uncharged slightly hydrophobic NIPAM or DAM comonomers into the polyacrylate chain makes the surfactant redissolution much more efficient even for long polyion chains. Polyions with a large fraction of nonionic comonomers could actually reproduce the key features previously found for a chemically very different system based on a cationic cellulose ether and (sodium) dodecyl sulfate. These features include a comparatively narrow miscibility gap with a finite intercept at the surfactant/water axis, enclosed in a single disordered micellar phase. In all these cases mentioned, we suggest that soluble, non-stoichiometric polyion-surfactant ion are formed at low concentrations of uncomplexed surfactant owing to an additional hydrophobic interaction between the polyion andthe surfactant aggregates.

A simple mean-field Flory-Huggins model, making only the essential assumptions that (i) there is a strong attraction between oppositely charged species and (ii) each equilibrium phase must be electroneutral, predicts the correct phase behavior found for complexes with

long homopolyions. As in the experiments, the key features of the calculated phase equilibria were a miscibility gap extending over all mixing ratios and an almost unbiased partitioning the surfactant component between a pure surfactant and a concentrated complex salt/surfactant phase. The model also predicts an increased tendency for surfactant redissolution when the complex salt contains very short polyions. Finally, the approach succeeds to capture the effect of an additional attraction between the simple anion and the surfactant ion aggregate, which again results in a wide miscibility gap at all surfactant/complex salt mixing ratios, but with a biased partitioning of the surfactant to the concentrated phase.

Acknowledgments. We thank Mats Leeman and Lars Nilsson for help in molecular weight measurements, and Wei Wang and Ola Karlsson for fruitful discussions. This study was funded by Fundação para a Ciência e a Tecnologia (SS, SFRH/BD/30929/2006), by POPH/FSE (SS) and by the Swedish Research Council (VR) through the Linnaeus Centre of Excellence on Organizing Molecular Matter (OMM).

Supporting Information Available. Additional table and figures as described in the text. This material is available free of charge via the Internet at http://pubs.acs.org.

References

(1) Leung, P. S.; Goddard, E. D. *Langmuir* **1991**, *7*, 608.

(2) Lee, B.-H.; Christian, S. D.; Tucker, E. E.; Scamehorn, J. F. *Langmuir* 1991, *7*, 1332.

(3) Magny, B.; Iliopoulos, I.; Zana, R.; Audebert, R. *Langmuir* **1994**, *10*, 3180.

(4) Iliopoulos, I. *Current Opinion Colloid Interf. Sci.* **1998**, 3, 493.

(5) Bronich, T.; Nehls, A.; Kabanov, V.; Kabanov, A. *Colloids Surf. B* **1999**, *16*, 243.

(6) Hössel, P.; Dieing, R.; Nörenberg, R.; Pfau; Sander, A. R. *International Journal of Cosmetic Science* **2000**, *22*, 1.

(7) Rodriguez, R.; Alvarez-Lorenzo, C.;. Concheiro, A. *Eu. J. Pharm. Sci.* **2003**, *20*, 429.

(8) Naderi, A.; Claesson, P. M.; Bergström, M.; Dédinaité, A. *Colloids and Surfaces A: Physiochem. Eng. Aspects* **2005**, *253*, 83.

(9) Mezei, A.; Pojják, K.; Mészáros, R. *J. Phys. Chem.* **2008**, *112*, 9693.

(10) Svensson, A. V.; Huang, L.; Johnson, E.; Nylander, T.; Piculell, L. *Applied Materials & Interfaces* **2009**, *1*, 2431.

(11) Santos, O.; Johnson, E. S.; Nylander, T.; Panandiker, R. K; Sivik, M. R.; Piculell, L. *Langmuir*, **2010**, *26*, 9357.

(12) Guillemet, F. ; Piculell, L. *J. Phys. Chem.* **1995**, *99*, 9201.

(13) Sjöström, J.; Piculell, L. *Colloids and Surfaces A: Physiochem. Eng. Aspects* **2001**, *183-185*, 429.

(14) Lynch, I.; Sjöström, J.; Piculell, L. *J. Phys. Chem.* **2005**, *109*, 4258.

(15) Borsos, A.; Acciaro, R.; Mészáros, R.; Gilányi, T. *Progr. Colloid Polym. Sci.* **2008** *135*, 188.

(16) Ananthapadmanabhan, K. P.; Leung, P. S.; Goddard, E. D. *Colloids and Surfaces* **1985**, *13*, 63.

(17) Svensson, A.; Sjöström, J.; Scheel, T.; Piculell, L. *Colloids and surfaces A: Physcochem. Eng Aspects* **2003**, *228*, 91.

(18) Thalberg, K.; Lindman, B.; Bergfeldt, K. *Langmuir* **1991**, *7*, 2893.

(19) Carnali, J. O. *Langmuir* **1993**, *9*, 2933-2941.

(20) Hansson, P.; Almgren M. *Langmuir* **1994**,*10*, 2115.

(21) Ilekti, P.; Martin, T.; Cabane, B.; Piculell, L. *J. Phys. Chem. B* **1999**, *103*, 9831.

(22) Svensson, A.; Piculell, L.; Cabane, B.; Ilekti, P. *J. Phys. Chem. B* **2002**, *106*, 1013.

(23) Svensson, A.; Piculell, L.; Karlsson, L.; Cabane, B.; B. Jönsson *J. Phys. Chem. B* **2003**, *107*, 8119.

(24) Svensson, A.; Norrman, J.; Piculell, L. *J. Phys. Chem. B* **2006**, *110*, 10332.

(25) Brady, J. E.; Evans, D. F.; Warr, G. G.; Grieser, F.; Ninham, B. W. *J. Phys. Chem.* **1986**, *90*, 1853.

(26) Piculell, L.; Lindman, B. *Adv. Colloid Interface Sci.* **1992**, *41*,149.

(27) Gottschalk, M.; Linse, P.; Piculell, L. *Macromolecules* **1998**, *31*, 8407.

(28) Piculell, L.; Lindman, B.; Karlström, G. In *Polymer-Surfactant Systems*; J. C. T. Kwak, ed., Marcel Dekker, New York, 1998, Chapter 3, p 65-141.

(29) Norrman, J.; Lynch, I.; Piculell, L. *J. Phys. Chem. B* **2007**, *111*, 8402.

(30) Knaapila, M.; Svensson, C.; Barauskas, J.; Zackrisson, M.; Nielsen, S.S.; Toft, K. N.; Vestergaard, B.; Arleth, L.; Olsson, U.; Pedersen, J. S.; Cerenius, Y. *J. Synchrotron Rad.* **2009**, *16*, 498.

(31) Hammersley, A. Grenoble. Private communication.

(32) Flory, P. J. *Principles of Polymer Chemistry*, Cornell University Press, Ithaca, 1953.

(33) Evans, D. F.; Wennerström, H. *The colloidal domain - where physics, chemistry, biology and technology meet*, 2nd ed.; John Wiley&Sons: New York, 1999.

(34) Bergfeldt, K.; Piculell, L.; Linse, P. *J. Phys. Chem.* **1996**, *100*, 3680.

(35) Dias, R.; Mel'nikov, S.; Lindman; B.; Miguel; M. G. *Langmuir*, **2000**, *16*, 9577.

(36) Skepö, M.; Linse, P. *Macromolecules* **2003**, *36*, 508.

(37) Shirahama, K. In *Polymer-Surfactant Systems*, J. C. T. Kwak, ed., Marcel Dekker, New York, 1998, Chapter 4, p 143-191.

(38) Linse, P.; Piculell, L.; Hansson, P. In *Polymer-Surfactant Systems*, J. C. T. Kwak, ed., Marcel Dekker, New York, 1998, Chapter 5, p 193.

Supporting information

Table S1. Structural Parameters Calculated from SAXS Results for the C_{16}TAPA-co-NIPAM(64:36)/C_{16}TABr/H_2O System

C_{16}TABr (wt%)	C_{16}TAPA-co-NIPAM(64:36) (wt%)	H_2O (wt%)	α (Å)	$N_{agg,theo}$	N_{agg}	D (Å)
11.8	42.1	46.1	102	95	102	
31.2	66.8	1.94				36.4

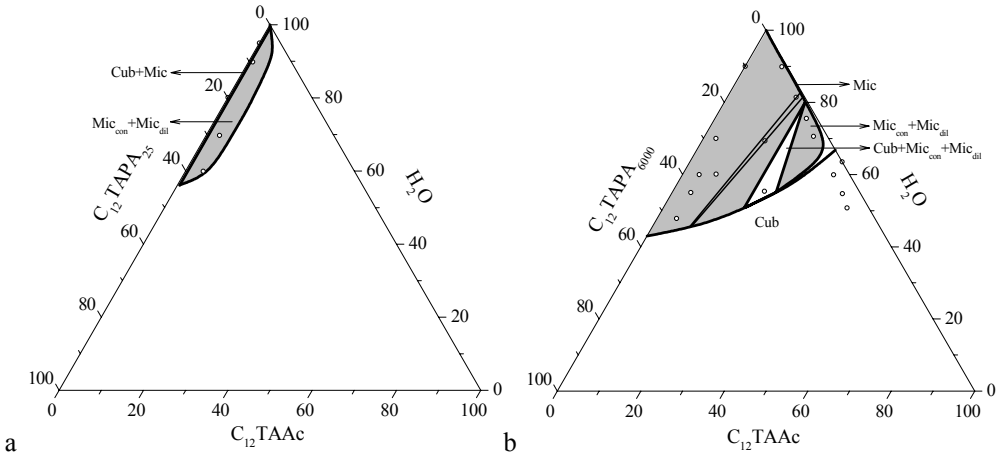

Figure S1. (a) $C_{12}TAPA_{25}/C_{12}TAAc/H_2O$ and (b) $C_{12}TAPA_{6000}/C_{12}TAAc/H_2O$ phase diagrams at 60ºC containing micellar (Mic) and cubic (Cub) phases. Estimated phase boundaries (solid curves) and tie-lines (straight lines) are given.

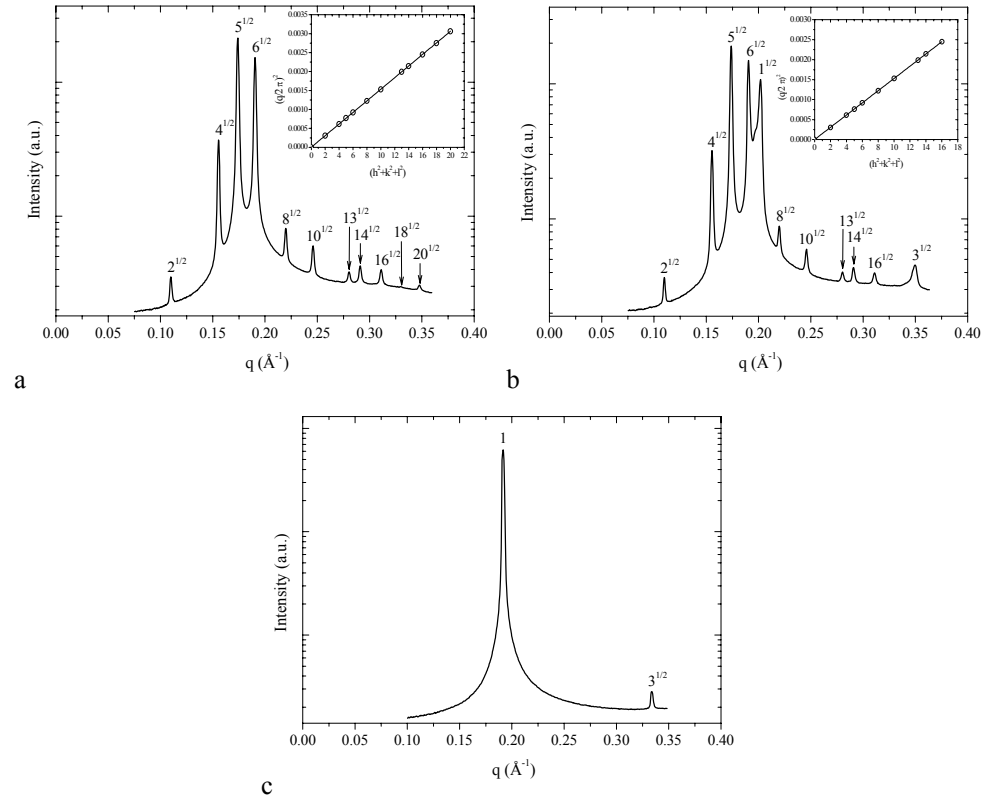

Figure S2. (a) SAXS results for the samples with compositions 6.59wt% C_{12}TAAc, 39.91wt% C_{12}TAPA$_{6000}$ and 53.50wt% H_2O. (b) Pm3n micellar cubic structure with peaks at the relative positions: $2^{1/2}$:$4^{1/2}$:$5^{1/2}$:$6^{1/2}$:$8^{1/2}$:$10^{1/2}$:$13^{1/2}$:$14^{1/2}$:$16^{1/2}$:$18^{1/2}$:$20^{1/2}$; 7.18wt% C_{12}TAAc, 63.29wt% C_{12}TAPA$_{6000}$ and 29.53wt% H_2O. (c) Mixture of Pm3n and hexagonal structures with peaks at the relative positions: $2^{1/2}$:$4^{1/2}$:$5^{1/2}$:$6^{1/2}$:$8^{1/2}$:$10^{1/2}$:$13^{1/2}$:$14^{1/2}$:$16^{1/2}$ and $1^{1/2}$:$3^{1/2}$, respectively, at the composition 7.29wt% C_{12}TAAc, 62.78wt% C_{12}TAPA$_{25}$ and 29.93wt% H_2O. Hexagonal structure with peaks at the relative positions 1:$3^{1/2}$. In (a) and (b), the insets show $(q/2\pi)^2$ versus $(h^2+k^2+l^2)$.

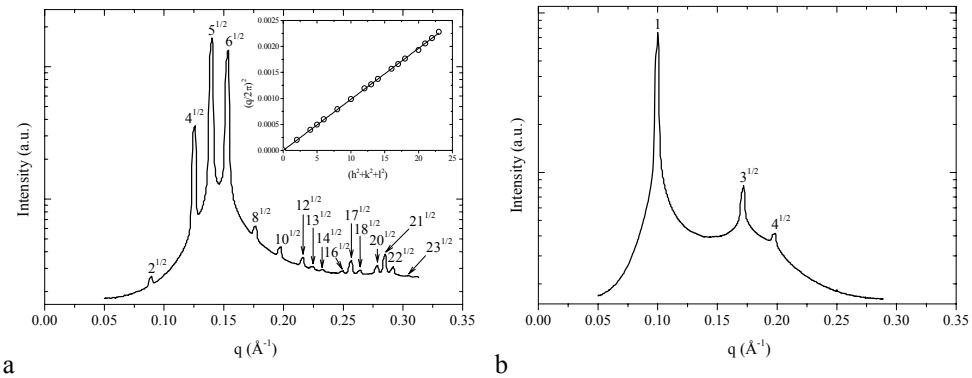

a b

Figure S3. (a) SAXS results for the samples with the compositions 42.1wt% C_{16}TAPA-co-NIPAM(64:36), 11.8wt% of C_{16}TABr and 46.1wt% of H_2O with the relative peak positions at $2^{1/2}$:$4^{1/2}$:$5^{1/2}$:$6^{1/2}$:$8^{1/2}$:$10^{1/2}$:$12^{1/2}13^{1/2}$:$14^{1/2}$:$16^{1/2}$:$17^{1/2}18^{1/2}$:$20^{1/2}$:$21^{1/2}$:$22^{1/2}$: $23^{1/2}$ and (b) 1.94wt% C_{16}TAPA-co-NIPAM(64:36), 31.24wt% of C_{16}TABr and 66.82wt% of H_2O with the relative peak positions at 1:$3^{1/2}$:$4^{1/2}$.

Paper IV

CREATED USING THE RSC ARTICLE TEMPLATE (VER. 3.1) - SEE WWW.RSC.ORG/ELECTRONICFILES FOR DETAILS

ARTICLE TYPE www.rsc.org/xxxxxx | XXXXXXXX

Phase diagrams come alive: understanding how to create, destroy or change ordered surfactant structures by polymerizing the counterions

Salomé dos Santos,[a] Lennart Piculell,*[a] Ola J. Karlsson,[a] and Maria da Graça Miguel[b]

Received (in XXX, XXX) Xth XXXXXXXXX 200X, Accepted Xth XXXXXXXXX 200X
First published on the web Xth XXXXXXXXX 200X
DOI: 10.1039/b000000x

Free radical polymerization of acrylate counterions to cationic alkyltrimethylammonium surfactant ions was performed in aqueous media. The results of the reactions were either formation, destruction or change of liquid crystalline surfactant structures, depending on the starting conditions such as the surfactant concentration, the content of inert counterions and the monomer-to-initiator ratio. The results were consistent with predictions inferred from equilibrium phase diagrams recently established for aqueous mixtures of the cationic surfactants alkyltrimethylammonium acetate or bromide (C_nTAAc/Br; n=12,16) with the "complex salts" C_nTAPA$_m$, in which the counterions to the surfactant ions were polyacrylate polyions (PA) of different degrees of polymerization (m = 25, 30 or 6000). Appropriate pathways, at constant water content, through the latter ternary phase diagrams show what happens, at equilibrium, when monomeric counterions to the surfactant ions are replaced by polymeric counterions. These pathways through the equilibrium phase diagrams thus "come alive" in the counterion polymerization processes performed here.

Introduction

There is a strong and long-standing interest in concentrated associating polymer-surfactant mixtures. The associative phase separation that gives rise to concentrated mixtures in aqueous polymer-surfactant systems of opposite charge is particularly well documented[1-8]. Owing to the self-association of the surfactant component, the concentrated phases that separate out from such mixtures often feature ordered liquid crystalline structures[5,6,9-14]. Important applications that stimulate the research on concentrated associating polymer-surfactant mixtures include templating for preparation of mesoporous ordered materials, surface deposition of concentrated polymer-surfactant layers, and the creation of soft structured particles[15-18].

Materials based on associating polymer-surfactant pairs can differ in structure, water uptake and mechanical properties depending on factors such as the lengths of the polymer and surfactant chains and the overall compositions. The materials can be produced using different routes, e.g. chemical synthesis, sequential addition of components, dilution and simple mixing. An important question is to what extent different routes of preparation give the same results, indicating that the systems have reached equilibrium. Of particular concern here are systems produced by polymerization reactions. Most approaches to polymerization reactions in surfactant systems so far seems to have been based on trial and error, and the resulting structures have often been found to be different from the original surfactant template[19,20]. That is, polymerization changes the equilibrium structure of system. One reason for such changes is the development of a repulsive depletion interaction between the formed polymers and the surfactant aggregates[19]. In fact, not much attention has been given to the fact that, as it happens for silica and its templates in hard mesoporous materials, the interaction between the different components in the system should be attractive in order to create long-ranged ordered structures containing polymer and surfactant[21]. The situation is further complicated since many systems, and certainly inorganic mesoporous materials, become kinetically arrested at some point during the polymerization.

Even for equilibrium systems, many questions regarding the properties of concentrated associating polymer-surfactant mixtures remain. Classically, the studies performed have involved mixing a polyelectrolyte (polyion + simple counterion) and a simple surfactant (surfactant ion + simple counterion) in water. Such mixtures are complex four-component systems, since they involve four ionic species and water. While the structures of the phases separating out from such mixtures can be studied, their compositions are rarely determined, since this is tedious work (in general, each phase contains all four ions)[1,5,7] However, the roles of polymer and surfactant architectures and overall compositions for the properties of oppositely charged mixtures have recently been systematically investigated for systems of minimum complexity (minimum number of components)[22-25]. In these studies, a novel simple approach has been utilized where at least one of the simple ions has been eliminated from the mixture. Specifically, equilibrium phase diagrams have been established for associating polymer-surfactant systems involving aqueous cationic alkyltrimethylammonium surfactant ions with two different counterions (C_{16}TAAc, C_{12}TAAc and C_{16}TABr) (Ac=acetate) mixed with "complex salts" containing the same surfactant ions, but with polyacrylate polyions of either very high or very low degrees of polymerization as counterions[22,23,25]. Interestingly, an appropriate chosen pathway through the latter type of phase

diagram shows what happens, at equilibrium, when a monomeric counterion to the surfactant is replaced by a polymeric counterion - a process that is closely analogous to a polymerization reaction. Thus, phase diagrams can be used to predict the results of polymerization reactions in surfactant systems, and this is a central message of the present study.

Here we build on and extend our previous studies by investigating polymerization reactions in systems of similar minimum complexity, by the use of alkyltrimethylammonium surfactants with polymerizable acrylate counterions. Two aspects make our approach to polymerization in surfactant media unique: i) it is based on our *a priori* knowledge of the phase behavior of ionic surfactants with monomeric versus polymeric counterions and ii) the synthesis is done under conditions where the surfactant aggregates are the sole counterions to the growing polyion chains. The latter is a strong constraint for the structure resulting from the polymerization.

The present investigation indeed confirms that the results of the polymerization reactions were predicted by the relevant equilibrium phase diagrams. The results also indicate general trends that should be relevant also for more complex systems, such as mesoporous silicates.

Materials and Methods

Materials

The following chemicals were used as received: acetic acid (Merck), ion exchange resin Dowex SBR dry mesh 20-50 (Sigma-Aldrich), sodium iodide (NaI) (Sigma-Aldrich), thermal initiator ammonium persulphate (APS) (Sigma-Aldrich) and azoinitiator 2,2'-Azobis[2-(2-imidazolin-2-yl)propane]dihydrochloride (VA-044) (Wako Pure Chemicals Industries, Ltd., Japan), sodium acrylate (Aldrich) and the surfactants cetyltrimethylammonium bromide (C_{16}TABr) (Merck), dodecyltrimethylammonium bromide (C_{12}TABr) (Merck) and cetyltrimethylammonium chloride (C_{16}TACl) (TCI Europe). Acrylic acid (Alfa Aeser), was received stabilized with 200ppm hydroquinone monomethyl ether, which was removed by passing through a column containing aluminum oxide (active base) (Merck).

Preparation of surfactants with different counterions

C_nTAAcr was prepared by titrating the hydroxide form of the surfactant C_nTAOH with acrylic acid. The first step was to convert C_nTABr into C_nTAOH by ion exchange as described elsewhere[22,23]. The ion exchange resin was charged with hydroxide by stirring in excess amount of 1 M NaOH for 2 hours and then rinsed with Millipore water until the pH of the rinsing water was below 7. Approximately 15 g of C_nTABr was then dissolved in a plastic beaker containing a large excess (100 g) of the hydroxide-charged ion exchange resin and 100 mL of Millipore water. The solution was stirred until all C_nTABr was dissolved (~1hour). The slurry was filtered and the filtrate was rinsed with Millipore water and then put into a new batch of 100 g resin and 100mL Millipore water, which was stirred for 2 hours. The last step was repeated once. The alkaline solution thus obtained contained C_nTAOH at a concentration of approximately 0.07M. A 0.8M solution of acrylic acid or acetic acid was added dropwise to the freshly prepared solution of C_nTAOH under stirring. The pH was measured with a standard pH KCl/AgCl electrode. The equivalence point was taken as the pH inflection point (pH≈8.7 for all the prepared surfactants (C_{16}TAAcr, C_{12}TAAcr and C_{16}TAAc) in a pH titration curve determined in a separate measurement. After equilibration overnight, the solution was freeze-dried. The compounds were obtained as white powders, which were stored over silica gel in a desiccator.

Surfactant characterization

For the characterization of the compounds, ^{1}H NMR, thermogravimetric analysis (TGA) and elemental analysis were performed. NMR integration of the peak areas confirmed a 1:1 ratio between the surfactant ions and their monomeric counterions. Peaks for acrylate were located at 5.96, 6.52, 6.1 and 12.0 ppm. For C_{16}TAAc the result corresponded to the results obtained by Svensson et al[27]. TGA was used to determine the amount of water in the samples of freeze-dried surfactants and also to determine the thermal stability of the surfactants, since the latter were used at 60ºC. Weight losses were recorded in the TGA at a programmed heating rate of 10ºC/min from ambient temperature to 300ºC. Elemental analysis was performed in C_{16}TAAcr to analyze the contents of sodium and bromide ions that remained after the counterion exchange. The obtained values were low (0.0075 and 0.0047wt%, respectively) and negligible.

Sample preparation and polymerization reactions

Samples were prepared using a range of different initial compositions (see Table 1). The free radical polymerization was performed under the following conditions. Samples with the desired monomer-to-initiator ratio were prepared in glass tubes and degassed by flushing nitrogen into the tubes for 30 minutes. The purge step was crucial as the presence of oxygen can inhibit the reaction. After the purge the tubes were sealed. The reactions were performed in a water bath at 60ºC for 7 hours. When C_{16}TAAcr was mixed with the APS initiator at room temperature there was a formation of $(C_{16}TA)_2S_2O_8$ crystals, which exhibit lamellar structure[28]. These crystals were fully dissolved at 60ºC. Stirring was performed for some of the dilute samples and all the other dilute samples were agitated inside the water bath to mix the initiator in the samples after the dissolution of the crystals.

Table 1 Different conditions of the polymerizations. Structures found before and after polymerization.

Case	Surfactant	Co-Surfactant	Initiator	r	Structure		α (Å)		d (Å)		Mw (g/mol)	PDI	DP_n
					Before	After	Before	After	Before	After			
1	C_{16}TAAcr (2wt%)		APS	30	Mic	Cub+Aq		105					
1	C_{16}TAAcr (5wt%)		APS	30	Mic	Cub+Aq		105					
1	C_{16}TAAcr (20wt%)		APS	30	Mic	Cub+Aq		105			2.2×10^3	1.5	33
1	C_{16}TAAcr (20wt%)		VA-044	30	Mic	Cub+Aq		107					
1	C_{16}TAAcr (20wt%)		APS	8	Mic	Cub+Aq		108					
1	C_{16}TAAcr (20wt%)		APS	70	Mic	Cub+Mic		109			4.6×10^3	1.4	68
1	C_{16}TAAcr (20wt%)		APS	100	Mic	Cub+Mic		107			8.3×10^3	1.3	115
1	C_{16}TAAcr (50wt%)		APS	30	Hex+Cub	Cub	109	104	50				
1	C_{12}TAAcr (20wt%)		APS	30	Mic	Cub+Aq							
1	C_{12}TAAcr(20wt%)		APS	100	Mic	Cub+Mic		83					
1	C_{12}TAAcr(11wt%)		APS	200	Mic	Cub+Mic		84					
1	C_{12}TAAcr(20wt%)		APS	200	Mic	Cub+Mic		84					
1	C_{12}TAAcr(20wt%)		APS	500	Mic	Cub+Mic		84					
2	C_{16}TAAcr (16wt%)	C_{16}TAAc(19wt%)	APS	30	Cub	Mic	110						
3	C_{12}TAAcr (49wt%)		APS	30	Cub	Cub	85	81					
4	C_{16}TAAcr (56wt%)		APS	30	Hex	Hex			50	47			
4	C_{16}TAAcr (51wt%)		APS	6000	Hex	Hex			52	51			
4	C_{12}TAAcr (65wt%)		APS	30	Hex	Hex			37	38			
5	C_{16}TAAcr (20wt%)		APS	110	Mic	Cub+Hex+Mic							
5	C_{16}TAAcr (20wt%)		APS	125	Mic	Hex+Mic				48			
5	C_{16}TAAcr (20wt%)		APS	250	Mic	Hex+Mic				50	12.2×10^3	1.6	208
5	C_{16}TAAcr (20wt%)		APS	400	Mic	Hex+Mic							
5	C_{16}TAAcr (20wt%)		APS	550	Mic	Hex+Mic							
	C_{16}TAAcr (16wt%)	C_{16}TAAc(5wt%)	APS	30	Mic	Mic+Mic							
	C_{16}TAAcr (13wt%)	C_{16}TABr(10wt%)	APS	30	Mic	Hex+Mic				50			

Molecular weight determination

After polymerization, the polyion and the surfactant ions of the complex were separated through the addition of 2 mL of a salt solution (0.5M NaCl). The best recovery of the polyion alone was obtained by removing the surfactants from the solution by precipitation by addition of NaI in excess (C_{16}TAI is insoluble at room temperature). The solution was then centrifuged and filtered with filter paper. The solution was collected and dialyzed during five days with daily change of water in order to remove the excess salt. The clear solution was freeze-dried for three days and a white powder was obtained.

The molecular weight determination was done with a Multi Angle Laser Light Scattering (Dawn-DSP photometer (eighteen detectors), Wyatt Technology Corporation) coupled with Size Exclusion Chromatography (SEC-MALLS). A differential refractive index detector (DRI) was also used and was placed after the Dawn-DSP photometer. A wide range (500 to 8×10^6 g/mol) Ultrahydrogel Linear 7.8×300 mm column (Serial Number: T02351A 13, Part no. WAT011545) designed for separation of water-soluble polymers was used at a flow rate of 0.3 mL/min. The polymer was dissolved (20 mg/ml) in a 0.1M solution of $NaNO_3$ and 0.2 wt% of sodium azide (NaN_3). The latter solution was also used as the mobile phase, which was degassed by a degasser connected to the water pump. The samples were inserted into a 100 µL loop and injected. The performance of the SEC-MALLS was checked using monodisperse pullulan standards. The data was analyzed using the Wyatt's ASTRA software.

Structures of equilibrium phases

The samples were investigated by visual inspection in normal light and between crossed polarizers to detect optically anisotropic phases. Small angle X-ray (SAXS) measurements were performed with two different setups. At the Max II Laboratory in Lund (beamline I711) the distance sample-to-detector used was 1250 mm and the wavelength 1.1 Å[29]. The analysis of the 2D SAXS scattering patterns was conducted by the Fit2D software[30]. Typically the acquisition time was ca. 15min. The other instrument was a Kratky compact small-angle system with linear collimation. The X-rays were detected with a position sensitive detector. The wavelength was 1.54Å, and the sample-to-detector distance was 277mm. In either instrument, a sample cell with mica windows, or a capillary of 1mm width, was maintained at room temperature. Apart from the resolution difference, no major differences were observed between spectra from these two sources.

The size of a cubic unit cell, α, can be obtained by plotting $(q/2\pi)^2$ versus the Miller indices $(h^2+k^2+l^2)$ of the cubic structures, according to Equation 1.

$$(q/2\pi)^2 = (1/\alpha)^2(h^2+k^2+l^2) \quad (1)$$

It follows from the geometry of the hexagonal structure that the center-to-center distance between adjacent rods, d, can be obtained from the first diffraction peak using Equation 2.

$$d = (2/3^{1/2})(2\pi/q_1) \quad (2)$$

The value of the scattering vector q_1 is the position of the first diffraction peak.

Results

Properties of C_nTA surfactants in water

The cmc of C_{16}TAAcr was determined to 1.6mM from a clear break point in a plot of the measured solution conductivity versus the surfactant concentration (not shown). Figure 1 presents the phase sequences of surfactant/water mixtures for the different surfactants used in this work. The phase sequence was obtained at 40ºC for C_{16}TABr (owing to its high Krafft temperature) and at 25ºC for all the other surfactants. The phases formed were disordered micellar (Mic), micellar cubic (Cub) of $Pm3n$ symmetry or hexagonal (Hex) as expected from previous studies[22,23]. The extension of the cubic phase was larger for the surfactants containing acetate as counterion when compared to the acrylate. Note the absence of a cubic phase for C_{16}TABr[7,22].

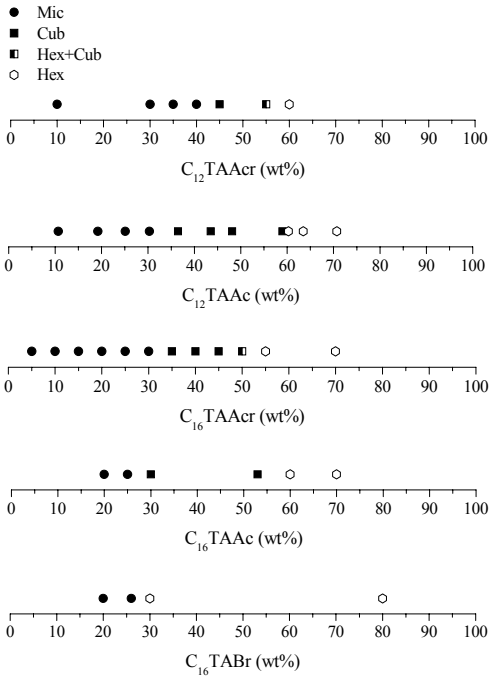

Fig. 1 Phase sequence as a function of surfactant concentration for the various binary surfactant/water systems at 40ºC for C_{16}TABr and at 25ºC for all other systems.

Polymerization reactions

We started the reactions from initial compositions at different points in the binary surfactant/water phase diagrams, covering the range from more dilute to highly concentrated surfactant/water mixtures. A few samples with mixed polymerizable and inert surfactant counterions were included in order to yield systems with mixed polymeric and simple counterions as a result of the polymerization. In Table 1, the

chosen starting compositions are shown. Table 1 also includes structural information on the systems before and after polymerization. Evidently, long-range ordered structures can be created, destroyed, changed or left unchanged on polymerization, depending on the initial conditions. This is a key result of our study.

The matrix of samples includes variations of the monomer-to-initiator ratio r to study of the effect of polyion length in the final system. The parameter r represents the target number-average degree of polymerization of the polymerized polyacrylate polyions, since one initiator molecule is consumed per polyion chain if the reaction terminates exclusively by radical combination. For a few selected systems, covering a range of r values, the molecular weights of the polymerized polyions were determined as described in the experimental section (see Table 1). In all these cases, the measured number average degree of polymerization, DP_n, differed by less than 20% from the target r value. A couple of samples with the alternative initiator VA-044 gave indistinguishable results from those with APS, despite the fact that VA-044 should give bulkier end groups on the polymer chains.

In most of the reactions starting from the micellar phase of the unpolymerized system, a rather high concentration (~20wt%) of surfactant was used to produce sufficient amounts of material after polymerization to enable other studies, such as molecular weight determinations, repeat SAXS measurements and studies of structure transformations caused by changes in temperature. The polymerization of these mixtures resulted in a separation of one or two concentrated, mostly liquid crystalline, phases from a more or less dilute micellar solution. For the $C_{16}TA$ surfactant, the structure of the concentrated liquid crystalline phase changed from cubic to hexagonal around $r \approx 100$. By contrast, for the surfactant with the shorter alkyl chain (12 carbons), samples with a high degree of polymerization retained the cubic structure, in agreement with recent studies of $C_{12}TAPA$ complex salts prepared by mixing, rather than polymerization[25]. For biphasic samples with concentrated phases showing cubic or hexagonal structures, some of the concentrated phase was removed from the reaction tube and put into another tube with pure water and the structure remained unchanged.

For reactions performed starting from disordered micellar solutions at $r > 70$, a significant concentration of surfactant with unreacted monomers was left in the dilute phase after phase separation, as was immediately apparent from the viscosity of the dilute phase. This was confirmed when more initiator was added to the dilute phase, since the reaction then proceeded after placing the sample at 60ºC. In Table 1 and henceforth in this paper, the notation Aq is used to designate a dilute phase that had a viscosity not noticably different from water, while the notation Mic refers to a dilute phase with a viscosity clearly different from water. During polymerization we observed that it took more time before a concentrated phase was observed for higher r, because some monomers were left unreacted and the viscosity of the dilute phase increased, slowing down the macroscopic separation of the concentrated phase.

When r was higher than ca. 300 no macroscopic phase separation of a concentrated phase was seen at 25ºC. However, cryo-TEM investigations performed on one of these samples (for r = 500) revealed that the sample actually contained particles in the 10-40 nm size range (see below). Similarly, $C_{12}TAPA_{r=400}$ was a clear apparently one-phase sample after polymerization but it presented a SAXS profile containing a broad correlation peak and the three characteristic peaks at relative positions of $4^{1/2}$:$5^{1/2}$:$6^{1/2}$, which are the signature of the *Pm*3*n* cubic structure.

To test that polymerization had actually occurred also in the initially very concentrated one-phase cubic and hexagonal samples, where no change of structure occurred on polymerization, water was added to these samples after polymerization. According to the results from the polymerizations of the more dilute samples, described above, the complex salt produced should be insoluble in excess water. The results obtained confirmed this prediction. Also in accordance with results for more dilute mixtures, the addition of water to the polymerized cubic and hexagonal phases obtained for the polymerizations of $C_{12}TAAcr$ (49wt%), $C_{12}TAAcr$ (65wt%) and $C_{16}TAAcr$ (56wt%) at r = 30 resulted in their transformations to cubic phases in equilibrium with very dilute aqueous phases.

To explore the significance of our salt-free approach to the synthesis of ordered structures, we performed the polymerization of sodium acrylate (0.0659 g ↔ 0.0007 mol) in the presence of $C_{16}TACl$ (Cl=chloride) (0.2249 g ↔ 0.0007 mol) in water (the total weight of the sample was 1.06 g). This means that we included stoichiometric amounts of simple inorganic counterions to the cationic surfactant and to the polymerizable anion. In the presence of the additional sodium and chloride ions, no phase separation was observed. When mixing the complex salt $C_{16}TAPA_{25}$ (0.249 g ↔ 0.0007 mol monomer) with NaCl (0.0406 g ↔ 0.0007 mol), that is, using the same equivalent concentrations as in the polymerization just described, we confirmed that the salt present influenced the interaction sufficiently to dissolve the complex salt into a single disordered micellar phase.

Influence of temperature

The effect of increasing the temperature on the structures of some biphasic samples after polymerization were investigated by visual inspection and SAXS measurements, see Table 2. For $C_{16}TAPA_{r=30}$, increasing temperature caused the surfactant aggregates to grow and the cubic structure changed into hexagonal. For $C_{16}TAPA_{r=8}$ the temperature increase changed a cubic/aqueous two-phase sample into a micellar/micellar two-phase sample. For the sample with a mixture of the polymerizable and inert surfactants, no structural change was observed. For $C_{16}TAPA_{r=250}$, the resulting sample from polymerization was a two-phase sample with a hexagonal phase in equilibrium with a dilute micellar phase. At 60ºC, the amount of precipitated material increased. For $C_{16}TAPA_{r=400}$ and $C_{16}TAPA_{r=550}$, the samples resulting from polymerization were clear solutions which did not visually appear to be different from the starting mixture (micellar), but with SAXS it was possible to see, in addition

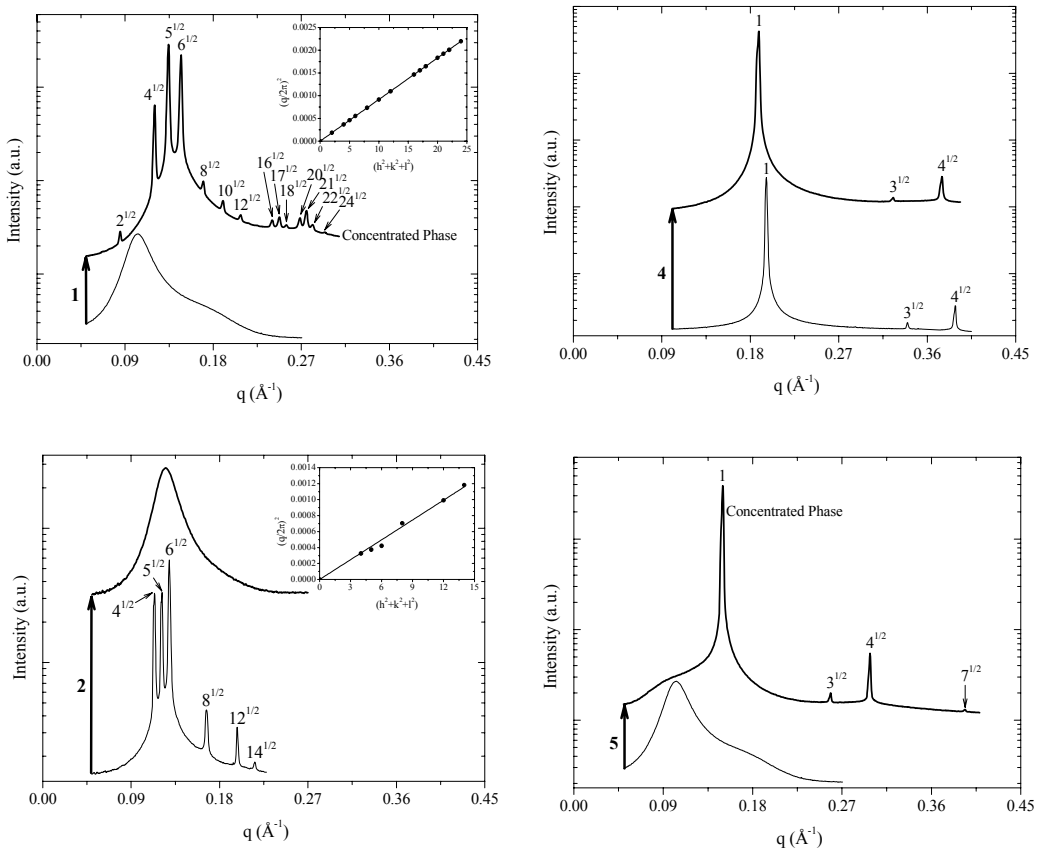

Fig. 2 SAXS profiles representing the different scenarios identified as cases 1-5 in Table 1, illustrating that long-range ordered structures can be produced, destroyed or preserved, depending on the choice of initial conditions, as a result of polymerizing the surfactant counterions. A case number is given in each profile, and the initial surfactant contents before synthesis were: **1** - C_{16}TAAcr (20wt%) (r=30), **2** - C_{16}TAAcr (16wt%) (r=30) and C_{16}TAAc(19wt%) (r=30), **3** - C_{12}TAAcr (49wt%) (r=30), **4** - C_{12}TAAcr (65wt%) (r=30) and **5** - C_{16}TAAcr (20wt%) (r=125). The thin and the thick line profile show the structure before and after polymerization, respectively. The relative peak positions are indicated. Inset: $(q/2\pi)^2$ versus $(h^2+k^2+l^2)$.

Table 2 Structure as a function of temperature.

Surfactant	Co-Surfactant	Initiator	*r*	Structure after reaction at 25ºC	T (ºC)		
					30	40	60
					Structure		
C_{16}TAAcr (20wt%)		APS	8	Cub+Aq			Mic+Mic
C_{16}TAAcr (20wt%)		APS	30	Cub+Aq	Cub+Aq	Hex+Mic	Hex+Aq
C_{16}TAAcr (20wt%)		VA-044	30	Cub+Aq	Cub+Aq	Hex+Mic	Hex+Aq
C_{16}TAAcr (20wt%)		APS	250	Mic	Hex+Mic		Hex+Mic
C_{16}TAAcr (20wt%)		APS	400	Hex+Mic	Hex+Mic	Hex+Mic	Hex+Mic
C_{16}TAAcr (20wt%)		APS	550	Hex+Mic	Hex+Mic	Hex+Mic	Hex+Mic
C_{16}TAAcr (16wt%)	C_{16}TAAc (19wt%)	APS	30	Mic			Mic
C_{12}TAAcr (20wt%)		APS	30	Cub+Aq			Mic+Mic
C_{12}TAAcr (20wt%)		APS	100	Cub+Mic			Mic
C_{12}TAAcr (20wt%)		APS	200	Cub+Mic		Mic	Mic

to the wide correlation peak typical of concentrated micellar solutions, one sharp peak at a *q* value consistent with the first diffraction peak of the hexagonal phase. Increasing the temperature in the latter two samples to 60ºC resulted in macroscopically phase-separated samples. For the systems containing C_{12}TA, we recall that the cubic structure was obtained at 25°C for the entire range of *r* studied. However, an increase in temperature to 60ºC lead to the destruction of the cubic structure for all studied *r* (30, 100 and 200).

Formation of particles

Although the focus of the present study is on the microscopic structures of the concentrated phases resulting from polymerization of surfactant counterions, we also made some preliminary observations regarding the meso- and macroscopic appearance of such concentrated phases. Increasing the value of *r* in a matrix of samples ($C_{16}TAPA_{r=250}$, $C_{16}TAPA_{r=400}$, $C_{16}TAPA_{r=550}$ and $C_{12}TAPA_{r=100}$, $C_{12}TAPA_{r=200}$, $C_{12}TAPA_{r=400}$) led to the formation of particles dispersed in solution. The particle size decreased with increasing *r* for both C_{16}TAPA and C_{12}TAPA systems. Particles with very different sizes ranging from ca 60μm ($C_{12}TAPA_{r=100}$) to 10nm ($C_{12}TAPA_{r=400}$) were observed by means of light microscopy and Cryo-TEM. The polydispersity was high. The size of the particles could also be decreased by dilution after polymerization.

Discussion

Phase diagrams come alive

The results obtained from our polymerization reactions may be summarized as five different cases, as indicated in Table 1:

- The polymerization of the counterions in a disordered micellar solution results in the formation of a concentrated, ordered cubic phase, containing polyions and the surfactant aggregates in equilibrium with essentially pure water (case **1**).
- A partial polymerization of the counterions in an originally cubic phase results in a change of the system to a viscous disordered micellar solution (case **2**).
- It is possible to polymerize the counterions of an initially cubic or hexagonal phase without changing the structure (cases **3** and **4**, respectively).
- Increasing the molecular weight of the polyion in the C_{16}TA system leads to a hexagonal phase instead of a cubic phase separating out from an originally micellar phase (case **5**).

Figure 2 shows SAXS profiles corresponding to the cases 1 to 5 before and after the polymerization reaction. The profile at the bottom always corresponds to the structure before polymerization and the arrow, symbolizing the polymerization process, ends at the top profile, which corresponds to the structure after the polymerization. For the polymerizations resulting in the two-phase samples (concentrated + dilute), the SAXS profile shown refers to the concentrated phase.

We will now show that all the obtained results are actually predicted by previously established equilibrium phase diagrams of mixtures of C_nTAAc and C_nTAPA_m (m=number of repeating units in the polymer) in water, shown in Figure 3. Of particular relevance in the present context are horizontal pathways (constant water content), emerging from the binary surfactant/water axis, which show what happens when an originally monomeric surfactant counterion is replaced by a polymeric counterion. The phase transitions occurring as a result of such a replacement have been interpreted in detail in the original references[22,23,25]. The special significance of the horizontal pathways here is that each path predicts the outcome of a polymerization of an initially monomeric counterion. Thus, the phase diagrams "come alive" as the systems evolve through the polymerization reactions.

Each of the arrows drawn in the diagrams in Figure 3 represents a specific case (**1** to **5** described above) of our polymerization reactions: It begins at the composition of the unpolymerized reaction mixture and ends either at the binary complex salt-water axis, for complete polymerization of all counterions, or earlier, for cases where the original reaction mixtures contained a fraction of inert acetate or bromide counterions. Although the comparison is approximate in the sense that the original monomeric counterion in the synthesis was acrylate, rather than acetate or bromide, and the final degree of polymerization was not exactly the one in the phase diagram, we can conclude that the qualitative correspondence is excellent. In all cases, the arrow beginnings describing the initial systems, as well as the arrow-heads predicting the results of the syntheses, are situated in the correct one- or two-phase regions of the phase diagrams.

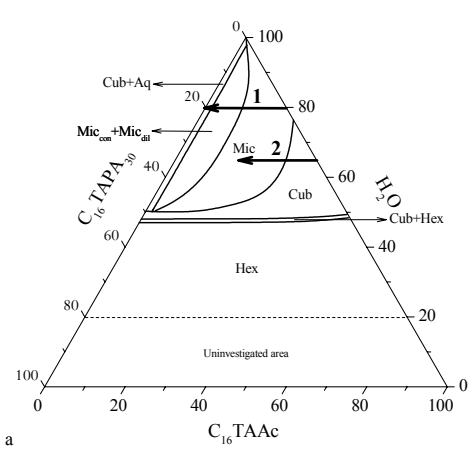

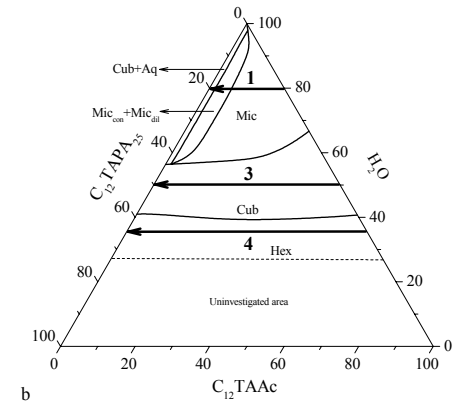

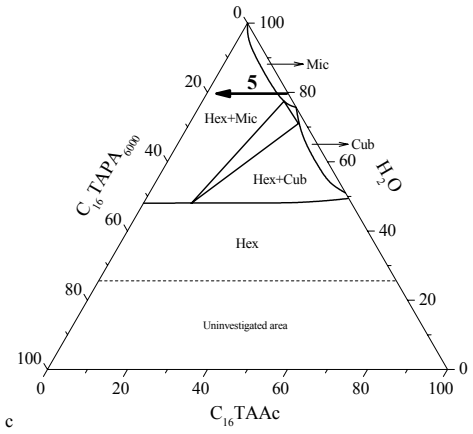

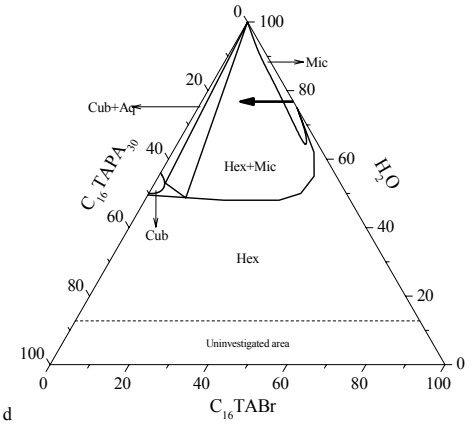

Fig. 3 Equilibrium phase diagrams for ternary mixtures of surfactant, complex salt and water. The phase diagrams are redrawn from those in references 24 (a), 23 (c), 25 (b) and 22 (d). The thick arrows with numbers in (a-c) represent the different outcomes from polymerization reactions identified as cases 1-5 in the text. The arrow in (d) is described separately in the text.

Figure 4 gives more detail on the transition from case **1** to **5** on increasing *r* for the $C_{16}TA$ system. The SAXS profiles after polymerization show that an increase in the molecular weight changed the structure of the concentrated phase that separated out from the $C_{16}TA$ system from cubic to hexagonal. This transition was already reported by Svensson et al to occur between the molecular weights 5000 and 20000 g/mol at 25ºC[23]. Interestingly, in Figure 4 at the intermediate *r* equal to 110, a three-phase sample was obtained, containing according to the SAXS profile both cubic and hexagonal structures in addition to the dilute phase. This indicates incomplete polymerization (a mixture of monomeric and polymeric counterions), since a three-phase coexistence requires a ternary mixture, according to the Gibbs phase rule. Indeed, the phase diagram for the longer polyion in Figure 3c features a region of coexistence of these three phases which is located in the interior of the phase triangle, where the system contains both monomeric and polymeric counterions. The exact location of the three-phase triangle should, of course, differ between the various systems in Figures 3 and 4, owing to differences in the degree of polymerization of the polyion.

When the monomer-to-initiator ratio was increased through the sequence of systems of Figure 4, the viscosity of the dilute phase remaining after polymerization was also found to increase, indicating that it contained surfactant with unreacted monomers, as described above. Again, the phase diagram in Figure 3c provides a possible explanation for this incomplete conversion: long polyions are predicted to partition essentially quantitatively to the concentrated phase from a dilute phase that contains only monomeric counterions. Hence, as the reacting polyions reach a sufficient length, they quantitatively separate out from a dilute micellar phase which is left without

reacting species and, therefore, does not react further. This interpretation is supported by the observation that the dilute phase could be polymerized further with the addition of more initiator. A similar phenomenon, where a polymerization reaction is terminated before completion owing to a phase separation of the growing polymer chains, occurs in the well-known dispersion polymerization process[31].

Table 1 includes a result of the polymerization of C_{16}TAAcr in the presence of C_{16}TABr, performed as a means to study the effect of ion specificity. In accordance with the prediction from the phase diagram presented in Figure 3d, the result (obtained at 40ºC as in the phase diagram) after polymerization was a concentrated phase with a hexagonal structure in equilibrium with a dilute micellar phase.

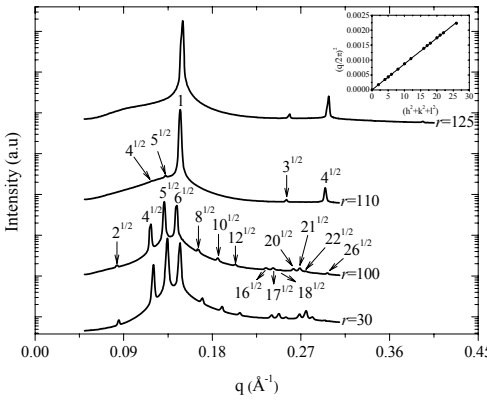

Fig. 4 SAXS profiles of the concentrated phases produced for different monomer-to-initiator ratios r (numbers on the side of respective profile) when polymerizing C_{16}TAAcr (20wt%) in water. The relative peak positions are indicated (for r=30 and r=125 see Figure 2). Inset: $(q/2\pi)^2$ versus $(h^2+k^2+l^2)$ for r=100.

Implications

Our results clearly illustrate that a successful incorporation of polymer and surfactant in an ordered liquid crystalline structure is most readily achieved if one uses an associating polymer-surfactant pair. This is indeed the case in formulations used in practice, and the scenarios here denoted as cases **1** and **5** correspond closely to a process that is used routinely in the synthesis of mesoporous inorganic materials, that is, polymerizing silicates in micellar solutions of cationic surfactants[15,32]. In contrast to our systems, the structures produced by polymerization of silicates eventually become kinetically trapped by solidification of the silica. Nevertheless, evolutions during polymerization of silicates have been observed that resemble the findings of the present study. Atluri et al performed the synthesis of silica in the presence of C_{16}TABr with direct condensation of (3-aminopropyl)triethoxysilane (APES)[15]. The result agrees with the phase study made by Svensson et al which is here reproduced as our Figure 3d. The latter equilibrium phase diagram shows that along a path from the C_{16}TABr/water axis to the complex salt/water axis there occurs a change in structure from hexagonal to cubic. The same transformation was seen in Atluri et al when APES was polymerized.

The effect of temperature was also studied by Atluri et al. At room temperature they obtained a cubic phase while at 50ºC and 70ºC, the resulting structure was hexagonal, in agreement with our results. In the synthesis of the kinetically arrested crosslinked silica network, the temperature of synthesis determined the final structure, while in our case the system was flexible enough to allow for an interchange between structures with changing temperature after the polymerization was terminated.

Conclusions

We have here demonstrated how established knowledge from equilibrium mixtures can make the results from polymerization reactions in surfactant-polymer systems clear and understandable. To use pathways through phase diagrams to predict the results of processes is, of course, nothing new; predictions of phase changes resulting from a change in temperature are commonplace. Also changes in composition are regularly used to predict, for instance, the results from dilution with excess solvent; the study in reference 5 may serve as an example. We believe, however, that the phase diagram pathways explored here - replacing a small molecule with its larger polymeric analogue - are unconventional, but could be exploited more widely to predict and rationalize results of polymerization processes in complex self-assembled systems. Based on such knowledge, one can predict strategies to retain structures during polymerization reactions, but also to transform disordered phases into ordered phases or *vice versa*.

Here we have thus shown that the appropriate choices of surfactant alkyl chain length, monomer-to-initiator ratio and overall reactant concentrations become tools with understandable roles in a rational design of the polymerization pathways to produce desired structures. The design can also include the incorporation of non-reactive counterions and different counterions to the surfactant ion, as well as added excess salt. Not only the resulting structures can be understood from the equilibrium phase diagrams, but also why, under certain conditions, reactions may terminate before full conversion owing to a phase separation of the growing polymer chains.

An important finding in its own right is that, for the C_nTAPA_m systems of our study, the polymerization of acrylate as performed gave the same structures and phases as previously obtained for direct mixtures, using a complex salt as one component. This strongly suggests that both methods give rise to equilibrium structures of these mixtures.

Although our studies were performed on a single class of complex salts (alkyltrimethyl polyacrylates) in systems of a minimum complexity (a minimum number of components), we found trends that should be quite general and which, indeed, agree with trends seen for polymerizing silica precursors in the same surfactant systems.

Acknowledgements

This study was funded by Fundação para a Ciência e a Tecnologia (SS, SFRH/BD/30929/2006), by POPH/FSE (SS) and by the Swedish Research Council (VR) through the Linnaeus Centre of Excellence on Organizing Molecular Matter (OMM). The authors thank Viveka Alfredsson for valuable discussions.

References

1 K. Thalberg, B. Lindman, G. Karlström, *J. Phys. Chem.*, 1991, **95**, 6004-6011.
2 K. Thalberg, B. Lindman, K. Bergfeldt, *Langmuir*, 1991, **7**, 2893-2898.
3 J. O. Carnali, *Langmuir* 1993, **9**, 2933-2941.
4 S. Ranganathan and J. C. T. Kwak, *Langmuir*, 1996, **12**, 1381-1390.
5 P. Ilekti, L. Piculell, F. Tournilhac, and B. Cabane, *J. Phys. Chem. B,* 1998, **102**, 344.
6 L. Piculell, B. Lindman and G. Karlström, in *Polymer-Surfactant Systems* (J. C. T. Kwak, ed.), Marcel Dekker, New York, 1998, Chapter 3, pp. 65-141.
7 P. Ilekti, T. Martin, B. Cabane and L. Piculell, *J. Phys. Chem. B,* 1999, **103**, 9831-9840.
8 R Dias, S Mel'nikov, B Lindman and M da Graça Miguel, *Langmuir*, 2000, **16**, 9577-9583.
9 Yu. V. Khandurina, V. L. Alexeev, G. A. Evmenenko, A. T. Dembo, V. B. Rogacheva and A. B. Zezin, *J. Phys. II France*, 1995, **5**, 337-342.
10 H. Okuzaki, Y. Osada, *Macromolecules*, 1995, **28**, 380-382.
11 F. Yeh, E. L. Sokolov, A. R. Khokhlov and B. Chu, *J. Am. Chem. Soc.*, 1996, **118**, 6615-6618.
12 S. Zhou, F. Yeh, C. Burger and B. Chu, *J. Phys. Chem.*, 1999, **103**, 2107-2112.
13 J. Merta, M. Torkkeli, T. Ikonen, R. Serimaa and P. Stenius, *Macromolecules*, 2001, **34**, 2937-3946.
14 K. Kogej, E. Theunissen and H. Reynaers, *Langmuir*, 2002, **18**, 8799-8805.
15 R. Atluri, Y. Sakamoto and A. E. Garcia-Bennett, *Langmuir*, 2009, **25** 3189-3195.
16 O. Santos, E. S. Johnson, T. Nylander, R. K. Panandiker, M. R. Sivik and L. Piculell, *Langmuir*, 2010, **26**, 9357-9367.
17 A. V. Svensson, L. Huang, E. Johnson, T. Nylander and Lennart Piculell, *Appl Mater Interfaces*, 2009, **11**, 2431-2442.
18 G. Nizri, A. Makarsky, S. Magdassi and Y. Talmon, *Langmuir*, 2009, **25**, 1980-1985.
19 M. Antonietti, C. Göltner and H.-P. Hentze, *Langmuir*, 1998, **14**, 2670.
20 H.-P. Hentze and E. W. Kaler, *Curr. Opin. Colloid. Interf. Sci.*, 2003, **8**, 164.
21 L. Piculell, A. Svensson, J. Norrman, J. S. Bernardes, L. Karlsson and W. Loh, *Pure Appl. Chem.* 2007, **79**, 1419-1434.
22 A. Svensson, L. Piculell, B. Cabane and P. Ilekti, *J. Phys. Chem. B*, 2002, **106**, 1013.
23 A. Svensson, J. Norrman and L. Piculell, *J. Phys. Chem. B*, 2006, **110**,10332-10340.
24 A. Svensson, L.Piculell, L. Karlsson, B. Cabane & B. Jönsson, *J. Phys. Chem. B*, 2003, **107**, 8119-30.
25 S. dos Santos, C. Gudmundsson, C. Gustavsson, P. Linse and L. Piculell, manuscript in preparation.
26 C. Leal, A. Bilalov, B. Lindman, *J. Phys. Chem. B*, 2006, **110**, 17221-17229
27 A. Svensson, D. Topgaard, L. Piculell and Olle Söderman, *J. Phys. Chem. B*, 2003, **107**, 13241-13250.
28 X. Zhang, J. Zhang, Z. Liu and C. Robinson, *Chem. Commun.*, 2004, 1852.
29 M. Knaapila, C. Svensson, J. Barauskas, M. Zackrisson, S.S. Nielsen, K. N. Toft, B. Vestergaard, L. Arleth, U. Olsson, J. S. Pedersen and Y. Cerenius, *J. Synchrotron Rad.*, 2009, **16**, 498-504.
30 A. Hammersley, Grenoble. Private communication .
31 R. Arshady, *Colloid Polym. Sci.*, 1992, **270**, 717-732.
32 K. Edler. *Aust. J. Chem.*, 2005, **58**, 627-643.

Notes

[a] *Division of Physical Chemistry, Center for Chemistry and Chemical Engineering, Lund University, P.O.Box 124, SE-22100 Lund, Sweden. E-mails: Salome.Santos@fkem1.lu.se , Lennart.Piculell@fkem1.lu.se & Ola.Karlsson@fkem1.lu.se*
[b] *Chemistry Department, Coimbra University, 3004-535 Coimbra, Portugal. E-mail: mgmiguel@ci.uc.pt*

Paper V

Responsive and Evolving Mixtures of a Hydrolyzing Cationic Surfactant and an Oppositely Charged Polyelectrolyte

Salomé dos Santos[1*], Dan Lundberg[1,2*] and Lennart Piculell[1]

1) Physical Chemistry, Center for Chemistry and Chemical Engineering, Lund University P.O. Box 124, 221 00 Lund, Sweden

2) Department of Chemistry, University of Coimbra, Rua Larga, 3004-535 Coimbra, Portugal

* Corresponding author

Abstract

The structure of concentrated phases formed when solutions of oppositely charged polyelectrolyte and surfactant are mixed was changed *in situ* via the hydrolysis of the surfactant, decyl betainate (DeB). The ester bond of DeB is highly susceptible to base-catalyzed hydrolysis, which causes degradation of the surfactant into decanol, and the amino acid betaine at only slightly alkaline conditions. At the conditions in question betaine is deprotonated, which gives a gradual decrease in the pH as the reaction proceeds. DeB was mixed either with a titratable polyelectrolyte, sodium poly(acrylate), NaPA, or with a non-titratable polyelectrolyte, sodium poly(styrene sulfonate), NaPSS. The first mixture is a "self-degrading" and "self-quenching" mixture; due to the high pH (~8) of the NaPA-DeB mixture, DeB degradation starts without addition of base and because pH is decreasing as the reaction proceeds the reaction stops by itself. As the reaction proceeds, the fraction of alcohol increases and, consequently, the curvature of the structure concentrated phase decreases. The structural sequence cubic-hexagonal-lamellar was obtained for macroscopic concentrated phases. For mixtures where polyion-surfactant ion nano-particles were studied, the cubic phase was not identified but the formation of multi-lamellar "onion-like" particles was obtained when decanol concentration increased. Mixtures containing not only NaPA and DeB but also a stable surfactant (dodecyltrimethylammonium chloride, DoTAC) were prepared in order to control the amount of alcohol produced. Mixtures of a non-titratable polyelectrolyte, NaPSS, DeB and DoTAC, produced a polyion-surfactant ion concentrated phase without long-range order. When exposed to NaOH, the structure of the concentrated phase changed into hexagonal. An interesting and dramatic swelling of the concentrated phase was observed when it was rinsed with large amounts of water. The swelling increased with the increasing amount of decanol produced in the structure. The hexagonal structure was kept in the swollen concentrated phases, inclusive the center-to-center distance between the cylinders.

1. Introduction

Dilute aqueous mixtures of polyelectrolytes and oppositely charged surfactants typically show a strong propensity for associative phase separation leading to the formation of concentrated phases containing polyion-surfactant ion complexes in equilibrium with a solution containing mainly the simple counterions. The concentrated phases often show different liquid crystalline structures (e.g. cubic, hexagonal or lamellar) depending on factors such as the polymer length, the surfactant akyl chain length and the presence of additional compounds, for instance, alcohols [1-3].

Stoichiometric "complex salts" of poly(acrylate) and alkyltrimethylammonium surfactant ions in water have been extensively investigated [1,3-5]. In excess water, a complex salt of dodecyltetramethylammonium ions ($DoTA^+$) and poly(acrylate) (PA^-) forms a micellar cubic structure [1,6,7]. Addition of increasing fractions of decanol to the DoTAPA complex salt induces transformations of the cubic structure into first a hexagonal and then a lamellar one due to a decrease in the spontaneous curvature of the surfactant-water interface on addition of a long-chain alcohol [2].

Long-chain esters of the amino acid betaine (trimethyl glycine) are cationic surfactants, which show a physicochemical behavior similar to that of surfactants of the alkyltrimethylammonium type [8,9]. However, the presence of an ester bond in their molecular structures makes them susceptible to hydrolysis, which degrades the surfactant into betaine (zwitterionic) and a long-chain alcohol, see Figure 1. The hydrolysis of betaine esters shows a rather dramatic pH dependence, and are much more prone to alkaline hydrolysis than esters in general, whereas they show higher stability in acidic environments; the compounds are hydrolyzed at a considerable rate at neutral pH (typically on the order of hours) by the base-catalyzed mechanism [10,11]. It is thus possible to produce an *in situ* transformation of cationic surfactant into a long-chain alcohol under rather mild conditions. This characteristic of betaine ester surfacatnts has been utilized to design different types of systems with dynamic, responsive or evolving, properties [12]. For instance, hydrolysis of oleyl betaine induces an *in situ* formation of small unilamellar vesicles [13] and appropriately composed aqueous mixtures of long-chain betaine esters with hydrophobically modified hydroxyethyl cellulose show time-dependent rheological properties [14].

In this paper we introduce a new type of dynamic system involving a betaine ester surfactant. Complexes of decyl betainate (DeB) and two different polyanions (poly(acrylate) (PA^-) or poly(styrene sulfonate) (PSS^-), see Figure 1b and c were investigated. DeB has the molecular structure shown in Figure 1a, and its critical micelle concentration (CMC) is similar to that of DoTAC, i.e. ~15 mM [11]. When such complexes are exposed to an environment where the betaine ester is hydrolyzed, and thus decanol is produced, they are expected to undergo

structural transformations similar to those observed by Bernardes et al. [2]. To control the maximum fraction of the total cationic surfactant that could be converted into alcohol we included varying fractions of inert dodecyltrimethylammonium chloride (DoTAC) in many of the investigated samples.

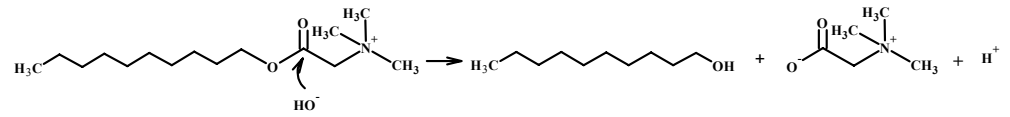

Figure 1. a – Base-catalyzed hydrolysis of decyl betainate, DeB, into decanol and betaine. b – Molecular structure of sodium poly(acrylate), NaPA. c – Molecular structure of poly(styrene sulfonate), NaPSS.

2. Evolving self-degrading and self-quenching systems

In the first series of samples to be discussed, sodium polyacrylate (NaPA) was mixed with DeB and DoTAC in different proportions, see Table 1. For all studied compositions the solutions had an initial pH of ~8. At this pH, hydrolysis of DeB is immediately initiated; the solutions containing NaPA and DeB can thus be characterized as "self-degrading" mixtures.

On mixing of the polyelectrolyte and surfactant solutions, a translucent concentrated phase containing polyion-surfactant ion complexes formed in all samples. However, for the mixtures containing DeB, the macroscopic appearance of the mixture immediately started to change. After equilibration for 2-4 days no further changes were observed and all samples were two-phase samples, presenting a concentrated phase in coexisting with a dilute aqueous phase.

Small-angle X-ray scattering (SAXS) experiments showed that the concentrated phases of mixtures containing DoTAC as the only surfactant component formed cubic structures for all investigated compositions (see Table 1), in agreement with previous findings. The final concentrated phases in mixtures containing DeB were all birefringent and SAXS revealed that they indeed presented either hexagonal or lamellar structures; example scattering profiles are shown in Figure 2 and the respective characteristic distances are presented in Table 1.

Table 1. Initial mixed compositions, pH values and SAXS results of the concentrated phases from NaPA, DoTAC and DeB mixtures.

NaPA[a] (mM)	DoTAC (mM)	DeB (mM)	pH_{Final}	Structure[b]
100	200		7.9	Cub
100	100		8.1	Cub
100	50			Cub
100	80	20	6.4	Hex, d_{hex}=4.4 nm
100	150	50	5.4	Hex, d_{hex}=4.5 nm
100	100	100	4.0	Lam, d_{lam}=4.2 nm
100		100	4.1	Lam, d_{lam}=4.1 nm
100		50	5.7	Lam, d_{lam}=4.1 nm

[a] Concentration in terms of monomer units; 100 mM ⇔ roughly 1 wt%

[b] Final structure of complexes; d_{hex} is the center-to-center distance between adjacent cylinders; d_{lam} is the distance between equivalent the planes in the lamellar structure.

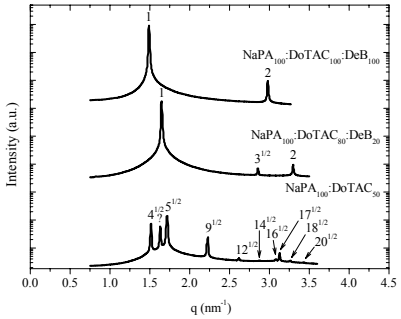

Figure 2. SAXS profiles of various concentrated phases from $NaPA_{100}$:$DoTAC_x$:DeB_y mixtures. Subscripts denote the concentrations of the respective components. The relative positions of the reflections are shown; $4^{1/2}$:$5^{1/2}$:$9^{1/2}$:$12^{1/2}$:$14^{1/2}$:$16^{1/2}$:$17^{1/2}$:$18^{1/2}$:$20^{1/2}$ for cubic, 1:$3^{1/2}$:2 for hexagonal and 1:2 for lamellar structures.

A factor with important influence on the system is that acid is formed on hydrolysis of DeB (compare to Figure 1a), which causes a gradual decrease in pH and a concomitant reduction in degradation rate as the reaction proceeds. The mixtures are thus also "self-quenching", which explains why there was still intact DeB available to form complexes in the final states of samples containing no other surfactant. The final pH in each sample, measured several weeks after preparation is shown in Table 1. One can see that the final pH is lower the higher the initial concentration of DeB. In the samples with the lowest total concentrations of DeB, where pH remained high, one can reasonably assume that the hydrolysis reaction had proceeded essentially to completion. Taking this into account, one can suggest that, since the sample with 80 mol% DoTAC formed a hexagonal phase, the final fractions of remaining intact surfactant in both the 50 and the 100 mM DeB samples was lower than 80 mol%. No attempts were made to determine the final compositions of the samples.

3. Particles with evolving structures

Nizri et al have recently shown that ordered polyion-surfactant ion nano-particles can be produced by simply mixing dilute solutions of NaPA and of single tailed cationic surfactants [14]. Mixtures that are off stoichiometry with respect to charge can form stable dispersions due to electrostatic stabilization from an excess charge at the surface of the complex particles. We prepared the corresponding dispersions with DeB to investigate if the particles would show a similar change in internal structure as observed for the macroscopic complexes discussed above. Samples were prepared using the procedure described by Nizri *et al* [15], by mixing 10 mM NaPA with 5 mM DeB, and then characterized after different times. pH was monitored every 24 h; the initial and final pH values for samples of different ages are shown in Table 2.

Immediately after mixing, all samples were homogeneous and visually clear. Generally, the samples became slightly hazy on storage, with the cloudiness increasing with time. The samples eventually showed a macroscopic separation of an oily liquid, presumably mainly decanol; it took at least 6 weeks until this was observed.

Table 2. pH values and SAXS results from NaPA and DeB mixtures.

Sample age	$pH_{Initial}$	pH_{Final}	q (nm^{-1})
just mixed			1.68
1 day	9.1	7.7	1.63
5 days	9.2	7.0	1.58
20 days	8.9	6.4	1.53

SAXS profiles for the samples consistently showed a single, broad reflection at the q values presented in Table 2. The change over time of the q value was consistent with the sequence of cubic-hexagonal-lamellar structures observed for the concentrated phases of the more concentrated samples discussed in section 2 (compare to Figure 2). The absence of higher order reflections are tentatively ascribed to low concentrations and/or small sizes of the ordered domains [16].

To verify that the internal structure changed with time, particles from selected samples were visualized using cryo-transmission electron microscopy (cryo-TEM). Figure 3 shows images of one freshly prepared sample and one that was 17 days old.

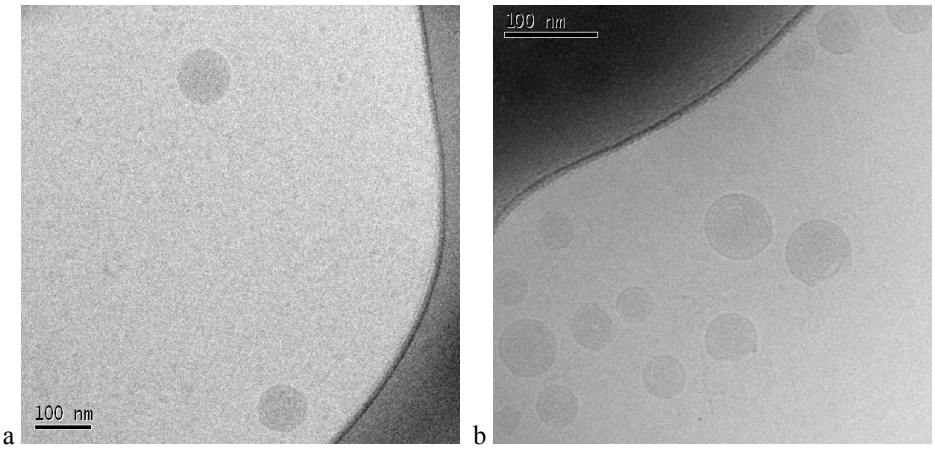

Figure 3: Cryo-TEM images of aliquots taken from samples freshly prepared (a) and 17 days old (b).

In the freshly prepared sample, the particles were essentially spherical, but with somewhat rough edges, and had diameter in a range of 30-80 nm. The internal structure of the particles was not possible to identify from the micrographs. After 8 days no significant change in particle appearance was apparent (images not shown). However, in the sample 17 days of age, a major fraction of observed particles showed a clear multi-lamellar ("onion-like") structure. The repeat distance between layers was 4-5 nm, consistent with that found for the macroscopic polyion-surfactant ion concentrated phases discussed in section 2 (compare with Table 1). It is appropriate to mention that for samples older than 8 days, a background pattern of "leopard-like" spots was consistently observed in the images (see images of the 17 days old sample in Figure 3). This is tentatively ascribed to patches of excess decanol.

4. Responsive systems triggered by alkali

Sections 2 and 3 show that mixtures of NaPA and DeB form complexes with "self-induced" structural changes. However, if polyacrylic acid (PAA) is used instead of the PA^- salt, one can obtain systems for which complex formation and subsequent surfactant hydrolysis can be triggered by the addition of alkali. When PAA was mixed with DeB and DoTAC in different proportions, see Table 3, clear, homogeneous solutions with a pH of ~2.5 were obtained; their appearance and pH remained unchanged with time. At these pH conditions PAA is practically uncharged and DeB should be reasonably stable towards hydrolysis [10]. Following equilibration at rest for 24h the homogeneous, acidic solutions were put in a dialysis bag and dialyzed against 0.5 M of NaOH (pH ~14) for 2.5 h.

Table 3. Initial mixed compositions and SAXS results of the concentrated phases from PAA, DoTAC and DeB mixtures.

PAA (mM)[a]	DoTAC (mM)	DeB (mM)	Structure[b]
100	100		Cub
100	100	20	Hex, d_{hex}=4.4 nm
100	100	100	Lam, d_{lam}=4.4 nm

[a] Concentration in terms of monomer units; 100 mM ⇔ roughly 1 wt%

[b] d_{hex} is the center-to-center distance between adjacent cylinders; d_{lam} is the distance between equivalent planes in the lamellar structure

Exposure of the PAA-surfactant mixtures to alkali has two immediate consequences: the PAA becomes deprotonated, and thus gains a negative charge, and hydrolysis of DeB begins. At the conditions in question DeB does, as expected, form a complex with the polyanion.

Data from SAXS experiments performed three weeks after the dialysis are presented in Table 3. These results show that the same sequence of structures with increasing initial DeB content is indeed shown, for the concentrated phases that separate out from solution, as in the NaPA-DeB-(DoTAC) mixtures. At the high pH of the dialysis experiment a complete conversion from DeB to decanol is expected to occurr. The same repeat distances were obtained irrespectively of whether the complexes were kept in alkaline solution or washed.

5. Responsive mixtures with a non-titrating polyelectrolyte

Finally, we will consider mixtures with sodium poly(styrene sulfonate), NaPSS, a polyelectrolyte, that has non-titratable anionic groups and thus a permanent negative charge. A range of samples containing NaPSS, DeB, and DoTAC, as detailed in Table 4, were prepared in the same way as the samples with PAA discussed in section 4. An important difference between the PAA and the NaPSS mixtures is that, in the latter, complexes were formed immediately on mixing.

Table 4. Initial mixed compositions and SAXS results of the concentrated phases from NaPSS, DoTAC and DeB mixtures.

NaPSS	DoTAC	DeB	Structure[a]	Structure[b]
100	100		Mic, d_{mic}=3.7 nm	Mic, d_{mic}=3.7 nm
100	90	10		Hex, d_{hex}=4.0 nm
100	80	20	Mic, d_{mic}=3.7 nm	Hex, d_{hex}=4.2 nm
100	70	30		Hex, d_{hex}=4.4 nm

[a] Structure of the the concentrated phases after mixing and before dialysis against NaOH. d_{mic} is the correlation distance between micelles.

[b] Structure of the the concentrated phase after dialysis against NaOH. d_{hex} is the center-to-center distance between adjacent cylinders

Before dialysis, the concentrated phase in all samples had a translucent appearance and, as exemplified in Figure 4a, a single broad reflection occurred in the SAXS profiles. This finding can likely be ascribed to a structure of by randomly distributed micelles, as found previously in mixtures of PSS^- and surfactant cations [17,18].

When the translucent concentrated phases collected from all non-dialyzed samples were rinsed with excess water, they became white and showed a slight shrinking. The observed compaction can likely be ascribed to removal of simple salt. However, no significant change in the structure was observed by SAXS.

On exposure to alkali the translucent concentrated phases showed a notable swelling and took on a whitish appearance. The swelling can be ascribed to a decrease in the surfactant ion content of a complex as DeB is hydrolyzed: to maintain electroneutrality, simple counterions to the polyion have to enter the complex and gives rise to an osmotic swelling. Consequently, the extent of swelling increases with an increasing initial fraction of DeB.

Figure 4a presents SAXS profiles of a concentrated phase before and after dialysis against NaOH. These profiles show a transition from a disordered micellar structure to a hexagonal structure as DeB was degraded. This transition was observed for all investigated samples: Figure 4b shows SAXS profiles of the concentrated phases collected from samples with varying initial concentration of DeB.

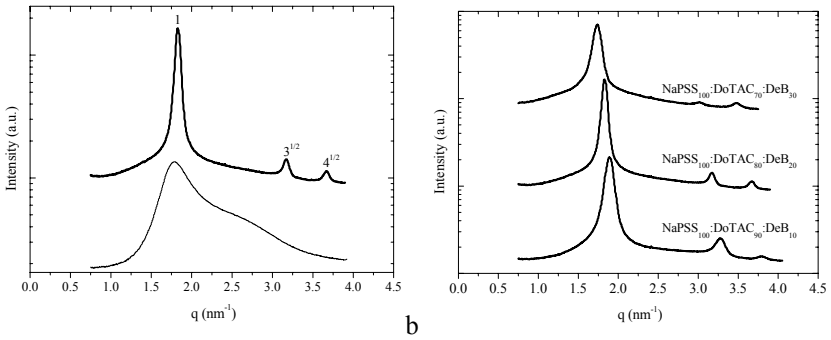

a b

Figure 4. SAXS profiles of the concentrated phases: a – for the sample $NaPSS_{100}$:$DoTAC_{80}$:DeB_{20} after mixing (thin line) and after dialysis in 0.5 M of NaOH (thick line); and b – for the samples with different DeB contents after dialysis. Subscripts denote the concentrations of the respective components. The relative positions of the reflections $1:3^{1/2}:2$ for the hexagonal structures are shown.

An important point to note is that the concentrated phases showed swelling without a notable increase in the characteristic distances of the respective hexagonal structures. From this finding one can tentatively describe the gels formed on dialysis as "domains" of hexagonal structure interconnected by stretches of "naked" PSS^-. (PSS^- becomes naked when it loses its surfactant counterion, due to a decrease in surfactant concentration as hydrolysis proceeds.) It can also be noted that the occurrence of hexagonal domains within the swollen gels could explain the cloudy visual appearance of the complexes.

When the concentrated phases from the dialyzed mixtures were washed with water they showed further substantial swelling, but remained birefringent, and the SAXS profiles were practically unchanged. Also at this stage the swelling was more pronounced for concentrated phases in samples with a larger initial fraction of DeB. The additional swelling on rinsing can be attributed to the removal of simple salt.

In this communication it has been demonstrated that aqueous mixtures involving anionic polyelectrolytes and betaine ester surfactant shows good potential for obtaining different types of responsive and evolving systems.

6. Acknowledgments

Cryo-TEM experiments were performed by Gunnel Karlsson from the department of Polymer and Materials Chemistry at Lund University. This study was funded by Fundação para a Ciência e a Tecnologia (SS, SFRH/BD/30929/2006 and DL, SFRH/BPD/48522/2008), by POPH/FSE (SS) and by the Swedish Research Council (VR) through the Linnaeus Centre of Excellence on Organizing Molecular Matter (OMM).

7. References

1 A. Svensson, J. Norrman and L. Piculell, *J Phys Chem B*, 2006, **110**, 10332.

2 J. Bernardes, J. Norrman, L. Piculell and W. Loh, *J Phys Chem B*, 2006, **110**, 23433.

3 J. Norrman and L. Piculell, *J Phys Chem B*, 2007, **111**, 13364.

4 A. Svensson, L. Piculell, B. Cabane and P. Ilekti, *J Phys Chem B*, 2002, **106**, 1013.

5 A. Svensson, L.Piculell, L. Karlsson, B. Cabane and B. Jönsson, *J Phys Chem B*, 2003, **107**, 8119.

6P. Nilsson, J. Unga and P. Hansson, *J Phys Chem*, 2007, **111**, 10959.

7 S. dos Santos, C. Gustavsson, C. Gudmundsson, P. Linse and L. Piculell, manuscript in preparation.

8 D. Lundberg, H. Ljusberg-Wahren, A. Norlin and K. Holmberg, *Colloid Interface Sci*, 2004, **278**, 478.

9 B. Rozycka-Roszak, S. Przestalski and S. Witek, *J Colloid Surface Sci*, 1998, **125**, 80.

10 M. Lindstedt, S. Allenmark, R. A. Thompson and L. Edebo, *Antimicrob Agents Chemother*, 1990, **34**, 1949.

11 D. Lundberg and K. Holmberg, *J Surfactants and Detergents*, 2004, **7**, 239.

12 *Surfactants and Polymers in Aqueous Solution*, K. Holmberg, B. Jönsson, B. Kronberg and B. Lindman, John Wiley & sons Ltd, 2003, pages 235-259.

13 D. Lundberg, M. Almgren, P. Jarvoll and G. Karlsson, *Langmuir*, 2010, **16**, 7996.

14 M. Karlberg, M. Stjerndahl, D. Lundberg and L. Piculell, *Langmuir*, 2005, **21**, 9756.

15 G. Nizri, A. Makarsky, S. Magdassi and Y. Talmon, *Langmuir*, 2009, **25**, 1980-1985.

16 G. Nizri, S. Magdassi, J. Schmidt, Y. Cohen and Y. Talmon, *Langmuir*, 2004, **20**, 4380.

17 K. Kogej, G. Evmenenko, E. Theunissen, H. Berghmans and H. Reynaers, *Langmuir*, 2001, **17**, 3175.

18 K. Kogej, *Adv Colloid Interface Sci*, 2010, **158**, 68.

19 M. Knaapila, C. Svensson, J. Barauskas, M. Zackrisson, S.S. Nielsen, K. N. Toft, B. Vestergaard, L. Arleth, U. Olsson, J. S. Pedersen and Y. Cerenius, *J. Synchrotron Rad*, 2009, **16**.

20 A. Hammersley, Grenoble. Private communication.

21 Bellare, J. R.; Davis, H. T.; Scriven, L. E.; Talmon, Y., *Journal of Electron Microscopy Technique*, 1988, **10**, 87.

8. Supporting Information

Materials. Sodium poly(acrylate), NaPA, (150 000 g/mol) poly(acrylic acid), PAA, (450 000 g/mol) sodium poly(styrene sulfonate), NaPSS, (1 000 000 g/mol), 1-Decanol, trimethylamine, chloroacetyl chloride, dodecyltrimethylammonium chloride, DoTAC and dialysis membrane with a cut-off of 500. All chemicals were used without further purification. All solutions were prepared using water purified with Millipore Milli-Q equipment.

Synthesis of DeB. Decyl betainate (DeB) was prepared via a two-step route based on previously described procedures, where decanol was first converted into the corresponding chloroacetate and then further reacted with trimethylamine to yield the final product [11].

Sample preparation.

NaPA:DoTAC:DeB. Each sample was prepared individually. Polymer and surfactant solutions with concentrations double (or triple) the desired final concentration were mixed and left for 20 min under stirring. For the mixtures containing both DoTAC and DeB, the surfactant solutions were mixed first and then the mixed surfactant solution was added to the polymer solution. The final volume of each sample was 3 mL. The samples were stirred for 30 min, and then left to equilibrate.

NaPSS:DoTAC:DeB and PAA:DoTAC:DeB. Samples were mixed the same way as for NaPA:DoTAC:DeB. After 24 hours each sample (one-phase or two-phase) was checked again and put into dialysis against 0.5 M of NaOH (pH~14). Final volume of each sample was 3 mL. The samples were dialyzed for 2.5 hours (after this time nothing seemed to change visually).

Structural characterization. Small angle X-ray scattering (SAXS) measurements were performed at the I711 line in Max-lab in Lund, Sweden [19]. The experimental setup involved the use of X-rays at the wavelength of 1.1 Å and a sample-to-detector distance around 1250 mm. A cell with mica windows was used and was maintained at the desired temperature (25 or 40°C). Typical acquisition times were 300 and 600 seconds. The volume between the sample and the detector was kept under vacuum during data collection to minimize the background scattering. The analysis of the 2D SAXS scattering data was conducted by the software Fit2D [20]. It follows from geometry that the center-to-center distance between adjacent rods, d, of the hexagonal structure can be obtained from the first diffraction peak (q_1) using

$$d_{\text{hex}} = (2/3^{1/2})(2\pi/q_1) \quad (1)$$

For the lamellar structures the distance between the equivalent planes, d_{lam}, is given by

$$d_{\text{lam}} = 2\pi/q_1 \quad (2)$$

The correlation distance between the micelles is given by

$$d_{\text{mic}} = 2\pi/q \quad (3)$$

Cryo-TEM. Samples for the cryo-TEM experiments were prepared using a controlled environment vitrification system (CEVS) [21], where the relative humidity was kept close to saturation at around 30°C. A 5 μL drop was placed on a lacey carbon-coated copper grid and the excess fluid was gently blotted away leaving a thin film of aqueous sample covering the grid. The grid was then plunged into liquid ethane at -180°C to allow rapid vitrification of the specimen (avoiding crystallization of water). All prepared grids were stored in liquid nitrogen until being transferred to the electron microscope. Images were digitally recorded using a Philips CM120 Bio TWIN electron microscope, operated at 120 kV, at around -183 °C, equipped with a Gatan MSC791 cooled-CCD camera system. To minimize beam damage, all samples were imaged under minimal electron dose conditions.

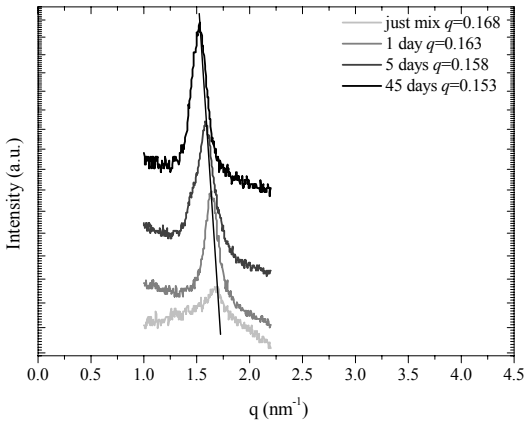

Figure S1. SAXS profiles of various dispersions of $NaPA_{10}$:DeB_5 mixtures.

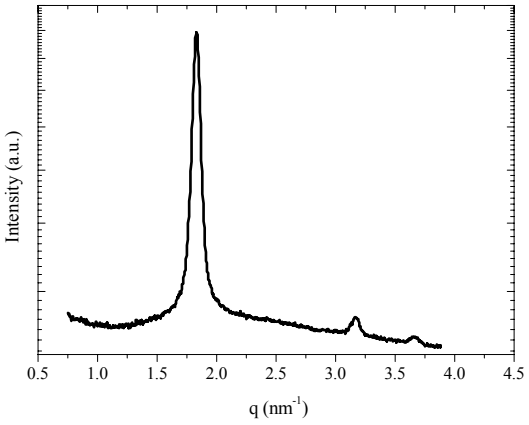

Figure S2. SAXS profiles from the swollen concentrated phase of $NaPSS_{100}$:$DoTAC_{80}$:DeB_{20} the system.